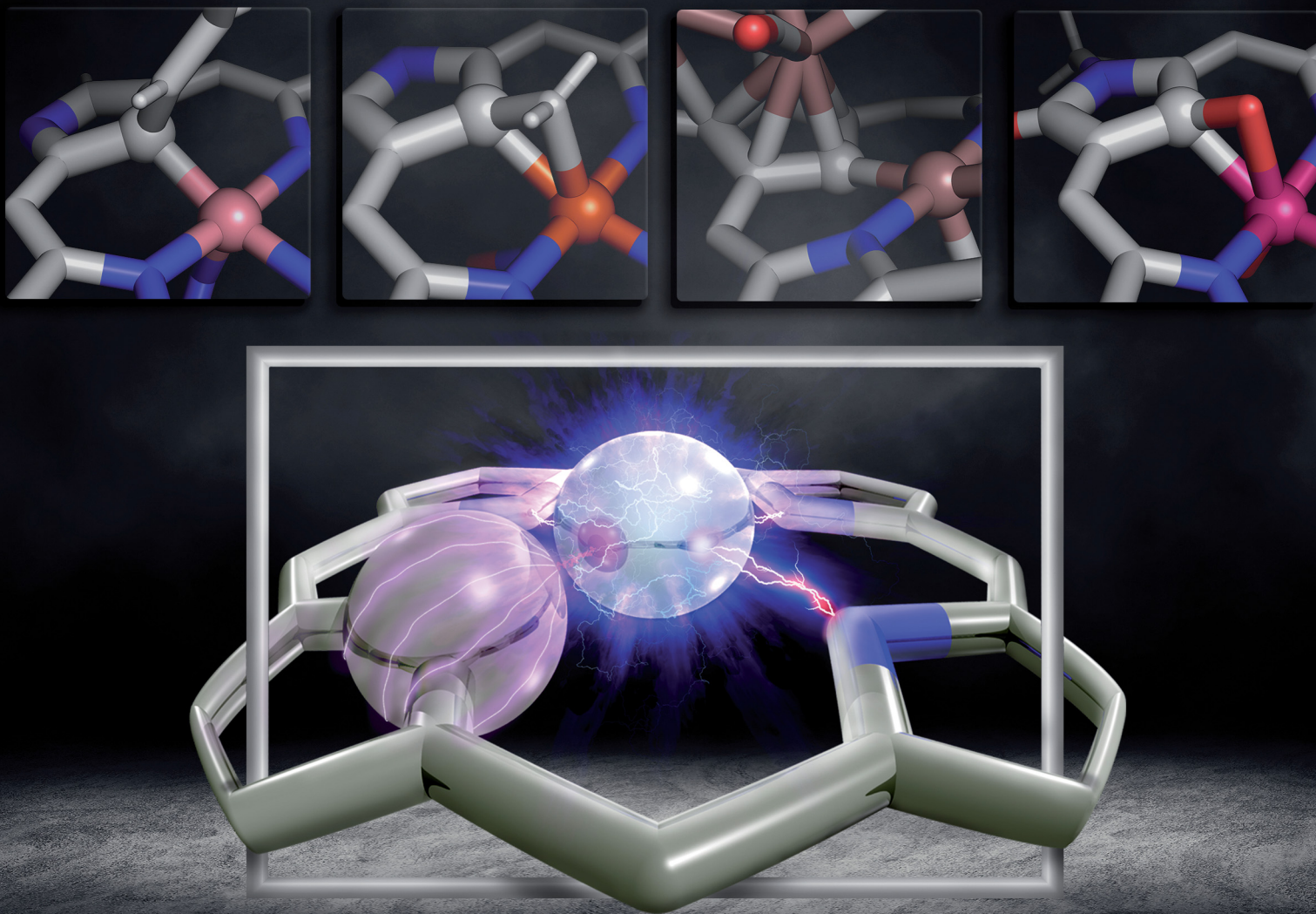


# Chem Soc Rev

Chemical Society Reviews

[rsc.li/chem-soc-rev](https://rsc.li/chem-soc-rev)



ISSN 0306-0012

## REVIEW ARTICLE

Hiroyuki Furuta, Lechosław Latos-Grażyński *et al.*  
Organometallic chemistry confined within a porphyrin-like  
framework



Cite this: *Chem. Soc. Rev.*, 2023, 52, 2082

Received 14th September 2022

DOI: 10.1039/d2cs00784c

rsc.li/chem-soc-rev

# Organometallic chemistry confined within a porphyrin-like framework

Michał J. Białek, <sup>a</sup> Karolina Hurej, <sup>a</sup> Hiroyuki Furuta <sup>\*b</sup> and Lechosław Latos-Grażyński <sup>\*a</sup>

The world of modified porphyrins changed forever when an N-confused porphyrin (NCP), a porphyrin isomer, was first published in 1994. The replacement of one inner nitrogen with a carbon atom revolutionised the chemistry that one is able to perform within the coordination cavity. One could explore new pathways in the organometallic chemistry of porphyrins by forcing a carbon fragment from the ring or an inner substituent to sit close to an inserted metal ion. Since the NCP discovery, a series of modifications became available to tune the coordination properties of the cavity, introducing a fascinating realm of carbaporphyrins. The review surveys all possible carbaporphyrins (1.1.1.1) and their spectacular coordination and organometallic chemistry.

## Introduction

Porphyrinoids, defined as porphyrin-inspired macrocycles, have undergone systematic evolution extending the original concepts.<sup>1–10</sup> The new research directions mainly originate from seminal porphyrin isomer<sup>11–15</sup> and heteroporphyrin<sup>4,16–20</sup> studies.

Porphyrinoids may be seen as a unique platform for coordination/organometallic chemistry, which creates a specific environment allowing for the observation of unusual oxidation and electronic states of bound metal cations. Consequently, they have created an opportunity to address fundamental issues investigated in such seemingly distant fields as the aromaticity of porphyrinoids, including those which adopt a Möbius topology,<sup>21–24</sup> organometallic copper(II) compounds,<sup>25,26</sup> the contraction of benzene to cyclopentadiene,<sup>27,28</sup> the inclusion of a d-electron subunit into a  $\pi$ -electron conjugation,<sup>29,30</sup> catalysis,<sup>31–33</sup> dioxygen activation,<sup>34</sup> or serving as a  $\pi$ -coordination platform to accommodate the  $\text{Ru}_4(\text{CO})_9$  cluster(s).<sup>35</sup>

<sup>a</sup> Department of Chemistry, University of Wrocław, 14 F. Joliot-Curie, 50383 Wrocław, Poland. E-mail: lechoslaw.latos-grazynski@chem.uni.wroc.pl

<sup>b</sup> Department of Chemistry and Biochemistry, Graduate School of Engineering, Kyushu University, 744 Moto-oka, Nishi-ku, Fukuoka 819-0395, Japan. E-mail: furuta.hiroyuki.165@m.kyushu-u.ac.jp



Michał J. Białek

Michał Białek was born in 1987. He graduated from the Wrocław University of Science and Technology in 2011. His PhD studies under the supervision of Lechosław Latos-Grażyński at the University of Wrocław focused on the organometallic chemistry and aromaticity of carbaporphyrinoids with an azulene motif. After completing PhD in 2017, he joined prof. Rafal Klajn's group at the Weizmann Institute of Science, Israel, a year later as a postdoc.

His current research at the University of Wrocław covers a range of topics from the organometallic chemistry of modified porphyrinoids to chemistry under confinement within host–guest systems or macrocycles.



Karolina Hurej

Karolina Hurej was born in 1988 in Lubin, Poland. In 2017, she completed her PhD under the supervision of Lechosław Latos-Grażyński. Her investigations were dedicated to carbaporphyrinoids and their rhodium and ruthenium complexes. In 2018, Karolina won the “Mobilność Plus” scholarship from the Polish Minister of Science and Higher Education and joined the group of Dr Paweł Dydio at the Institute of Supramolecular Chemistry and Engineering,

France. Currently, she works at the University of Wrocław. Her research interests include C–H activation within the carbaporphyrinoid frameworks and in simple organic molecules using porphyrin-based catalysts.

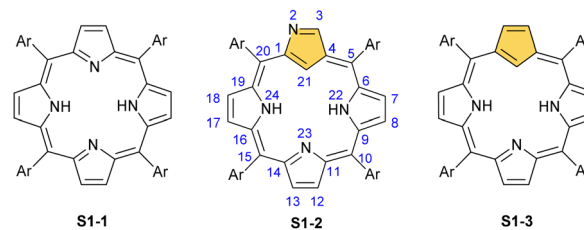




Since its discovery by Rothemund,<sup>36</sup> *meso*-tetraarylporphyrin **S1-1** has become a ubiquitous building block used in biomimetic chemistry to investigate metalloporphyrin-catalysed reactions or as working elements of molecular devices. The progress in the field has been confirmed by the development of efficient synthetic strategies for preparing *meso*-tetraarylporphyrins introduced by Adler and Longo<sup>37</sup> and subsequently by Lindsey<sup>38</sup> in a version adjusted for milder conditions. Remarkably, the synthesis of *meso*-tetraaryl-N-confused porphyrin<sup>12,13</sup> (2-aza-21-carbaporphyrin, inverted porphyrin) **S1-2** – a constitutional isomer of **S1-1**, formed in the Lindsey-type condensation of pyrrole and arylaldehyde – triggered the interest in the original class of macrocycles, 21-carbaporphyrins, to be later extended to a broader group of carbaporphyrinoids.

This specific subclass of core-modified porphyrins, *i.e.*, 21-carbaporphyrins, can be formally constructed after a confinement of a carbocyclic moiety within the porphyrin **S1-1** scaffold. A perfect match between the metal cation radii and the crevice diameter, so significant for the coordination chemistry of porphyrins, remains conserved in 21-carbaporphyrin. This provides a crucial incentive to explore unique macrocyclic organometallic chemistry. Today, replacing a porphyrin's single pyrrole ring with cyclopentadiene or N-confused pyrrole rings, as shown in Scheme 1, seems to be a natural strategy for creating porphyrin-type frames containing a paradigmatic [C<sub>4</sub>NNN] coordination core. The several advances in the broader field of carbaporphyrinoids are comprehensively accounted for in a series of recent review articles.<sup>1,39–43</sup>

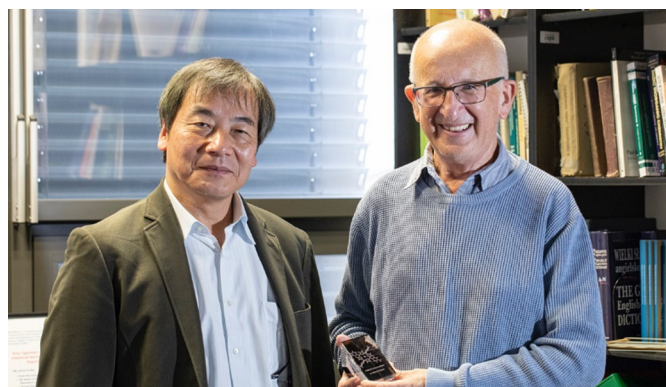
For the purpose of this review, we would like to remain focused on a basic porphyrin scaffold – tetraphyrin(1.1.1.1) with four five-membered rings closed in a macrocycle with *meso*-bridges. The apparent structural resemblance of N-confused porphyrin **S1-2** and 21-carbaporphyrin **S1-3** frames to those coined “the working horses” of metalloporphyrin chemistry – *meso*-tetraarylporphyrin or  $\beta$ -octaethylporphyrin – provides the



**Scheme 1** *meso*-Tetraarylporphyrin **S1-1** and its carba analogues: N-confused porphyrin **S1-2** and *meso*-tetraaryl-21-carbaporphyrin **S1-3**.

well-founded expectation for similar roles of **S1-2** and **S1-3** in organometallic chemistry. The conformation and strain within the macrocycle remain unaltered. However, by forcing a carbon fragment into close contact with the metal centre, organometallic reactions occur that would otherwise not progress if there was no confinement of these two species. Consequently, because of macrocyclic stabilisation, one is also able to witness and detect unstable transient forms solving mechanistic riddles. Eventually, the formation of organometallic complexes with suitably labile carbon–metal bond(s) can create an avenue to practical applications for catalysis, in a way the pincer ligands are famously used for.<sup>44–47</sup> Finally, seemingly slight scaffold modifications are powerful means for determining new structure–property relationships in the spectral properties and reactivity of modified macrocycles.

The start of the review seems to be predictable because of the authors' involvement in the originating field. The enlightening modification, namely N-confusion, introduced a carbon atom into the cavity and started a broad family of carbaporphyrins. The next step in creating an organometallic environment imprinted in porphyrin was introducing a carbocyclic unit. Thus, the presentation is split into a few complementary parts (Scheme 2). The first section covers the chemistry of N-confused porphyrin (**S2-2**); the second one addresses the properties of further modifications, including X-confused (**S2-3**) and

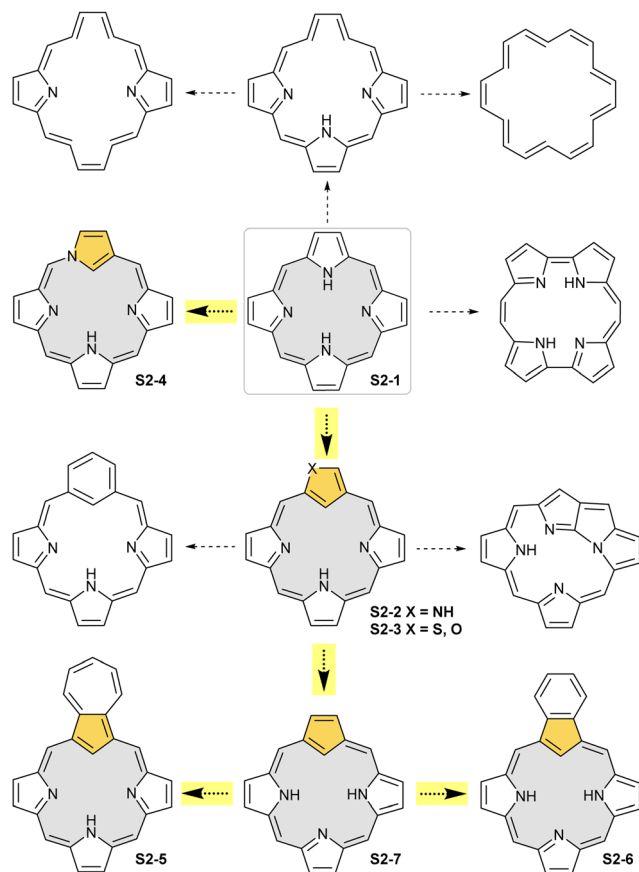


**Hiroyuki Furuta (left) and Lechosław Latos-Grażyński (right)**

*La Mar* at the University of California, Davis (1979–1981), he returned to Wrocław, where he achieved professorship in 1992 and was nominated as the Head of the Organic Chemistry Division in 2002. Lechosław Latos-Grażyński is interested in the chemistry of porphyrins and N-confused porphyrins and their analogues, including various carbaporphyrinoids. His current interests include the synthesis of new porphyrinoids, their coordination and organometallic chemistry, and NMR spectroscopy of paramagnetic systems.

Hiroyuki Furuta (left) received his BSc (1980), MSc (1982), and PhD (1986) degrees from Kyoto University. After postdoctoral research at the Mitsubishi-Kasei Institute of Life Sciences, Tokyo, and at the University of Texas, Austin, he started his independent academic career in 1992 as an Associate Professor at Oita University, where the “N-confused porphyrin” was found. In 1997, he moved to Kyoto University as an Associate Professor. In 2002, he was named a Full Professor in Chemistry at Kyushu University. In 2022, he retired from Kyushu University and became professor emeritus. His current research focuses on the synthesis of N-confused porphyrinoids with novel functionality. Lechosław Latos-Grażyński (right) received his PhD in 1978 from the University of Wrocław for the work supervised by Bogusława Jeżowska-Trzebiatowska. After postdoctoral research on highly oxidized iron porphyrins with Alan L. Balch and Gerd N.





**Scheme 2** Basic structural motifs leading from regular porphyrin (**S2-1**) to carbaporphyrin (**S2-7**) and isomeric porphyrins (**S2-2** and **S2-4**), while preserving the regular porphyrin framework. The inner parts of the described macrocyclic frameworks are grey-coloured to underline the leading motif together with an orange-coloured crucial five-membered ring that donates an inner carbon atom for coordination. Highlighted arrows indicate general pathways followed in this review. The remaining structures underline the great richness of the modified and isomeric porphyrinoid family, including other carbaporphyrinoids, not covered by this review.

neo-confused porphyrins (**S2-4**). The third part is focused on azuliporphyrin (**S2-5**) and benziporphyrin (**S2-6**). The fourth one presents true carbaporphyrins (**S2-7**). The fifth section introduces 'higher complexity' systems containing more than one carbon atom in the inner core. Finally, the last one looks at selected examples closely related to the previous sections.

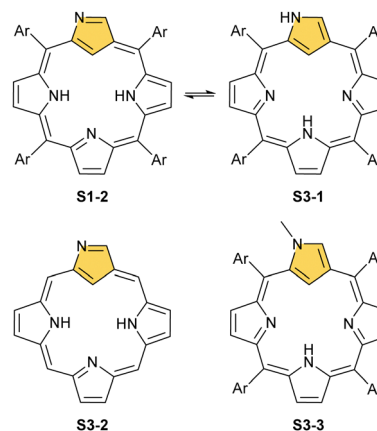
## NCP – an origin of carbaporphyrinoids

The story of carbaporphyrins started with discovering *meso*-tetraaryl-2-aza-21-carbaporphyrin (N-confused porphyrin, inverted porphyrin) as a side-product of Lindsey-type condensation of pyrrole and arylaldehyde that typically leads to regular *meso*-tetraarylporphyrin. Our two groups isolated and determined the structure of this molecule independently as early as 1994.<sup>12,13</sup> However, the preliminary suggestions addressing the potential existence and the structure of this peculiar porphyrin

isomer were reported by Aronoff and Calvin in 1943<sup>48</sup> and Pauling in 1944 in his laboratory notes.<sup>15</sup>

Originally, N-confused porphyrin was identified as an additional macrocyclic product of *meso*-tetraarylporphyrin synthesis carried out under classical Lindsey conditions.<sup>12,13</sup> The first studies reported relatively low yields (4% Latos-Grażyński and 5–7% Furuta). The first preparative breakthrough required the synthesis of predesigned dipyrromethanes containing a pyrrole ring attached at a  $\beta$ -position (N-confused pyrrole), and the procedure afforded a 25% yield.<sup>49</sup> The absolute game-changer resulted from the optimised Lindsey-type condensation of regular pyrrole and arylaldehyde. Lindsey *et al.* upgraded the process, eventually achieving the impressive *ca.* 40% yield of **S1-2**. Here, the skillful selection of an acidic catalyst, namely methanesulfonic acid, was crucial.<sup>50</sup> This paved the way for extensive multidirectional studies of NCP – the constitutional porphyrin isomer with a carbon atom in the coordination core and the pyrrolic nitrogen atom at its perimeter. Finally, an appropriate design and the [3+1] reaction of protected N-confused tripyrrane and 2,5-bis(hydroxymethyl)pyrrole resulted in the formation of the N-confused isomer of porphine (**S3-2**).<sup>51</sup>

N-confusion could not go unnoticed in spectroscopic characterisation studies.<sup>12,52</sup> The macrocycle containing an N-confused pyrrolic moiety is still aromatic, thus exhibiting a strong Soret band at 440 nm in an electronic spectrum and the overall red-brown colour of the chloroform solution. These features are typical as long as the experiment is carried out in a solvent with low polarity. In polar solvents such as DMF, the solution becomes green, Q-bands shift, and the Soret gets broader and slightly less intense. The differences are much more apparent in <sup>1</sup>H NMR spectroscopy. In chloroform-*d*, strong macrocyclic aromaticity shifts upfield the inner proton signals and is a consequence of a sharp peak at *ca.* –5 ppm from an internal C(21)–H. In contrast, the solution in DMF-*d*<sub>7</sub> reveals a different pattern, with a C(21)–H signal at 0.76 ppm and an increasing peak at 13.54 ppm. This alone allowed for a conclusion that two tautomers of NCP exist (**S1-2** three inner protons – 3H and **S3-1** (Scheme 3) two inner protons – 2H) and



**Scheme 3** N-confused porphyrin tautomers (**S1-2** – 3H and **S3-1** – 2H) and other derivatives.



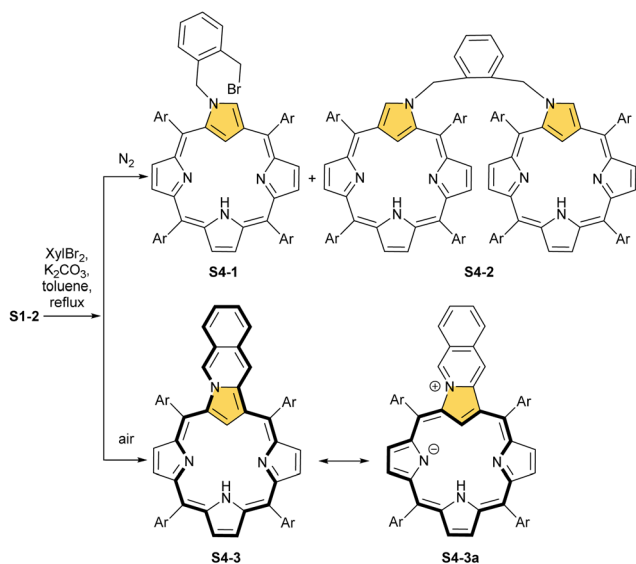
that one is able to control the formation of a particular tautomer by picking the right solvent<sup>52,53</sup> and, as further studies show, substituents.<sup>53,54</sup> Indeed, the signal at 13.54 ppm comes from the NH proton located outside the cavity. The conjugation pathway in **S3-1** is formally disturbed; thus, the macrocyclic aromaticity is somewhat diminished.

The described aromaticity control within a preserved porphyrin scaffold of NCP shows a clear difference with the behaviour of the regular porphyrin. The tautomeric structural reorganisation of N-confused porphyrin **S1-2** implies substantial coordination flexibility.

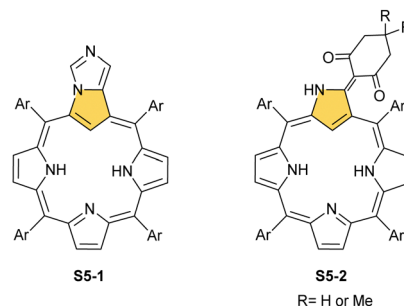
### Reactivity of N-confused pyrrole – fundamental routes

**N(2) reactivity.** Certainly, NCP tautomers **S1-2** and **S3-1** are expected to act differently once engaged in coordination. The readily accessible yet fundamental modification involves a structural locking of the tautomer **S3-1** via N(2) methylation. The methylation reaction proceeds regioselectively, yielding N(2)-methyl NCP **S3-3** as the N(2) outer nitrogen atom is sterically more accessible and nucleophilic than competing inner core nitrogen atoms. The process is straightforward and involves the reaction of NCP and methyl iodide in excess under mild conditions.<sup>55</sup> The extension of this transformation comes from using various alkylating agents, including haloalkyl esters, amides, and allyl bromide.<sup>56,57</sup>

Typically, such reactions are facilitated by the presence of a base. The reactivity of dihaloderivatives, including 1,2-bis(bromomethyl)benzene as a representative example, was tested as a logical next step in such studies.<sup>58</sup> As expected, a reaction in an inert atmosphere provides, aside from an N(2)-alkylated product, a dimer **S4-2** in which two NCP units are bridged through N(2) positions using an *o*-xylene moiety. Significantly, the presence of dioxygen triggers an alternative route. An annulation of a transient N(2)-substituted derivative **S4-1** (Scheme 4) involves the reaction of an adjacent



Scheme 4 N(2)-Substituted derivatives of N-confused porphyrin **S1-2**.



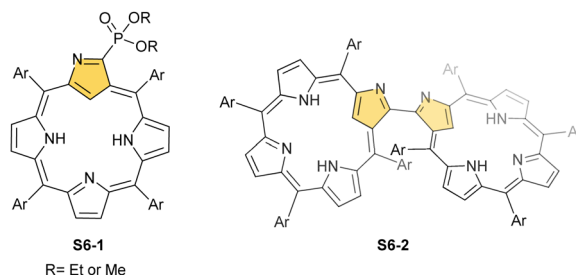
Scheme 5 C(3)-Substituted derivatives of N-confused porphyrin **S1-2**.

bromomethyl site with a C(3) atom. This affords, after oxidation, pyrrolo[1,2-*b*]isoquinoline-embedded macrocycle **S4-3**.

**C(3) reactivity.** The N-confused pyrrole ring of **S1-2** reveals characteristic reactivity centred at the C(3) position. For example, using tosylmethylisocyanide, a substitution reaction occurs in the course of which another type of annulation yields imidazole-fused macrocycle **S5-1** (Scheme 5).<sup>59</sup> This transformation locks the molecular structure resembling the inner core arrangement of **S1-2**. It contains three dissociable protons in the cavity, allowing for eventual coordination as the macrocyclic trianionic ligand. The outer nitrogen atom may undergo further selective protonation or methylation. A diversity of C(3)-substituted derivatives can be generated from NCP **S1-2** in reactions with appropriately selected reagents, including, among others, active methylene compounds.<sup>60</sup> The reaction of **S1-2** and cyclohexane-1,3-dione affords a peculiar derivative **S5-2** in which an external C(3)=C double bond forms. Accordingly, the molecular pattern related to **S1-2** was enforced, which in the properties is reminiscent of a 3-oxo N-confused porphyrin (lactam) derivative.<sup>61</sup>

A different porphyrin skeleton, yet with inner 3H, can be warranted by the location of bulky substituents at the C(3) position. A phosphonate group of **S6-1** (Scheme 6) (introduced in a reaction of NCP with trialkyl phosphite) is attached through a P-C(3) linkage.<sup>62</sup> Phosphorylation of NCP occurs regioselectively. Initially, the reduction at the *meso* C(5) position was detected in this substitution process. Eventually, the reduced intermediary species was oxidised with 2,3-dichloro-5,6-dicyano-*p*-benzoquinone (DDQ) to form the final derivative **S6-1**.

A spectacular C(3)-centred reactivity of N-confused porphyrin can be illustrated by the formation of covalently linked



Scheme 6 Selected results of C(3) reactivity in NCP.



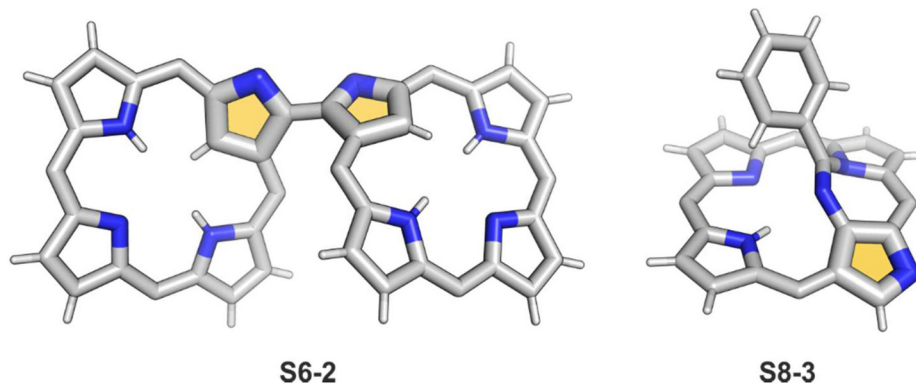
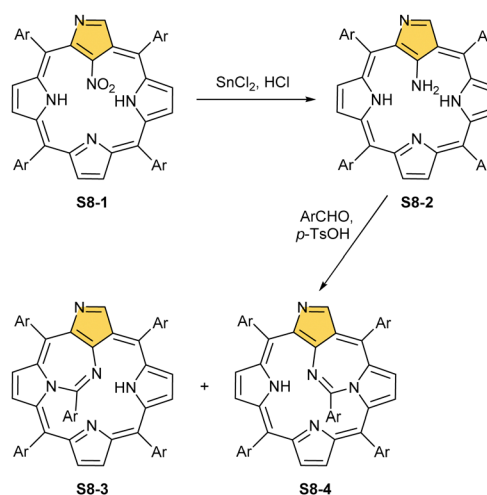


Fig. 1 Products of C(3)/C(21) reactivity in NCP. *meso*-Substituents not shown.

dimers represented here by **S6-2**.<sup>63</sup> **S6-2** is readily produced by acid-catalysed dimerization of N-confused porphyrin **S1-2** carried out in a toluene/dichloromethane mixture under reflux. In **S6-2**, two NCP subunits are linked by the C(3)–C(3') bond of 1.468(3) Å length (Fig. 1).

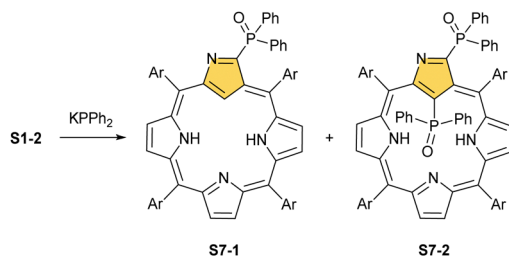
**C(21) reactivity.** Phosphorylation of NCP **S1-2** using six equivalents of potassium diphenylphosphide also results in a respective C(3) substitution. It gets oxidised into a diphenylphosphoryl derivative **S7-1** (Scheme 7) during the work-up.<sup>64</sup> Noticeably, though, this is not the only product as the subsequent step involves the substitution at the C(21) position producing doubly phosphorylated porphyrin **S7-2**. This transformation points to the particular reactivity of the internal C(21) atom. Significantly, the C(21) substitution is important in metal coordination or the possible modes of metal–carbon interactions. Thus, the confined fragment may directly participate in the coordination or get transformed into a different moiety. Alternatively, the cleavage of the C(21)-substituent bond can be stimulated, affording its controlled release. Examples of such transformations will be presented within the coordination chemistry section.

Another C(21) functionalisation example is regioselective nitration leading to **S8-1** (Scheme 8). The process occurs solely at the C(21) position when using  $\text{HNO}_2$  or diluted  $\text{HNO}_3$  acids.<sup>65</sup> The reduction of the introduced  $\text{NO}_2$  group generates the respective amino derivative **S8-2** – a suitable starting point for further transformations.<sup>66</sup> The addition of arylaldehyde to **S8-2** results in intramolecular annulation, which delivers two isomeric products (**S8-3** and **S8-4**). In fact, in the oxidative step, the carbon atom of the imine moiety forms a single bond with

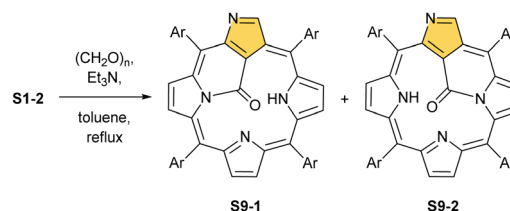


Scheme 8 Reactivity of 21-nitro N-confused porphyrin **S8-1**.

one of two available internal NH atoms (N(22)H or N(24)H), completing the closure of novel seven-membered rings. Interestingly, **S8-3**, with the C(21)/N(24) link (Fig. 1), forms in higher yields. Upon heating, the isomers interconvert, yet the original preference under thermodynamic equilibrium is preserved. A reaction of N-confused porphyrin and paraformaldehyde (at elevated temperatures and under basic conditions) provides another illustrative example of intramolecular ring fusion.<sup>67</sup> The initial incorporation of the formyl group at the C(21) position is followed by a bridge formation reaching the adjacent N(22) or N(24) nitrogen atoms. Consequently, this step leads to fusion, making the six-membered rings in **S9-1** (Scheme 9) and **S9-2** with a clear preference toward a C(21)/N(24) bond of **S9-1**.

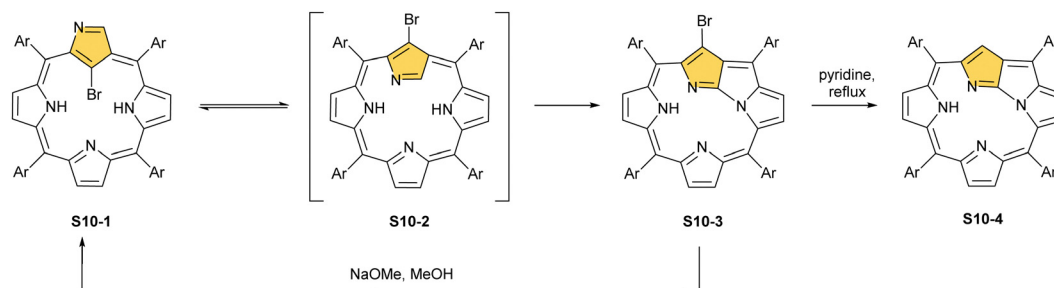


Scheme 7 Phosphorylation of N-confused porphyrin **S1-2** using potassium diphenylphosphide.



Scheme 9 Reactivity of N-confused porphyrin with paraformaldehyde.



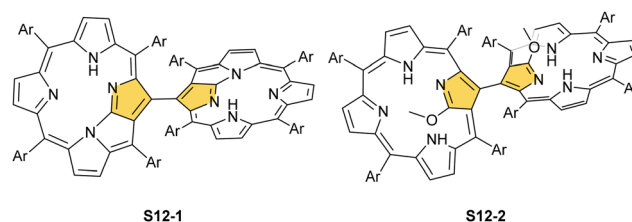
Scheme 10 Reactivity of 21-bromo N-confused porphyrin **S10-1**.

**Inversion and N-fusion.** Already described fused systems (**S8-3**, **S8-4**, **S9-1**, and **S9-2**) are shaped by initial functionalisation at the C(21) atom followed by annulation. Thus, they acquire a completely altered coordination cavity. This results in the shrinking of its accessible size and marked variations in possible donor centres.

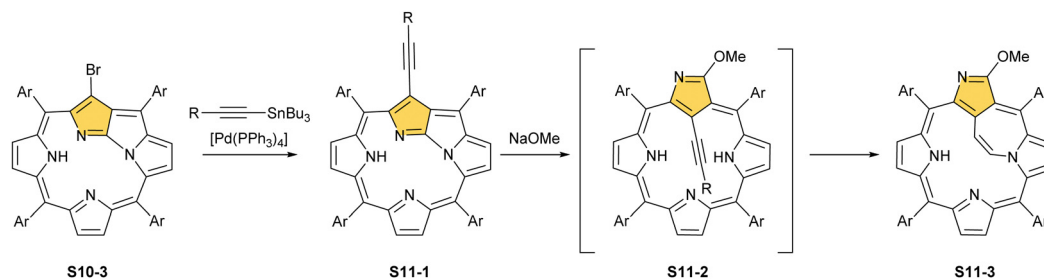
It is significant to emphasise that the N-confused porphyrin's conformationally flexible nature creates a route for a peculiar intramolecular fusion concept.<sup>68,69</sup> Thus, the regioselective bromination of **S1-2** with NBS affords 21-bromo N-confused porphyrin **S10-1** (Scheme 10).<sup>70</sup> In a pyridine solution, **S10-1** readily converts into N-fused porphyrin, NFP-Br (**S10-3**), a new type of porphyrinoid with a fused pyrrole ring in the macrocyclic core.<sup>71</sup> Presumably, the presence of a bulky bromide substituent at the centre of NCP-Br **S10-1** accelerates the flip of the N-confused ring. The geometry of transient species **S10-2** imposes an adjacency of C(3) and N(22) atoms. Their proximity facilitates the oxidative ring fusion resulting in the formation of the C(3)–N(22) bond. The formation of NFP-Br creates a novel coordination platform, allowing for an unprecedented architecture of metal binding.<sup>72</sup> The macrocyclic framework of N-fused porphyrin is markedly rearranged. After the N-confused pyrrole ring flip, the originally internal C(21) atom resides outside the coordination cavity.

Furthermore, debromination of **S10-3** *via* reflux in pyridine afforded a fundamental frame of NFP **S10-4**. The addition of sodium methoxide to **S10-3** results in the recovery of the NCP-Br frame, albeit after the cleavage of the N(22)–C(3) bond, the substitution by the methoxy group occurs at the C(3) position. Such a rearrangement can be induced by various nucleophiles, including thiols,<sup>73</sup> which can be subsequently removed from the macrocycle.

Interestingly, **S10-3** can be considered as a convenient starting point to generate suitably C(21)-substituted NCP due to the significant exposure of now the outer C(21) atom and an accessible NFP–NCP conversion.<sup>74</sup> Thus, a facile Br(21) substitution with an alkynyl moiety produced an appropriate NFP alkynyl derivative **S11-1** (Scheme 11). The subsequent conversion triggered by methoxide creates 21-alkynyl-substituted NCP **S11-2**. The further internal fusion of the triple bond with the adjacent NH provides etheno-bridged N-confused porphyrin **S11-3** and, in terms of electronic structure, the endocyclic extension of the porphyrin  $\pi$ -system.<sup>74,75</sup> In contrast to previously mentioned fusions, this one occurs regioselectively with the N(22) atom (**S11-3**), probably due to kinetic reasons. The exposed C(21) position of NFP **S10-4** may also be functionalised with another NFP unit in an oxidative coupling reaction forming a covalently linked dimer **S12-1**.<sup>76</sup> The NFP–NCP conversion triggered by methoxide allows for a stereoselective transformation of **S12-1** (Scheme 12) into the original structure of **S12-2**, in which the subunits are C(21)-covalently linked (Fig. 2). The C(21)–C(21') bond distance is similar to the C(3)–C(3') bond length determined for **S6-2**, *i.e.*, 1.480(7) Å, despite possible steric strains.



Scheme 12 C(21)–C(21') dimers.

Scheme 11 Reactivity of 21-bromo N-fused porphyrin **S10-3**.



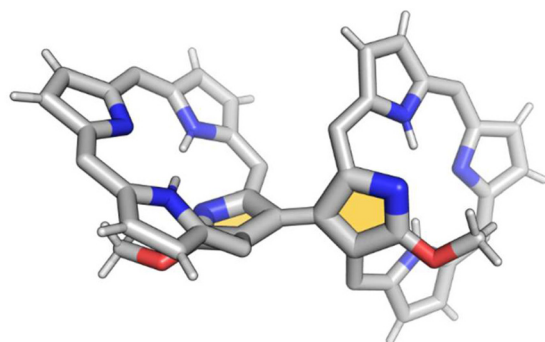
**S12-2**

Fig. 2 C(21)–C(21') NCP dimer. *meso*-Substituents not shown.

### Organometallic chemistry

**General comment.** Research efforts in ours and other groups have been constantly stimulated by the fact that the original 2-aza-21-carbaporphyrins **S1-2** are, at least in principle, able to accommodate a large variety of transition metal cations. They can frequently adopt unusual oxidation states. Thus, uncommon electronic structures can be stabilised by the suitably adjusted anionic charge of macrocyclic coordination centres. A possibility has been created to enforce a location of a metal cation close to carbon atom(s), creating an environment for typical and atypical organometallic interactions.

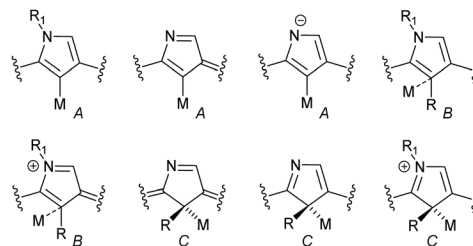
Such induction of metal–carbon interactions provides a unique opportunity to analyse them and translate the results into more reactive and dynamic (*e.g.*, catalytic) systems. **S1-2** enabled extensive studies on organometallic chemistry in macrocyclic surroundings.

One can notice that the coordination crevices of NCP can be adjusted in several ways *via* specific internal or peripheral modifications. Alternatively, a response to axial coordination to the transition metal ion can be probed. Fundamentally, the preferences for an oxidation state and/or tendency to form a direct M–C bond vary considerably. Thus, the higher oxidation states prefer the ligand structure related to tautomer **S1-2**. The lower oxidation state revealed the preference for the ligand structure visualised already for tautomer **S3-1**. The developments in the organometallic chemistry of N-confused porphyrin created a firm background for further, more general explorations of the organometallic chemistry of carbaporphyrinoids. In the following paragraphs, we will describe the highlights of organometallic chemistry in N-confused porphyrin surroundings.

In general, three fundamentally different modes of coordination can be identified for the inner core C(21) atom of the N-confused pyrrole ring defined by the C(21) donor geometry (Scheme 13):

- $\sigma$ -bonding of trigonal ( $sp^2$ ) carbanion (A),
- side-on coordination involving the trigonal ( $sp^2$ ) unit (B),
- $\sigma$ -bonding of tetrahedral ( $sp^3$ ) carbanion (C).

**Zn, Cd, Hg.** The insertion of a metal ion from the 12th group is not warranting the efficient activation of the C(21)–H bond. In this case, the side-on  $\eta^2$ -coordination and a very weak

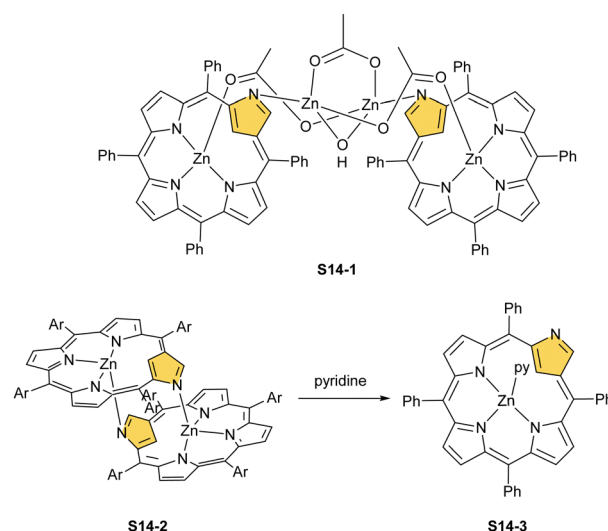


Scheme 13 Different coordination modes of N-confused porphyrin.

side-on  $\eta^1$ -interaction with the protonated C(21)  $sp^2$  atom have been typically established.

Zinc(II), when inserted using zinc(II) acetate, coordinates to three internal nitrogen atoms and the external axial acetate ligand.<sup>77</sup> The side-on  $\eta^1$  coordination of zinc(II) to the C(21) atom was also documented. NCP accommodates the structure of the **S1-2** tautomer; thus, the zinc(II) charge is compensated by the equatorial ligand. The availability of the outer N(2) donor centre resulted in the formation of a tetranuclear zinc(II) NCP dimer **S14-1** (Scheme 14). Two additional zinc(II) cations are involved in the construction of the bridging unit (Fig. 3). The reaction of **S14-1** with  $Et_4NOH$  leads to a more compact dimer, **S14-2** – the natural conjunction of a zinc(II) preferred coordination number and [CH,NNN] core coordination. Finally, the saturation with pyridine breaks the dimer **S14-2** affording a monomer **S14-3**. The Zn...C distance from the X-ray structure in **S14-3** is 2.414(10) Å.

The structure of **S14-2** was also confirmed by X-ray crystallography, showing *Z(cis)*-symmetry with vectors from C(3) to N(2) pointing in the same direction (Fig. 3).<sup>78</sup> The similar behaviour of cadmium(II) and mercury(II) N-confused porphyrins was detected, although  $[Hg(NCP)]_2$  **S15-3** is somewhat unstable. The Zn...C distance in the dimer **S14-2** increases to 2.534(8) Å. Interestingly, after mixing Zn and Cd dimers together, the heterodimer formation was observed during equilibration due to N(2) de- and recoordination. Inserting



Scheme 14 Zinc(II) complexes of N-confused porphyrin derivatives.

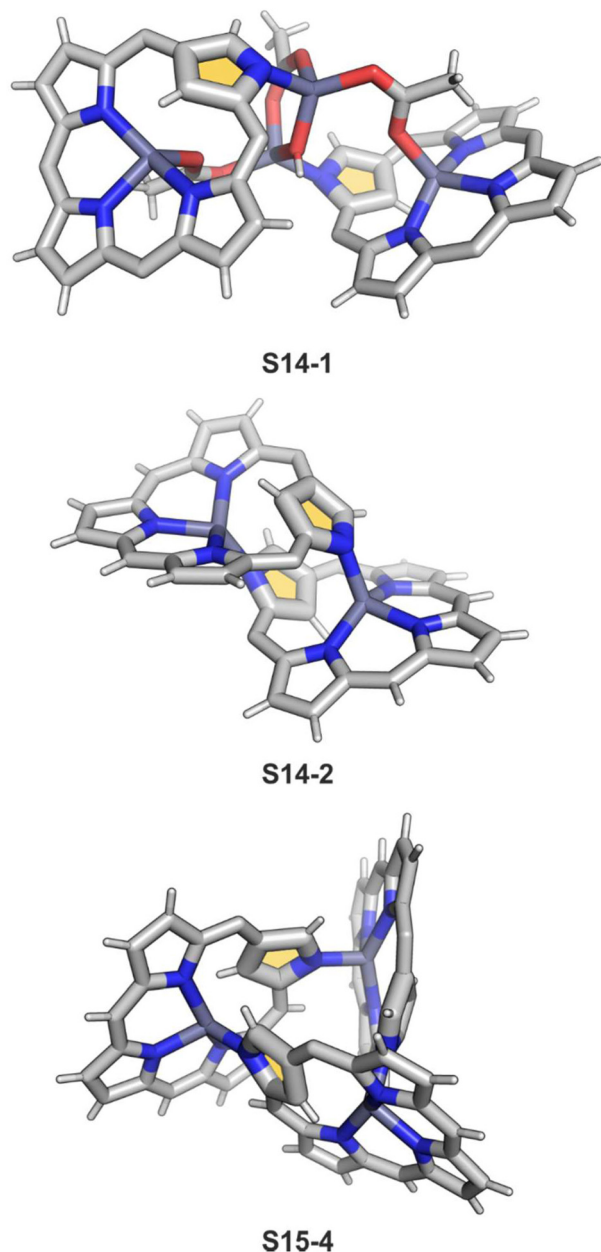
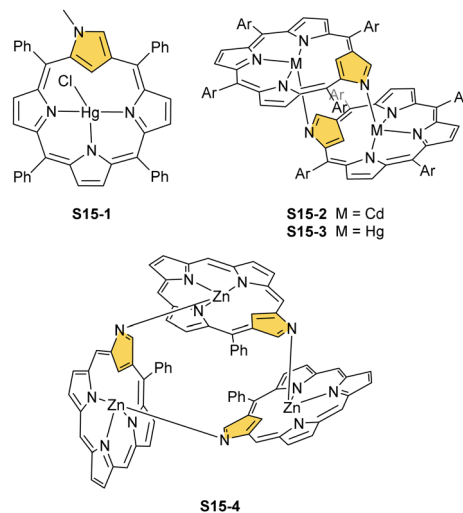


Fig. 3 Oligoporphyrinic assemblies induced by zinc(II) coordination. meso-Substituents not shown.

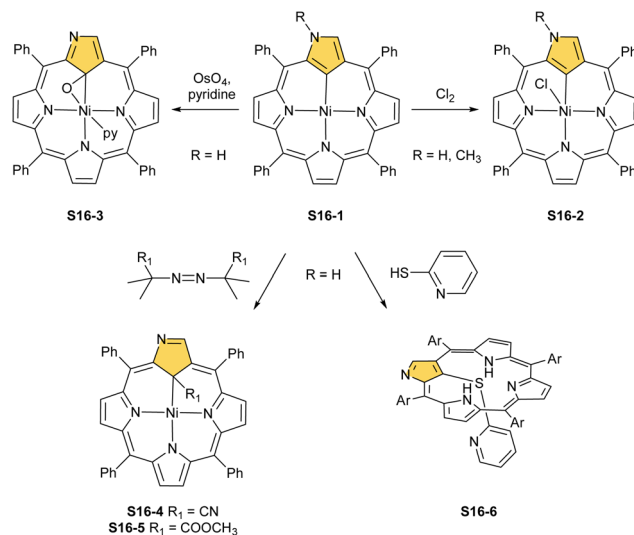
mercury(II) into N(2)-methyl NCP, which adopts an **S3-1**-like cavity with one inner NH, resulted in a monomeric complex **S15-1** (Scheme 15) supplemented with chloride for the charge balance.<sup>79</sup> The same coordination mode can be found in the Zn<sup>II</sup> and Cd<sup>II</sup> complexes of phosphonylated N-confused porphyrin (**S6-1**)<sup>62</sup> or the zinc(II) complexes of the C(3)–C(3') dimer (**S6-2**).<sup>80</sup> Complex **S15-1** exhibits the Hg<sup>II</sup>⋯C(21) distance of 2.711(6) Å and, together with similar derivatives, demonstrate the agostic interaction, which has significant consequences in communication between closely located interacting atoms. In the case of **S15-1** and related species, the scalar coupling of the internal H(21) and <sup>199</sup>Hg is reflected in an appropriately split <sup>1</sup>H NMR pattern. Depending on NCP substituents, e.g., mono-5-



Scheme 15 Complexes of N-confused porphyrin derivatives with mercury(II), cadmium(II), and zinc(II).

phenyl substitution, coordination trimers **S15-4** can be formed as sole products (Fig. 3).<sup>81,82</sup>

**Ni, Pd, and Pt.** A coordination mode of the N-confused porphyrin described as the deprotonated  $\sigma$ -bonding carbanion was detected in this macrocycle's very first reported complex.<sup>12</sup> The insertion occurs when NCP is treated with nickel salt in a mixture of chloroform and ethanol. Isolated nickel(II) N-confused porphyrin **S16-1** (Scheme 16) acquires a strictly planar geometry and stabilises a direct Ni<sup>II</sup>–C(21) organometallic bond. The structure of **S16-1** adopted the form of the **S3-1** tautomer. The analogous ligand geometry was also detected in nickel(II) 2-methyl NCP.<sup>55</sup> Such a molecular frame seems to be preserved during a swift oxidation process. Thus, the oxidation of **S16-1**, with a range of one-electron oxidants (e.g., halogens), leads to paramagnetic nickel(III) species **S16-2**. Nickel(III) NCP contains the five-coordinate central metal ion with an axially



Scheme 16 Reactivity of nickel(II) N-confused porphyrin **S16-1**.

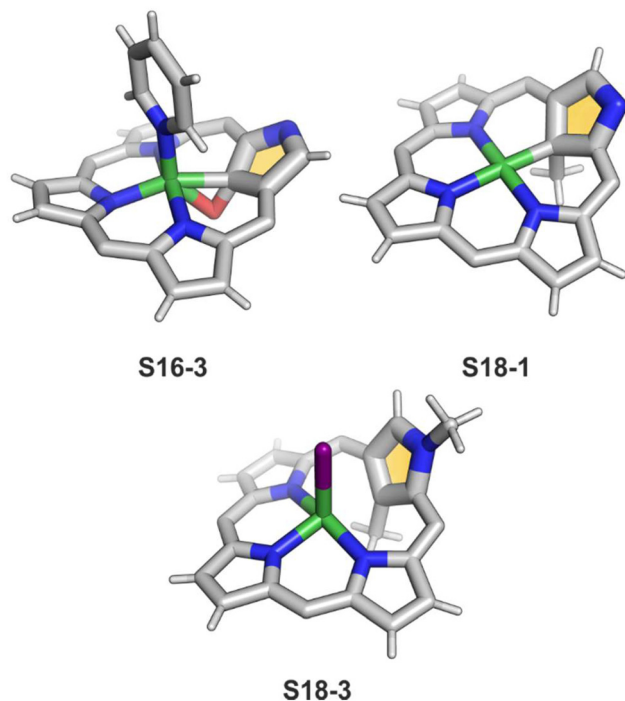


Fig. 4 Coordination motifs in nickel(II) NCP complexes. *meso*-Substituents not shown.

attached anionic ligand.<sup>83</sup> The [CNNN] coordination remains undisrupted.

A different oxidation product can be obtained in a reaction of **S16-1** and  $\text{OsO}_4$ .<sup>84</sup> During the reaction, an oxygen atom is transferred onto the C(21) atom (**S16-3**). As confirmed by the X-ray structure (Fig. 4), organometallic bonding is still in place being indicated by a short C(21)–Ni distance of 2.069(4) Å. In the course of this process, the one-electron oxidation of nickel(II) takes place, and the charge is balanced by O(21) coordination in its phenolic state (C(21)–O(21) distance equals 1.377(5) Å). The nickel(III) coordination sphere is supplemented by pyridine used in the reaction. A very interesting transformation is enabled by the: (I) initial internal C–H activation by a nickel(II) ion, (II) adjustable coordination properties of the NCP macrocycle, *i.e.*, the possibility of nickel(III) stabilisation, (III) close proximity to the metal centre and the carbon fragment. The same molecular motif is obtained after nickel(II) is inserted into 3-ethoxy NCP and then exposed to air.<sup>85</sup> As the primarily formed nickel(II) 3-ethoxy NCP complex **S17-1** (Scheme 17) is

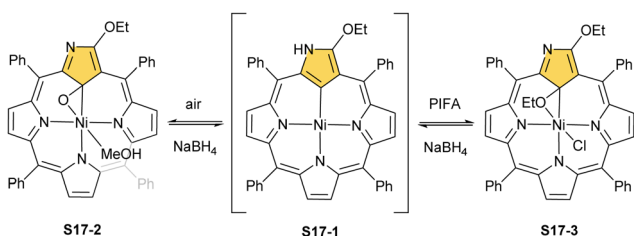
unstable, transformation leads to a 3-ethoxy complex **S17-2**. The oxidation of the nickel(II) centre with [bis(trifluoroacetoxy)-iodo]benzene (PIFA) conducted in the presence of ethanol leads to the incorporation of an additional ethoxy substituent at the C(21) position. This complex **S17-3** bears additional chloride at the nickel(III) centre, which also interacts with the inner ethoxy group as indicated by a Ni–O(21) contact of 2.331(3) Å. The Ni–C(21) distance is 2.065(3) Å. Both inner oxide (in **S17-2**) and ethoxide (in **S17-3**) can be removed in a reversible reduction using  $\text{NaBH}_4$ , leading to the starting nickel(II) complex **S17-1**. This study points to differences in reactivity induced just by adding a 3-ethoxy substituent. In other studies, when nickel(II) NCP (**S16-1**) is exposed to azo radical initiators, like 2,2'-azobis(2-methylpropionitrile) (AIBN) and dimethyl 2,2'-azobis(2-methylpropionate), the isolated product contains the new C(21) substituent originating evidently from the azo-source.<sup>86</sup> In the case of AIBN, it is a CN group (**S16-4**) and, for the second one, an ester moiety (**S16-5**).

As the final complex is diamagnetic, square-planar nickel(II) is expected. Thus, a C(21)–Ni bond must remain intact for the charge balance. The transformation involves a nickel(III) N-confused porphyrin intermediate, which eventually coordinates the generated radical. Then, an  $\text{R}_1$  substituent is transferred onto C(21) with the cleavage of either the C–CN or the C–COOMe bond and reductive elimination of a remaining carbon fragment from the metal centre. After demetallation, free 21-substituted porphyrins can be obtained. The coordination sphere flexibility of nickel has its limitation. After the reaction of **S16-1** and 2-mercaptopyridine, the C(21)–S bond is formed, but the complex is demetallated at the same time (**S16-6**), in contrast to cobalt(II) and ruthenium(II) chemistry (see below).<sup>33</sup> Substitution at the activated C(21) position will be a frequent motif reported throughout this review.

Another example of **S16-1** reactivity is regioselective methylation which occurs upon mixing with methyl iodide.<sup>87</sup> Firstly, a methyl group is attached at the C(21) position forming diamagnetic nickel(II) 21-methyl N-confused porphyrin **S18-1** (Scheme 18). The reversible concerted addition of HX converts diamagnetic **S18-1** into paramagnetic **S18-2**. In contrast, it was proposed that nickel(II)  $\beta$ -alkylated NCP **S19-1** (Scheme 19) undergoes the protonation of the internal, coordinated C(21) atom after adding TFA affording aromatic **S19-2**.<sup>88</sup> Similarly, reversible C-protonation is observed in the case of *N*-methylated NCP.<sup>89</sup>

The methylation of **S16-1** at the C(21) position may also be followed by the reaction at the peripheral N(2) atom to afford the paramagnetic dimethylated derivative nickel(II) 2,21-dimethyl NCP (**S18-3**). The reaction route does not include the alternative path, namely the peripheral methylation to form diamagnetic nickel(II) 2-Me NCP like **S19-1**. However, the treatment of **S19-1** with methyl iodide results in the methylation of the C(21) position.

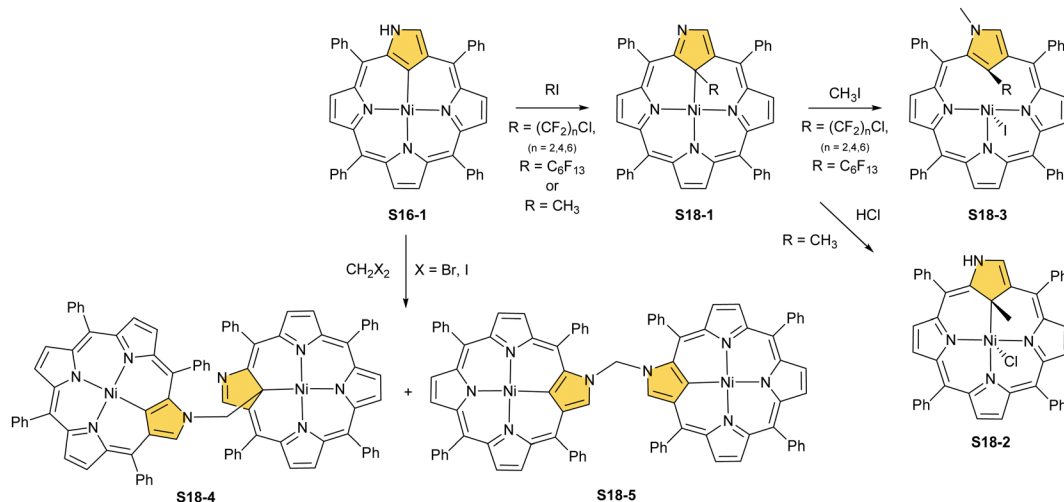
In contrast to methylation with methyl iodide, perfluoroalkyl iodides react selectively at the C(21) position of **S16-1**.<sup>90</sup> The molecular structures of **S18-1** and **S18-3** were determined by X-ray crystallography (Fig. 4). The Ni–C(21) bond length in



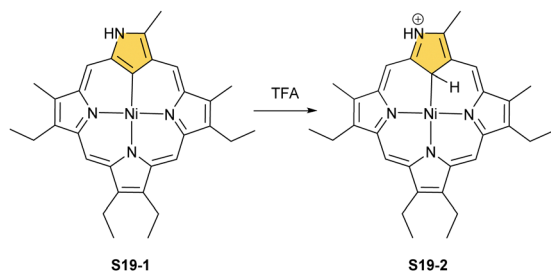
Scheme 17 Reactivity of nickel(II) 3-ethoxy N-confused porphyrin **S17-1**.



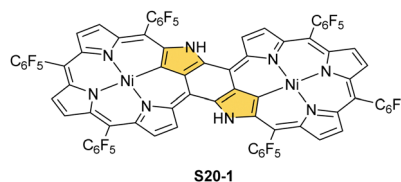




Scheme 18 Regioselective alkylation of nickel(II) N-confused porphyrin **S16-1**.



Scheme 19 Protonation of nickel(II)  $\beta$ -alkylated N-confused porphyrin **S19-1**.



Scheme 20 Nickel(II) NCP dimer **S20-1**.

**S18-1** (2.005(6) Å) indicates direct bonding to the clearly  $sp^3$ -hybridised carbon atom. The structure of **S18-3**, with iodide attached to nickel(II), gives a longer distance (2.406(9) Å) corresponding to the strong  $Ni \cdots C(21)$  interaction enforced by macrocyclic constraints, leaving  $C(sp^2)$  substituted with the methyl group.

An application of substrates with more halide atoms attached can promote the formation of covalently linked dimers. Such a reaction was reported with dihalomethanes as the precursors of bridging units. The representative treatment of **S16-1** with dihalomethanes in the presence of a base afforded preferentially the dimer **S18-4**.<sup>91</sup> Overwhelming majority of the product (even above 90%) acquired the  $N(2)-C(21)'$   $CH_2$  linkage (**S18-4**). The only other dimeric product identified is **S18-5** with the  $N(2)-CH_2-N(2)'$  bridge.

Coordination with nickel(II) may induce the formation of a strapped NCP dimer complex **S20-1** (Scheme 20) when starting from 3,7,23,27-tetrabromo[36]octaphyrin bearing two unsubstituted *meso* positions.<sup>92</sup> It was suggested that the initial  $Ni^{II}$  complexation occurs in two NNNC pseudo-cavities ( $Ni-C$ : 1.885(4) Å; Fig. 5). It imposes proximity between positions 5,27 and 7,25, leading to a fusion reaction and bromides leaving positions 7 and 27. This step is followed by debromination at the perimeter. The whole molecule exhibits weak paratropic features due to the domination of the  $36\pi$ -electron ring current.

Two other metals accompanying nickel in the 10th group, *i.e.*, palladium and platinum, efficiently react with NCP.

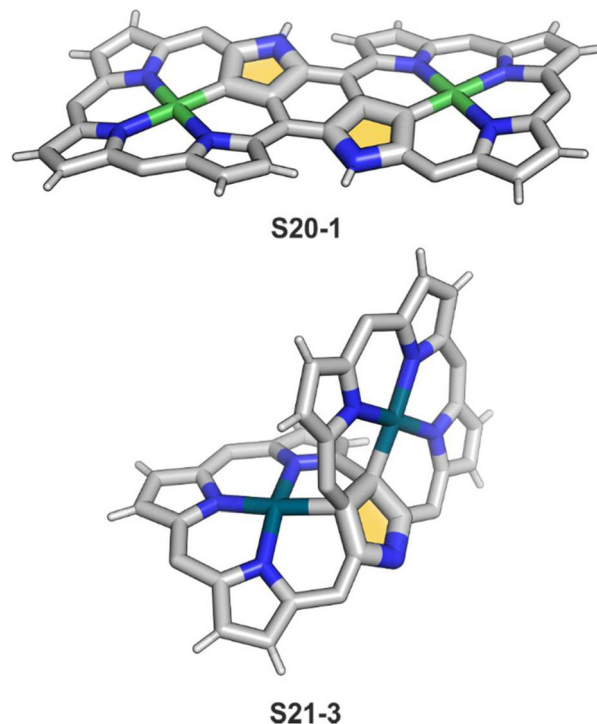
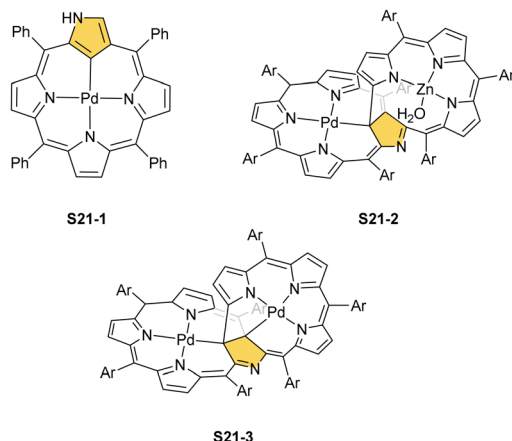


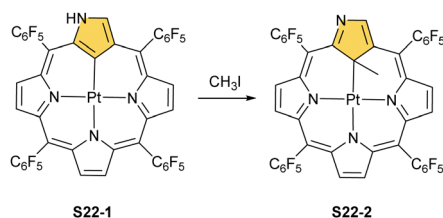
Fig. 5 Bis-N-confused porphyrin skeletons formed after expanded porphyrin coordination. *meso*-Substituents not shown.

A simple insertion of palladium(II) into NCP using palladium(II) acetate in boiling chloroform affords a regular





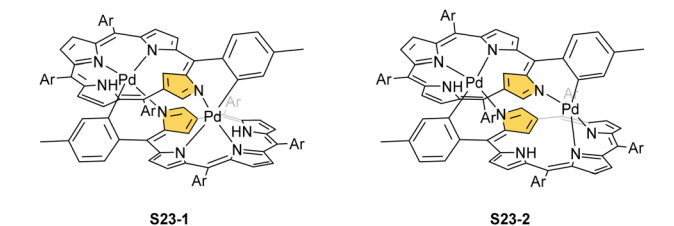
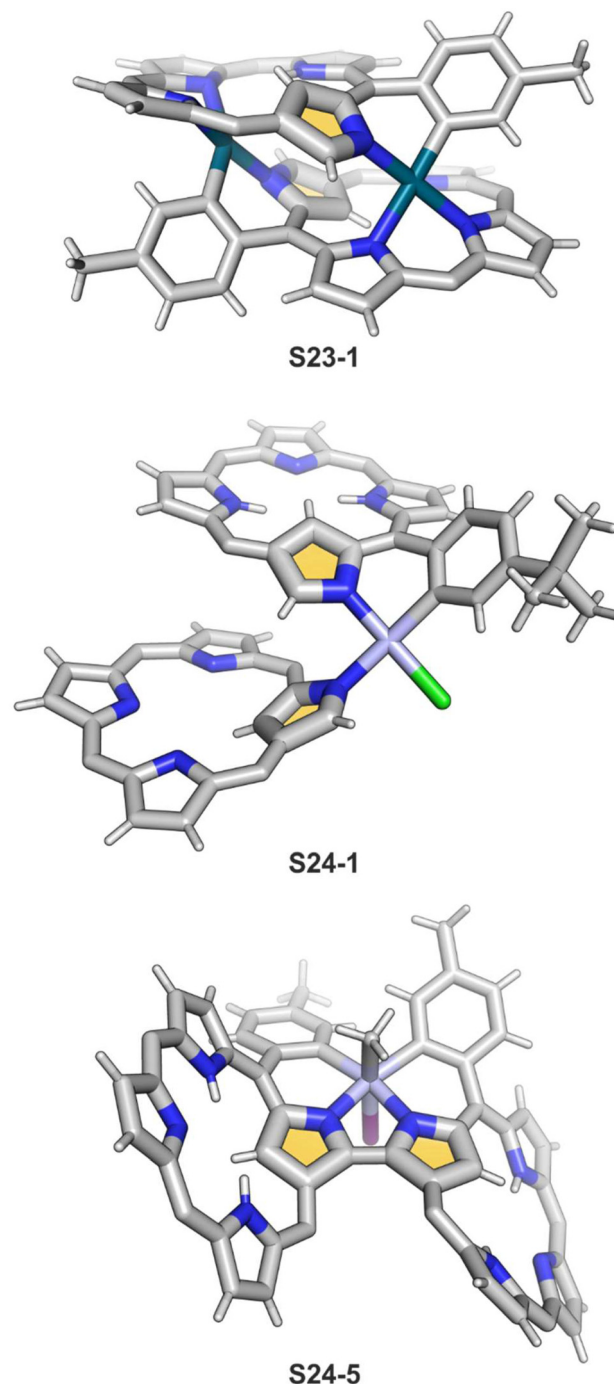
Scheme 21 Palladium(II) complexes of N-confused porphyrin derivatives.

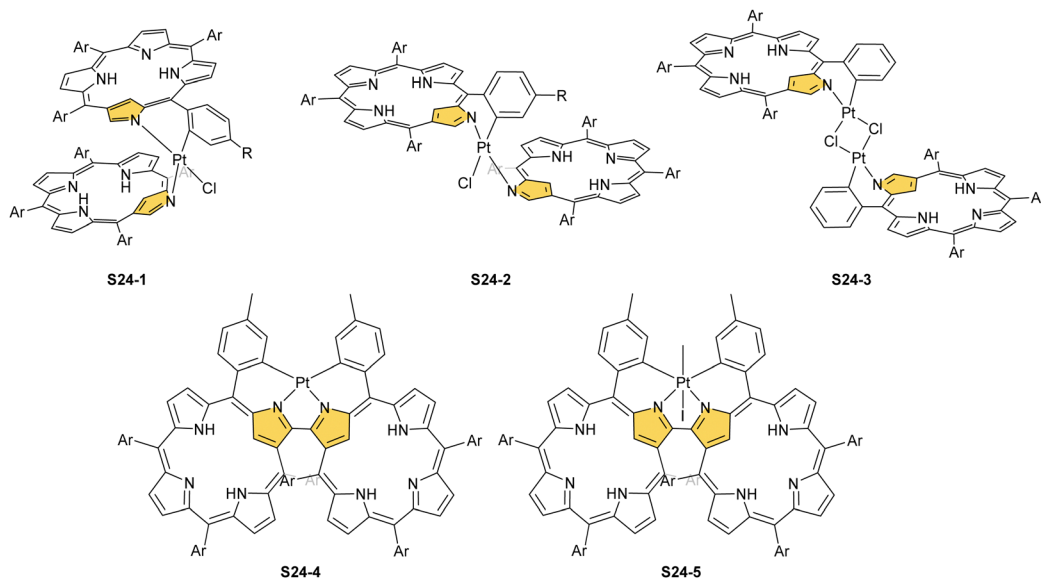
Scheme 22 Regioselective methylation of platinum(II) N-confused porphyrin **S22-1**.

square-planar complex **S21-1** (Scheme 21),<sup>93</sup> analogous to the nickel(II) complex **S16-1**.

Platinum(II) NCP **S22-1** (Scheme 22) is formed efficiently in a reaction of  $[\text{PtCl}_2(\text{MeCN})_2]$  and NCP with perfluorinated *meso*-phenyls ( $-\text{C}_6\text{F}_5$ ) in boiling 1,2-dichlorobenzene.<sup>94</sup> This complex undergoes swift regioselective methylation on the activated C(21) atom (**S22-2**) like the nickel analogue does. Interestingly, a C(3),C(21)-disubstituted complex of palladium(II) can be obtained in an unexpected transformation using [32]heptaphyrin and palladium acetate at room temperature.<sup>95</sup> Initially, in the course of the insertion, palladium(II) is accommodated into a [CNNN] surrounding. The structure of formed intermediary species promoted the profound heptaphyrin bond rearrangement affording a peculiar architecture **S21-2** with the readily identified moiety based on the skeleton of 3,21-disubstituted NCP. A more prolonged reaction with a 20 eq. excess of  $\text{Pd}(\text{OAc})_2$  leads to interesting dipalladium(II) species **S21-3** (Fig. 5).

In fact, the outcome of the regular palladium(II) or platinum(II) insertion depends enormously on the choice of conditions. As already mentioned, the insertion of palladium(II) under mild conditions afforded regular palladium(II) NCP **S21-1**. Two additional products, **S23-1** (Scheme 23) and **S23-2**, were identified once boiling toluene was used as a solvent.<sup>93</sup> As one can see, the presence of outer N(2) facilitates the formation of isomeric  $\text{Pd}_2\text{L}_2$  dimers, in which each palladium(II) ion coordinates two core nitrogen atoms of one NCP subunit and the outer N(2) atom from the second subunit (Fig. 6). This geometry brings palladium(II) close to a proximal *meso*-aryl

Scheme 23 *meso*-Aryl-coordinated palladium(II) NCP-based complexes.Fig. 6 *meso*-Aryl-coordinated NCP-based complexes. Other *meso*-substituents not shown.



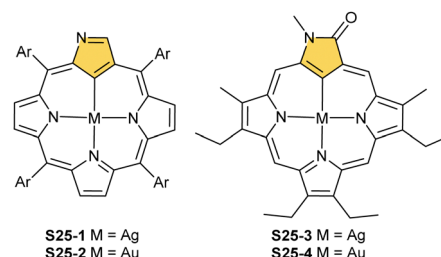
Scheme 24 *meso*-Aryl-coordinated platinum(II)/IV NCP-based complexes.

substituent. The proximity of palladium(II) and the *ortho*-CH fragment seems to be instrumental in activating the  $C_{ortho}$ -H bond and eventually forming the palladium(II)- $C_{ortho}$  bond.

The insertion of platinum(II) (0.5 eq.  $PtCl_2$ ) into NCP, carried out in boiling toluene, affords the diporphyrinic species  $[PtCl(NCP)_2]$  **S24-1** (Scheme 24) and **S24-2**.<sup>96</sup> Two NCP subunits are solely linked *via* perimeter N(2), N(2)', and  $C_{ortho}$  donors coordinated to a single platinum(II) cation. The fourth coordination site is occupied by chloride. The *cis* vs. *trans* location of  $C_{ortho}$  and Cl is responsible for forming two isomers, with **S24-1** (*cis*) existing as a major product (Fig. 6). In the specific structures **S24-1** and **S24-2**, both the cavities of NCP subunits remain unoccupied, potentially leaving some room for the accommodation of other metal cations to form composite trimetallic species. The reaction outcome changes quite drastically when 1 eq. of platinum(II) chloride is used. The regular platinum(II) NCP and the diporphyrinic species  $[PtCl(NCP)_2]$  **S24-1** and **S24-2** can be detected but as minor side-products. The major product  $[PtCl(NCP)]_2$  forms as a dimeric and symmetric structure **S24-3** in which two chloride ligands bridge the subunits.

The preorganised environment of a covalently linked NCP C(3)-C(3') dimer **S6-1** enforces the specific external coordination to a platinum ion.<sup>97</sup> Two proximal N(2) and N(2') atoms and two adjacent  $C_{ortho}$  positions participate in platinum(II) coordination, providing an external CCNN environment (**S24-4**). The NCP cores remain available for further coordination. When treated with methyl iodide, the platinum(II) centre of **S24-4** undergoes oxidative addition yielding the platinum(IV) complex with equatorial ( $Pt^{IV}$ - $C_{ortho}$ ) and axial ( $Pt^{IV}$ -CH<sub>3</sub>) organometallic bonding (**S24-5**; Fig. 6).

**Cu, Ag, and Au.** Interesting organometallic chemistry was reported for group 11 metals: copper, silver, and gold. In contrast to palladium, platinum, and even nickel, for which the N-confused porphyrin seems to accommodate metal(II)



Scheme 25 Silver(III) and gold(III) complexes of N-confused porphyrin and its derivative.

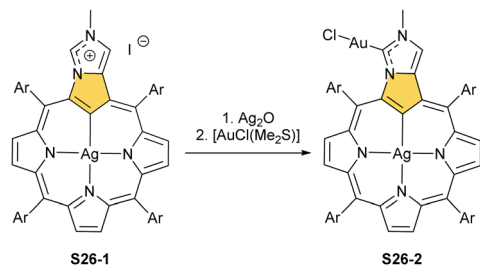
cations preferentially, the coordination of a metal(III) cation seems to be favoured for group 11 metals. The reaction of N-confused porphyrin and  $Ag(CF_3COO)$  affords silver(III) NCP with the silver cation located in the square-planar [CCNN] surrounding **S25-1** (Scheme 25).<sup>98</sup>

Thus, the dissociation of inner core protons of tautomer **S1-2** (two (N)H and one (C)H) generates a trianionic, aromatic macrocyclic ligand allowing the initial insertion of silver(I) to be followed by two-electron oxidation with an excess of silver(I). The metal centre can be removed through acidification.<sup>99</sup> Interestingly, when the complex is substituted with an ethoxy group at the C(3) position, demetallation is accompanied by the halogenation of the C(21) atom coming from the HX molecule.

The treatment of NCP with  $[AuCl(S(CH_3)_2)_2]$  in refluxing toluene yields small amounts of gold(III) NCP **S25-2**, with the source adopting the same roles (insertion and oxidising reagent).<sup>100</sup> Remarkably, N-fused porphyrin **S10-4** is mainly produced while using regular NCP. Before complexation, C(21) bromination must be performed to obtain **S25-2** efficiently. The reaction of activated 21-Br NCP (**S10-3**) and  $[AuCl(S(CH_3)_2)_2]$  provides desired **S25-2**. The organometallic contact of 2.016(12) Å clearly points to direct bonding.







Scheme 26 Gold-carbene coordination at the periphery of silver(III) imidazole-fused NCP **S26-1**.

One can form a bimetallic species by using imidazole-fused NCP **S5-1**.<sup>59</sup> In the first step, the silver(III) imidazole-fused NCP is formed. Subsequently, the methylation with methyl iodide yields cationic species **S26-1** (Scheme 26), in which the methyl group is attached to the outer nitrogen atom. **S26-1** reacted with  $\text{Ag}_2\text{O}$  acquires the initial N-heterocyclic carbene functionality. The following metallation with  $[\text{AuCl}(\text{S}(\text{CH}_3)_2)]$  affords a  $\text{Ag}^{\text{III}}/\text{Au}^{\text{I}}$  hybrid **S26-2** (Fig. 7). The insertions of silver and gold to N(2)-methyl ( $\beta$ -substituted) N-confused porphyrin were probed as well.<sup>89</sup> The inner core of N(2)-methyl N-confused porphyrin **S3-3** contains only two dissociable hydrogen atoms (NH and C(21)H); the frame of tautomer **S3-1** and, as predictable, tends to promote the stabilisation of metal(II) cations. Consequently, the silver(III) or gold(III) insertions have been accompanied by oxygenation at position C(3) to form the lactam units of **S25-3** and **S25-4**.

When silver(III) NCP **S25-1** reacts with  $\text{KPPH}_2$ , it gives C(21) substitution regioselectively with diphenylphosphine (**S27-1**, Scheme 27).<sup>64</sup> At the same time, the macrocycle gets demetallated, probably due to the difficulties of a new form in stabilising  $\text{Ag}^{\text{III}}$ . The substituent can be oxidised to a diphenylphosphoryl form. The interesting fact is that the C(21)–P bond is cleaved after the reinsertion of silver [from  $\text{Ag}(\text{CF}_3\text{COO})$ ], meaning one returns to starting **S25-1**. Another example is a reaction with dimethylamine.<sup>101</sup> After C(21) substitution with  $-\text{N}(\text{CH}_3)_2$ , the silver ion leaves the molecule. It was also shown that the outer N(2)=C(3) bond in the silver(III) complex might act as an electrophilic site, and alcohol addition to the C(3) position is possible.<sup>102</sup> Silver(I) trifluoroacetate-catalysed transformation yields a methoxy substituent after a reaction with ethanol and, per analogy, with different alcohols.

An interesting transformation is induced when **S25-1** reacts with methyl iodide and lithium hydroxide in THF.<sup>103</sup> N(2) and N(22) get methylated, which is associated with the silver(III) centre removal. More importantly, the bond between the C(3) and C(4) atoms breaks, leaving the C(3) atom oxidised in a formyl functionality held merely by the N(2)–C(3) bond. The formed **S27-2** remains cyclised with C(21) and C(4) atoms forming a triple bond. The so-called porphyrin remains aromatic with a  $-3.89$  ppm chemical shift for the N(22) methyl group. Nickel(II) NCP and the free ligand did not exhibit the same type of reactivity.

Finally, the insertion of silver into C(3),C(3)'-dimer **S6-2** using  $\text{Ag}(\text{CF}_3\text{SO}_3)$  results in unprecedented species.<sup>104</sup> Besides

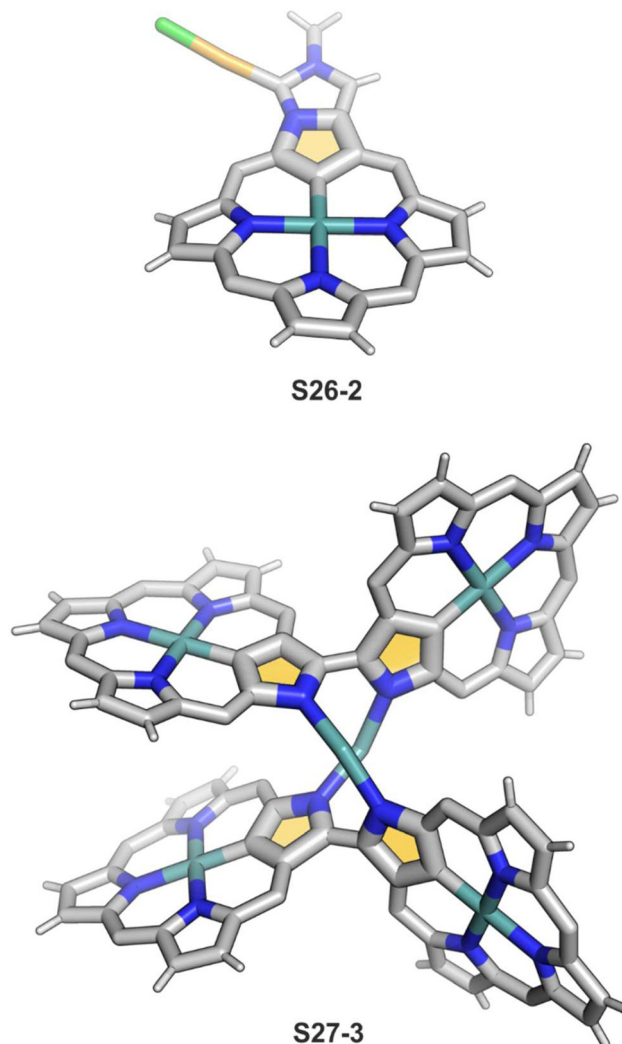


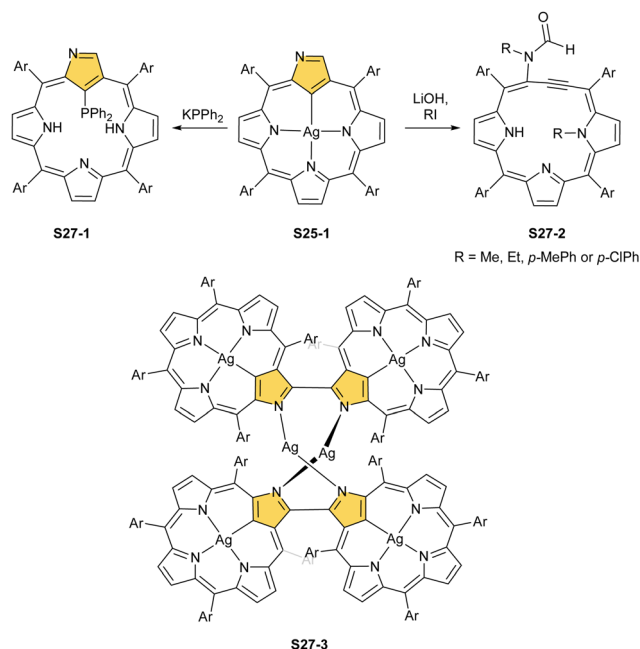
Fig. 7 Specific silver(III) NCP coordination motifs. *meso*-Substituents not shown.

the regular silver(III) insertion (two cavities of **S6-2** occupied by the metal ions), the outer N(2) atom coordination is instrumental and shown in “the dimer of dimers” ensemble **S27-3**. Two perimetral silver(I) cations coordinate linearly two N(2) nitrogen atoms from the different dimeric subunits (Fig. 7). The cationic charge of **S27-3** is balanced by two nonbonding counterions forming the  $[\text{Ag}_4^{\text{III}}\text{Ag}_2^{\text{I}}\text{L}_2]$  complex eventually.

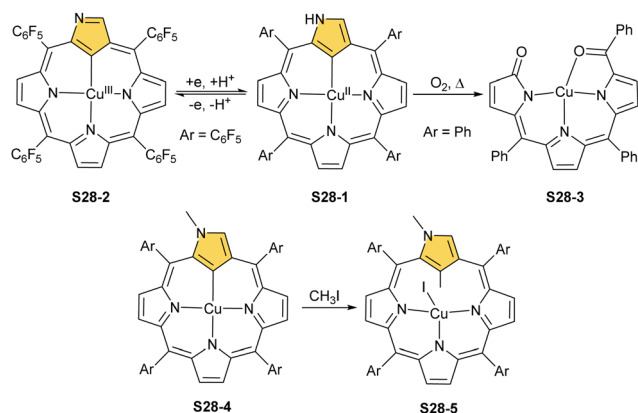
The third metal completing the discussed coinage group, *i.e.*, copper, is known for forming organometallic compounds adopting three fundamental oxidation states, *i.e.*, copper(I), copper(II), and copper(III). Thus, its organometallic chemistry in the NCP environment varies significantly once related to the heavier counterparts – silver and gold.

The reaction of copper(II) acetate and NCP under mild conditions (inert atmosphere, THF, 298 K) results in the formation of paramagnetic square-planar copper(II) N-confused porphyrin **S28-1** (Scheme 28) belonging to the small group of organocopper(II) species.<sup>105</sup> The stabilisation of the copper(II) centre implies that the ligand frame acquires the



Scheme 27 Reactivity of silver(III) N-confused porphyrin **S25-1**.

geometry of tautomer **S3-1** and N(2) nitrogen is protonated. Accordingly, 2-Me NCP **S3-3**, having already the appropriately prearranged molecular structure, readily coordinates to copper(II) to form **S28-4**. Protonation (HCl) or methylation ( $\text{CH}_3\text{I}$ ) of **S28-1** occurs at the initially activated C(21) centre and is followed by the axial coordination of accompanying anions. Thus, in the case of **S28-4**, already N(2)-methylated, the inner core methylation at C(21) was detected, eventually generating copper(II) 2,21-dimethyl NCP **S28-5**. The reactive organometallic copper(II) NCP complexes (**S28-1** and **S28-4**) gain additional stabilisation once perfluorophenyl substituents are located at *meso* positions.<sup>106</sup> Such a complex (**S28-1**) was shown to undergo a swift and reversible one-electron metal-centred oxidation with DDQ to form diamagnetic square-planar copper(III) (**S28-2**).<sup>25</sup> This is facilitated by switching to the 3H tautomer of NCP. On the other hand, the alternative insertion

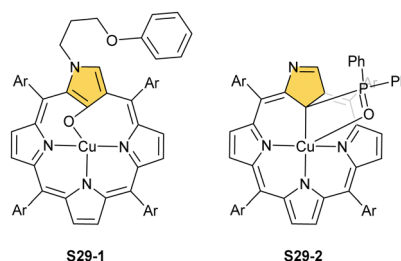
Scheme 28 Reactivity of copper(II) N-confused porphyrin **S28-1**.

procedure ( $\text{Cu}(\text{OAc})_2$ , NCP, reflux in toluene,  $\text{O}_2$ ) provides harsh conditions that result in controlled degradation.

Oxygenolysis of **S28-1** includes cleavage of C–C bonds adjacent to the N-confused pyrrolic ring and eventually, this sub-unit linked to one *meso* phenyl is extruded from the framework.<sup>107</sup> The remaining tripyrrinone-like fragment of **S28-3** incorporates C(6) and C(20) carbon atoms of starting NCP, albeit transformed into the carbonyl units. In fact, the degradation proceeds regioselectively and introduces a larger structural transformation than the photooxidation of a free macrocycle.<sup>108,109</sup> The tripyrrinone derivative conserves the coordination to copper(II), completing the fourth coordination site with the terminal C(20)–carbonyl oxygen atom. Oxygenation of copper(II) N(2)-methyl NCP **S28-4** under milder conditions (reflux in a mixture of chloroform and acetonitrile,  $\text{O}_2$ ) results in an insertion of an oxygen atom into the Cu–C(21) bond affording copper(II) oxo-NCP (or 21-hydroxy NCP) **S29-1** (Scheme 29).<sup>110</sup>

The  $\text{Cu}^{\text{II}}\text{--C}(21)$  distance increases to 2.530(3) Å, consistent with the side-on  $\eta^1$ -type interaction. On the other hand, the regular  $\text{Cu}^{\text{II}}\text{--O}$  bond has been encountered ( $\text{Cu}\text{--O}(21)$  1.900(2) Å). The  $\text{O}(21)\text{--C}(21)$  distance is relatively short (1.307(4) Å) but longer than the typical bond length of the regular carbonyl group. One can conclude that, in **S29-1**, the ligand preserves features of 21-hydroxy NCP. Finally, there is an example of copper(II) insertion into C(21)-substituted NCP. A diphenylphosphoryl functionalised porphyrin obtained in a reaction of  $[\text{Ag}^{\text{III}}(\text{NCP})]$ ,  $\text{KPPH}_2$  was used.<sup>111</sup> The insertion occurs under mild conditions and, in contrast to silver, a metal complex with C(21) substitution is formed (**S29-2**). The C(21) atom gets rehybridised to  $\text{sp}^3$  and the  $\text{Cu}^{\text{II}}\text{--C}(21)$  contact is in a bonding range (2.154(3) Å; Fig. 8). The phosphoryl oxygen atom is located at the centre of porphyrin and forms an axial bond yielding a square pyramid coordination mode.

**Co, Rh, and Ir.** Inserting cobalt into N-confused porphyrins creates a highly versatile and reactive coordination centre. Two oxidation states, *i.e.*, cobalt(II) and cobalt(III), can be stabilised in the [CNNN] coordination sphere. Cobalt insertion from  $[\text{Co}_2(\text{CO})_8]$  (but also chloride<sup>112</sup> and perchlorate<sup>113</sup>) into either free or N(2)-locked NCP produces cobalt(II) NCP (**S30-1**, Scheme 30).<sup>56,114</sup> The recrystallization from pyridine affords the square pyramidal structure with pyridine in the axial position of **S30-2**. The  $\text{Co}\text{--C}(21)$  distance (1.938(2) Å) reflects the existence of the regular  $\text{Co}^{\text{II}}\text{--C}$  bond. The reaction



Scheme 29 Copper(II) complexes of N-confused porphyrin derivatives.



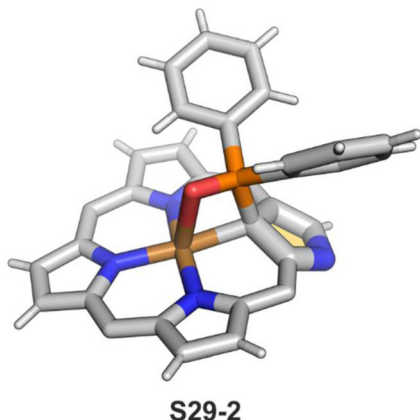
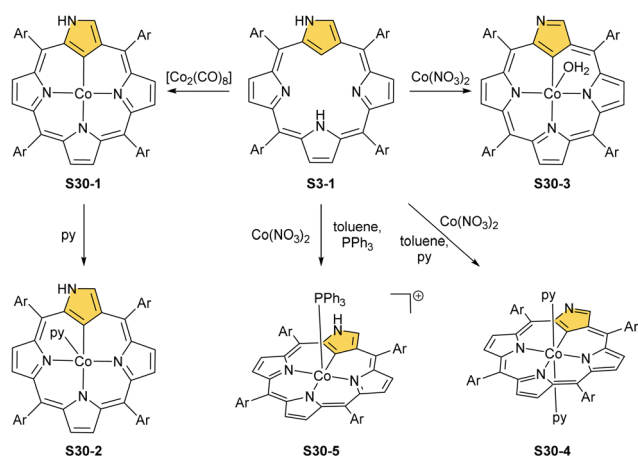


Fig. 8 Copper(II) organometallic complex with C(21)-substituted NCP. *meso*-Substituents not shown.



Scheme 30 Cobalt(II) insertion into N-confused porphyrin **S3-1**.

of NCP with  $\text{Co}(\text{NO}_3)_2$  results in cobalt(III) N-confused porphyrin containing the trianionic equatorial macrocyclic ligand.<sup>115</sup> The axial site is occupied by a water molecule (**S30-3**). The product is not particularly stable when exposed to air. Additions of pyridine convert **S30-3** into a six-coordinate species with two axial pyridine ligands replacing water (**S30-4**). The difference in oxidation states in **S30-2** and **S30-4** is markedly reflected in the alteration of  $\text{Co}-\text{N}_{\text{py}}$  bond lengths. The  $\text{Co}-\text{N}_{\text{py}}$

distance equals 1.983(3) Å for diamagnetic **S30-4**, whereas for the high-spin cobalt(II) complex **S30-2**, the essential elongation to 2.162(2) Å was determined, reflecting the contribution of the half-filled  $d_{z^2}$  orbital in bonding. The stable cobalt(III) five-coordinate complex **S30-5** forms in the presence of triphenylphosphine as well. In this case, despite cobalt(III) stabilisation, a dianionic macrocyclic form is preferred rendering cationic **S30-5**. The  $\text{Co}^{\text{III}}-\text{C}(21)$  distance equals 1.903(5) Å.

The cobalt(II) NCP **S30-1** reacts with nitric oxide, which effectively binds as the fifth axial ligand.<sup>112</sup> In this process, carried out in dichloromethane solution, a peculiar transformation occurs. The complex activates two solvent molecules and forms a C(21) 2-chlorovinyl substitution (**S31-1**, Scheme 31).

The organometallic bond is preserved as illustrated by the  $\text{Co}-\text{C}(21)$  distance (2.046(5) Å); thus, C(21) becomes tetragonal (Fig. 9), and the electronic state of the centre is  $\{\text{Co}(\text{NO})\}^8$ . Prolonged NO bubbling through solutions of **S30-1** and **S31-1** results in oxygen atom insertion into the  $\text{Co}-\text{C}(21)$  bond of **S30-1** associated, however, for **S31-1** with the extrusion of a 2-chlorovinyl substituent. It was suggested that the incorporated

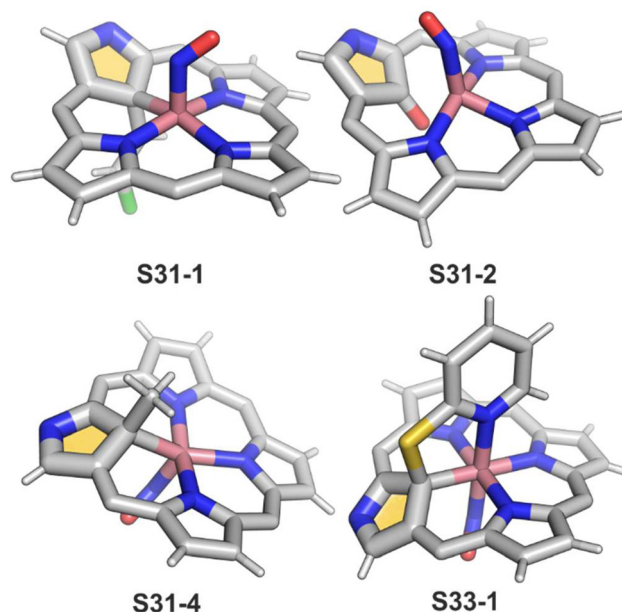
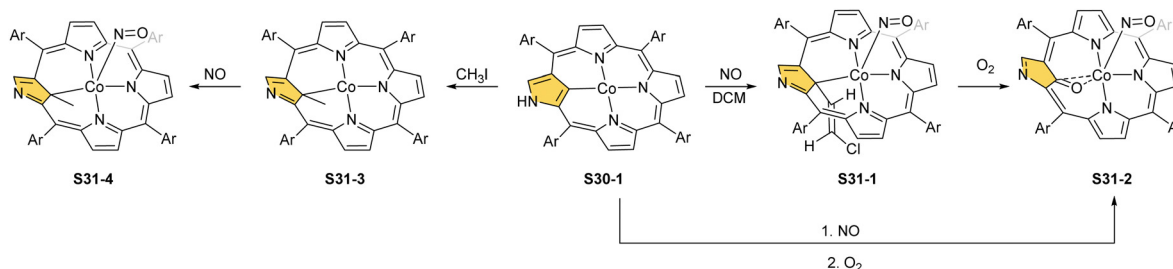


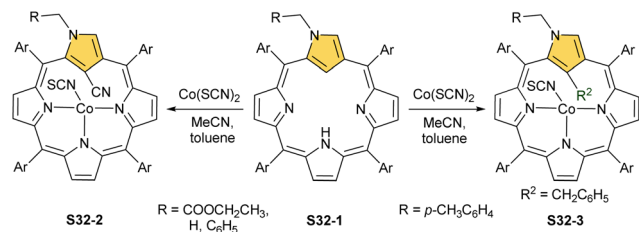
Fig. 9 Cobalt-coordinated NCP derivatives. *meso*-Substituents not shown.



Scheme 31 Reactivity of cobalt(II) N-confused porphyrin **S30-1**.







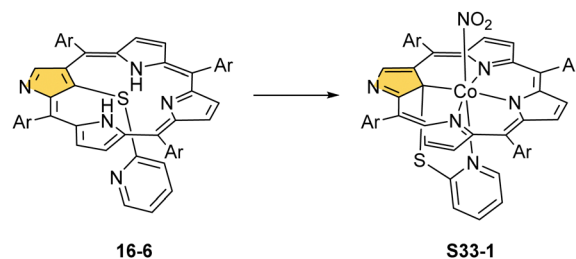
**Scheme 32** Cobalt(II) insertion into N(2)-substituted N-confused porphyrin **S32-1**.

oxygen atom came from NO contamination. The formed species (**S31-2**) can be characterised as a  $\{\text{Co}(\text{NO})\}^7$  electronic state. The C(21)–O(21) distance suggests a double bond (1.301(9) Å)  $\eta^2$ -interaction with the metal centre (Fig. 9). This is in line with Co–O(21) and Co–C(21) distances (2.051(5) and 2.175(8) Å, respectively). Treatment of **S30-1** with methyl iodide produces a C(21)-methylated complex **S31-3**, which reacts in the next step with NO, forming a structural analogue of **S31-1**, *i.e.*, **S31-4** (Fig. 9).<sup>116</sup> This  $\{\text{Co}(\text{NO})\}^8$  complex can be then reduced to a stable  $\{\text{Co}(\text{NO})\}^9$  anion using  $[\text{Co}(\text{Cp}^*)_2]$ .

The insertion of cobalt(II) into N(2)-substituted N-confused porphyrin **S32-1** (Scheme 32) using  $\text{Co}(\text{SCN})_2$  in a mixture of acetonitrile/toluene gives quite unexpected results, however, evidently controlled by the nature N(2) substitution.<sup>117</sup> The *p*-xylyl substitution connected through one of the aliphatic carbon atoms leads to a product with a cobalt(II) centre coordinating to three nitrogen atoms and supplemented with  $\text{SCN}^-$  for the charge balance. Thus, the inner C(21) atom links the benzyl moiety derived from toluene (**S32-3**). Switching N(2) substitution to methyl, benzyl, or ethoxycarbonylmethyl leads to C(21) cyanation (**S32-2**), assuming the cleavage of the former  $\text{SCN}^-$  anion assisted by a cobalt cation.

The Co–C(21) distances of **S32-2** and **S32-3** type species are in a range of 2.52–2.56 Å suggesting the effective side-on Co...C(21) interactions. Different charge distributions over C(21) caused by the N(2) substituents explain the identified differences in reactivity. When **S32-1** containing the ethoxycarbonylmethyl N(2) substituent is used but with another cobalt(II) source, namely  $\text{CoCl}_2$ , one can still obtain a C(21)-benzylated  $\text{Co}^{\text{II}}$  complex *via* toluene activation, the structural analogue of **S32-3** but with axially coordinated chloride.<sup>118,119</sup> These results clearly outline that moderately subtle molecular changes in N-confused porphyrin substitution and/or of reaction conditions may result in remarkably different outcomes pointing at the richness of chemistry conceivable to be induced. These results also suggest that, at first, the C(21)–H bond is activated by adjacent cobalt(II) firmly located *via* coordination with three nitrogen donors. Then, a vulnerable inner C(21) atom undergoes substitution. The order of actions may also be reversed. The already mentioned reaction of a nickel(II) regular complex of NCP with mercaptopyridine leads to the C(21) substitution and demetallation (**S16-6**).<sup>33</sup>

Prearranged macrocycle **S16-6** can be remetalated with cobalt(II) (reflux of **S16-6** and  $\text{Co}(\text{NO}_3)_2$  in THF) to the transient cobalt(II) complex. The subsequent one-electron oxidation



**Scheme 33** Preparation of cobalt(III) 21-substituted N-confused porphyrin **S33-1**.

produces six-coordinate cobalt(III) 21-substituted N-confused porphyrin **S33-1** (Scheme 33) with a direct organometallic bond to an  $\text{sp}^3$ -hybridised C(21) atom (Co–C(21): 2.022(4) Å, Fig. 9). The axial coordination is supplemented with a nitrogen atom from attached pyridine accompanied by the *trans*-located nitrite-N anion as the sixth ligand. Alternatively, **S33-1** can be directly formed starting from cobalt(II) insertion into NCP in the presence of mercaptopyridine. Mechanistically, the process naturally involves activating the C(21)H unit, which precedes the formation of **S33-1**.

In contrast to cobalt, the heavier elements of group 9 of the periodic table, *i.e.*, rhodium and iridium, demonstrated a preference for metal(I) and metal(III) oxidation states in NCP environments.

A product formed by reacting NCP and  $[\text{RhCl}(\text{CO})_2]_2$  (under relatively mild conditions of boiling dichloromethane) constitutes a bimetallic species (**S34-2**). None of the rhodium(I) cations managed to activate the internal C(21)–H bond; thus, one  $\text{Rh}^{\text{I}}$  centre is bound through N(22) and N(23) atoms and its coordination sphere is supplemented with two carbonyl groups (Fig. 10).<sup>120</sup> The other centre is attached through the external N(2) donor and the coordination is completed by two carbonyl groups and one chloride to balance the rhodium(I) charge. By using only 0.5 eq. of the dirhodium source, selective outer-only coordination can be achieved (**S34-1**, Scheme 34).<sup>121</sup>

In a similar trial, a reaction of 2 eq. of  $[\text{IrCl}(\text{CO})_2(\textit{p}$ -toluidine)] with NCP (in boiling toluene) gives two  $\text{Ir}(\text{CO})_2$  fragments coordinated to two nitrogen atoms each (**S34-6**).<sup>122</sup> In this case, a complex reminiscent of a dirhodium(I) complex with regular porphyrin<sup>120</sup> is obtained. Such a coordination mode means one ion coordinates to N(22) and N(23) and the other one to N(24) and N(2) (Fig. 10). Surprisingly, the inverted ring flips to facilitate coordination, but no N-fusion is observed. The structure is confirmed by X-ray crystallography and through the observation of chemical shifts for protons H(21) and H(3) in  $^1\text{H}$  NMR spectra. As the macrocycle preserves aromaticity, H(21) relocates from –5.01 ppm to 10.11 ppm. The complex is stable and the conversion to a regular form with Ir–C(21) is not observed.

However, for rhodium, one is able to obtain a regular complex with an organometallic bond when the metal centre gets oxidised.<sup>121,123</sup> Pyridine enables the oxidation of **S34-2** to form monorhodium(III) species **S34-3**. The outer  $\text{Rh}^{\text{I}}$  ion is removed and the macrocycle acts as a trianionic ligand



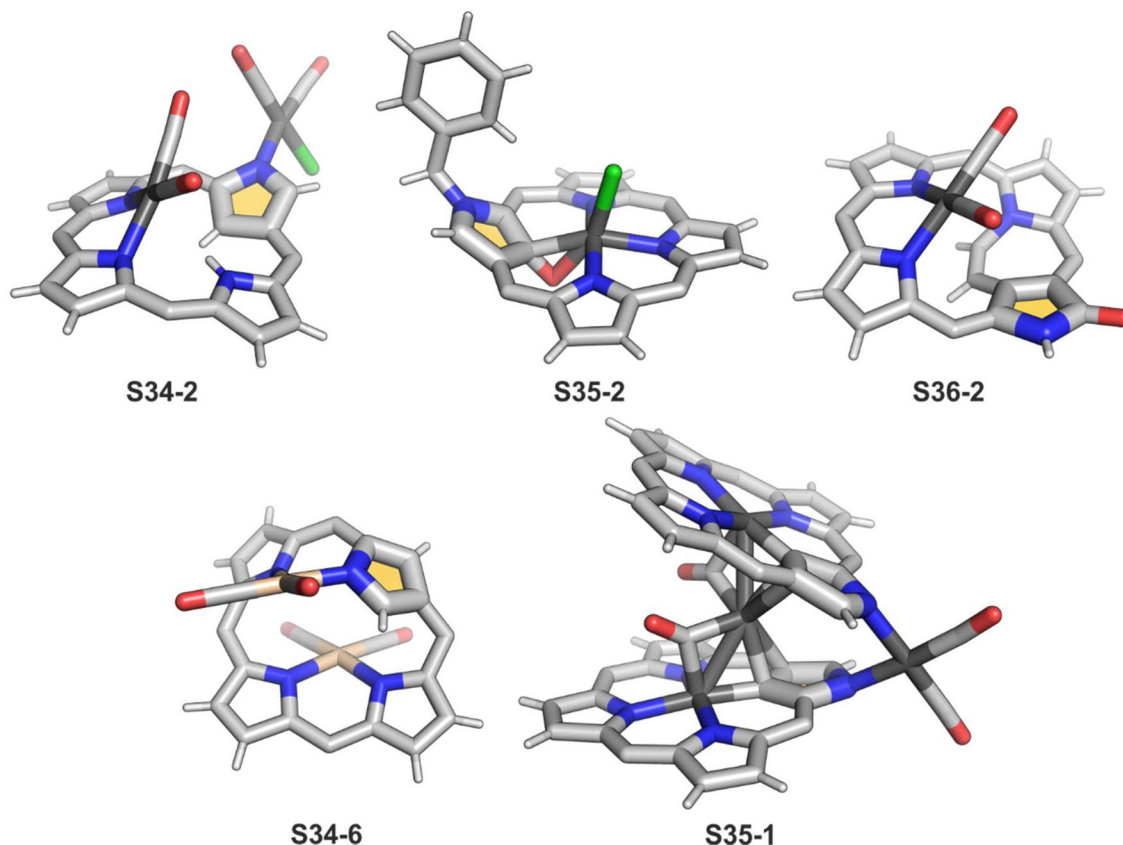
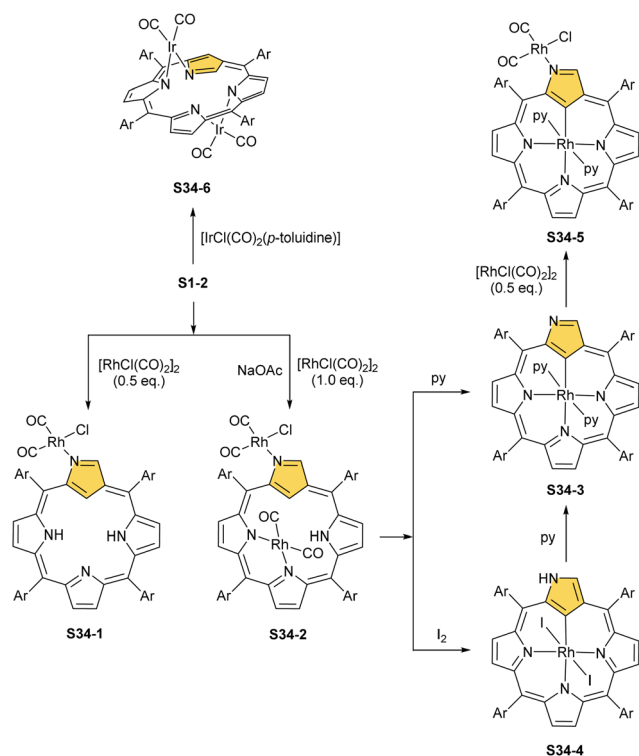


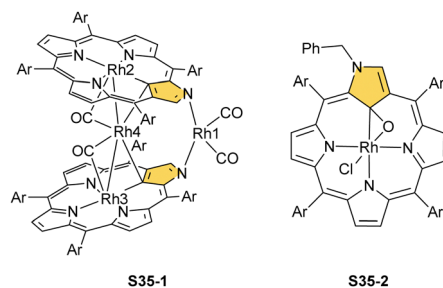
Fig. 10 Rhodium and iridium coordination motifs. *meso*-Substituents of NCP not shown.



Scheme 34 Iridium and rhodium N-confused porphyrin complexes.

stabilising rhodium(III) accompanied by two axial pyridines. It is possible to transform to the bimetallic species when an additional 0.5 eq. of the dirhodium(I) source is added to isolated **S34-3**. It forms a mixed rhodium(III)/(I) system **S34-5**. A situation looks different when iodine is added to the solution of **S34-2** at room temperature. The resulting complex becomes paramagnetic and possesses two axial iodide ligands, which suggests a rhodium(IV) centre (**S34-4**), while the porphyrin acts as a dianionic species. The reaction with pyridine initiates the reduction of the metal centre to rhodium(III) and yields diamagnetic **S34-3** as a consequence.

Another fascinating construction (**S35-1**, Scheme 35) is formed when  $[\text{RhCl}(\text{CO})_2]_2$  reacts with NCP in boiling toluene.<sup>124</sup> An identified  $[\text{Rh}_4(\text{NCP})_2(\text{CO})_4]$  complex is a dimer



Scheme 35 Rhodium complexes of N-confused porphyrin derivatives.



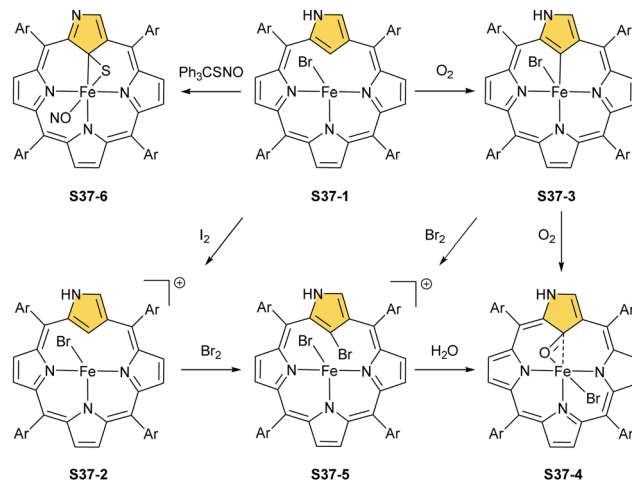
bridged through Rh coordination; thus, there are three coordination motifs (Fig. 10): (I) the Rh1 ion binds to both N(2) and N(2)' atoms introducing the stable N-confused porphyrin motif, (II) Rh2 and Rh4 cations inserted into C(21)NNN cores form the C(21)–Rh bonds, and (III) Rh3 with Rh2 and Rh4 (the Rh2...Rh3 distance is *ca.* 2.71 Å) afford an Rh<sub>3</sub> cluster. The rest of the coordination sphere is filled up by carbonyl groups but also the  $\eta^1$  interaction of Rh3 with C(21) and C(21)' atoms (2.262(5) and 2.214(5) Å). Only one isomer has been identified for **S35-1**. The total oxidation state of the multimetallic species must be fully stabilised by two trianionic macrocycles, as there are no counterions in the crystal lattice. Thus, a total of 6+ charge has to be distributed over four rhodium centres to yield a diamagnetic species.

A rhodium insertion in a boiling mixture of dichloromethane and acetonitrile into an N(2)-substituted NCP and without protection from oxygen results in a C(21) atom oxygenation in the final rhodium(III) complex (**S35-2**; Fig. 10).<sup>110</sup> The Rh–C and Rh–O distances indicate direct  $\eta^2$  bonding (Rh–C(21) 2.170(3) and Rh–O(21) 2.043(2) Å) with an internal carbonyl (C(21)–O(21) 1.330(4) Å), similarly to an oxygenated complex with cobalt (**S31-2**).

Eventually, the internally locked system **S11-3** was tested as a potential non-trivial molecular platform to accommodate rhodium(*n*).<sup>74</sup> A reaction of **S11-3** with [RhCl(CO)<sub>2</sub>]<sub>2</sub> yields a dirhodium(I) complex **S36-1** (Scheme 36), an analogue of **S34-2**. The double bond of the bridging ethene is preserved. The internally incorporated Rh(CO)<sub>2</sub> moiety, linked to two pyrrolic nitrogen atoms, is located at the opposite porphyrinic side with respect to the ethene bridge. Interestingly, after treatment with silica gel, **S36-1** transforms to **S36-2** *via* demethylation, forming a lactam moiety. This is accompanied by decooordination of an N(2)-attached centre (Fig. 10).

**Fe and Ru.** Iron porphyrin chemistry – very rich due to the biological importance of heme – provides the stimuli to explore the impact of the replacement of an [NNNN] inner coordination sphere by the organometallic [CNNN] arrangement of N-confused porphyrin.

Iron(II,III) NCP and their mono-, dimethylated, or C(21)O derivatives were characterised by <sup>1</sup>H and <sup>2</sup>H NMR spectra, revealing the typical isotropic shift patterns of paramagnetic iron porphyrins in given oxidation and spin states.<sup>125–127</sup> The high-spin bromoiron(II) NCP **S37-1** (Scheme 37) displays a distinctively large isotropic shift of the inner H(21) atom (812 ppm, 298 K), which indicates that an Fe<sup>II</sup>...C(21)–H

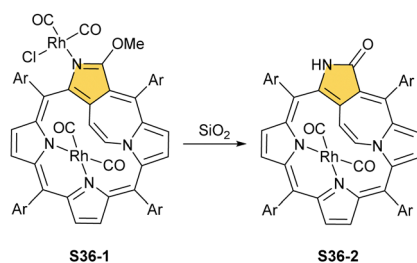


Scheme 37 Reactivity of iron(II) N-confused porphyrin **S37-1**.

agostic interaction also reflected in its molecular structure (Fig. 11).<sup>125</sup> In the case of C(21)-methylated NCP derivatives, the characteristic C–Me resonances occur in a unique window (420–520 ppm) for iron(III) C(21)-methylated NCP, which remains in contrast to relatively small values found for iron(II) C(21)-methylated NCP (50–80 ppm).<sup>127</sup>

Aside from important spectroscopic findings, organometallic chemistry was also intensively explored. Oxygen-sensitive high-spin iron(II) NCP **S37-1** is formed in a reaction of NCP with FeBr<sub>2</sub> heated in a mixture of MeCN/THF.<sup>128</sup> Iron(II) coordinates three inner nitrogen atoms and one axial bromide. The coordinated NCP is in its **S3-1** tautomeric form, having protonated N(2). The framework constraints result in the mentioned enforced equatorial agostic interactions with C(21)–H as confirmed by a close Fe...C(21) distance of 2.361(10) Å. A replacement of a bromide anion with a thiolate ligand in a reaction of **S37-1** and sodium 4-methylbenzenethiolate produces a structurally related compound with a comparable Fe...C(21) distance of 2.398(3) Å.

The treatment of **S37-1** with iodine causes the one-electron oxidation of iron(II) to produce iron(III) NCP **S37-2**. Iron(II) NCP **S37-1** exposed to dioxygen quickly transforms, at first, into five-coordinate intermediate-spin iron(III) NCP **S37-3**, creating a direct Fe–C(21)  $\sigma$ -bond (Fig. 11).<sup>126</sup> **S37-2** demonstrates sensitivity toward dioxygen as well. The further exposure of **S37-3** results in an oxygen atom insertion into the Fe–C(21) bond, forming high-spin iron(III) C(21)-oxygenated NCP **S37-4**, similarly as presented already for copper, cobalt, or rhodium NCPs. The bond distances (Fe–C(21) 2.199(7), Fe–O(21) 2.041(5), and C(21)–O(21) 1.299(7) Å) point at the iron(III)  $\eta^2$  interaction with the internal carbonyl group (Fig. 11). The addition of Br<sub>2</sub> to the solution containing **S37-2** or **S37-3** results in bromination at C(21), yielding **S37-5** in accord with typical N-confused porphyrin reactivity. The subsequent reaction with water finally results in forming the mentioned C(21)=O fragment (**S37-4**). The demetallation of **S37-4** with strong acid affords 21-hydroxy NCP.<sup>129</sup> The X-ray structure of the isolated free base is



Scheme 36 Rhodium(I) complexes of N-confused porphyrin derivatives.



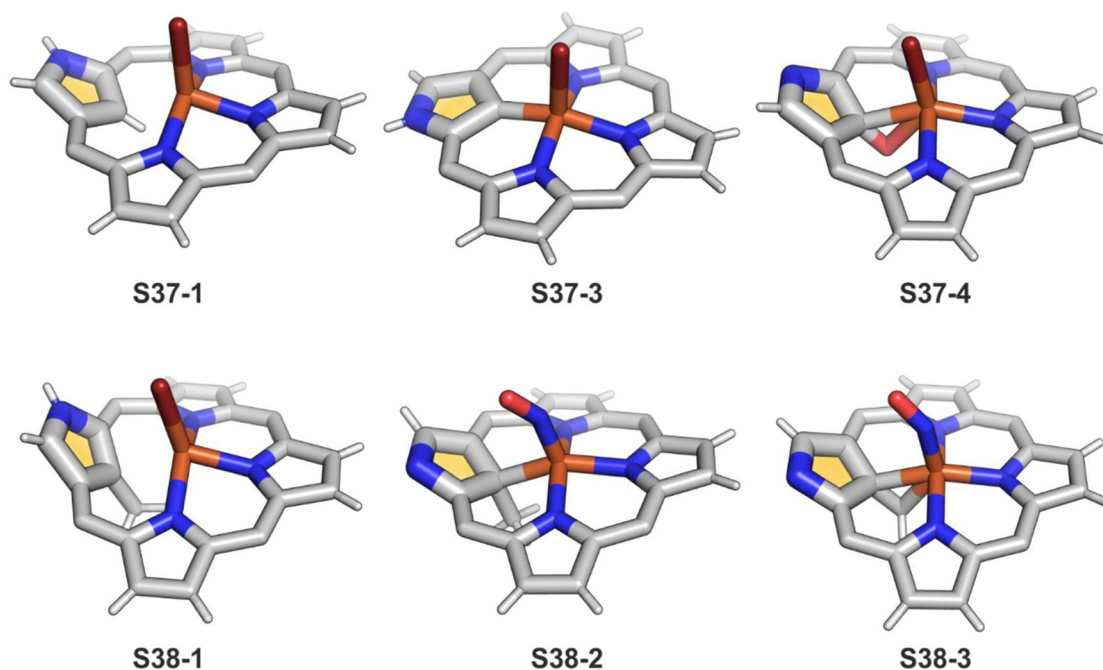
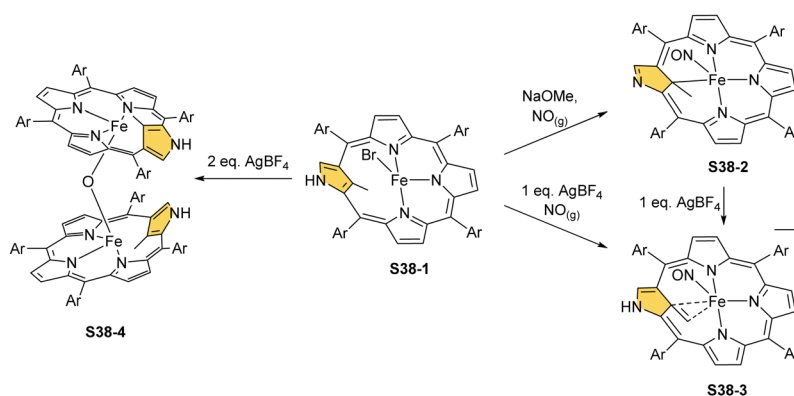


Fig. 11 Iron coordination motifs for C(21)-substituted and regular NCP. *meso*-Substituents not shown.



Scheme 38 Reactivity of iron(III) 21-methyl N-confused porphyrin **S38-1**.

disordered over the inversion centre, but it points at a C(21)–OH rather than a C(21)=O distance (1.497(5) Å).

Incorporating a sulphur atom into Fe–C(21) was also documented. It is achieved in the reaction of **S37-1** with *S*-nitrosotriphenylmethanethiol giving **S37-6**.<sup>130</sup> An NO molecule dissociates from nitrosothiol and is captured as an axial ligand replacing bromide. The transformation also involves a C–S bond cleavage followed by the incorporation of a liberated sulphur atom into the Fe–C(21) bond. **S37-6** is diamagnetic and acquires the {Fe(NO)}<sup>6</sup> electronic structure. The C(21) atom acquires the tetrahedral geometry and forms a stable organometallic bond as the Fe–C(21) distance equals 2.051(6) Å. The C(21)–S(21) bond length equals 1.763(5) Å being close to a single bond. The Fe–S(21) distance (2.2432(17) Å) confirms the binding of the thiolate-like sulphur atom to the iron centre.

Thus, species **S37-6** incorporates the ferrathiacyclopropane motif into its structure. Similar chemistry was observed for **S38-1** (Scheme 38) (Fig. 11) – the C(21)-methylated analogue of **S37-1**.<sup>131</sup>

The replacement of bromide with NO triggers the subsequent rearrangement leading to the formation of **S38-2** with a characteristic direct Fe–C(21)  $\sigma$ -bond (2.072(6) Å) and a {Fe(NO)}<sup>7</sup> configuration (Fig. 11). After the gentle oxidation of **S38-2** with AgBF<sub>4</sub>, activation of the inner methyl occurs and a double bond between CH<sub>2</sub> and C(21) forms with a length equal to 1.439(4) Å (**S38-3**; Fig. 11). The short contacts with the metal centre suggest that the formed alkene unit participates in an  $\eta^2$  type  $\pi$ -bonding (distances of Fe–C(21) and Fe–CH<sub>2</sub> are equal to 2.103(3) and 1.974(3) Å). The reaction of iron(II) 21-Me NCP **S38-1** with two equivalents of AgBF<sub>4</sub> under anaerobic conditions



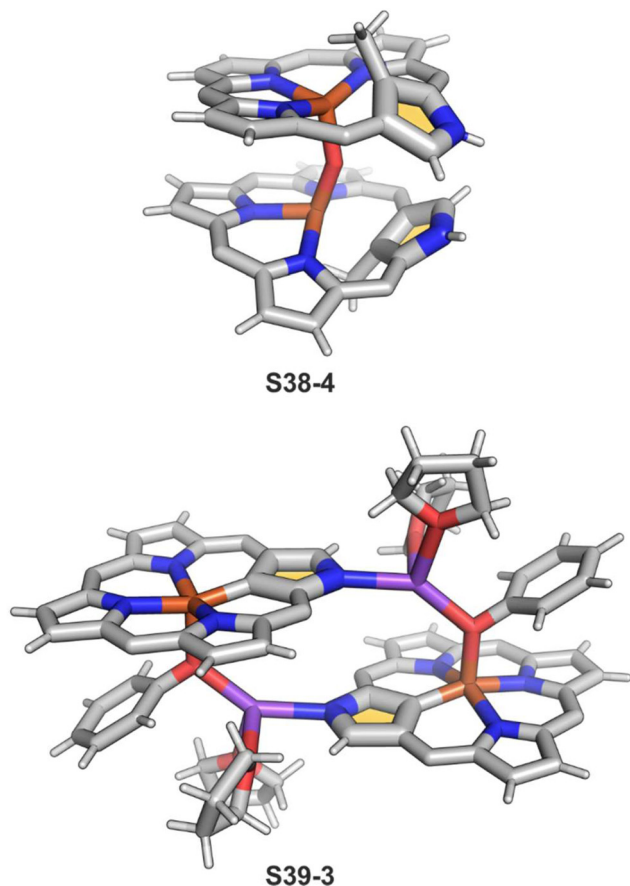


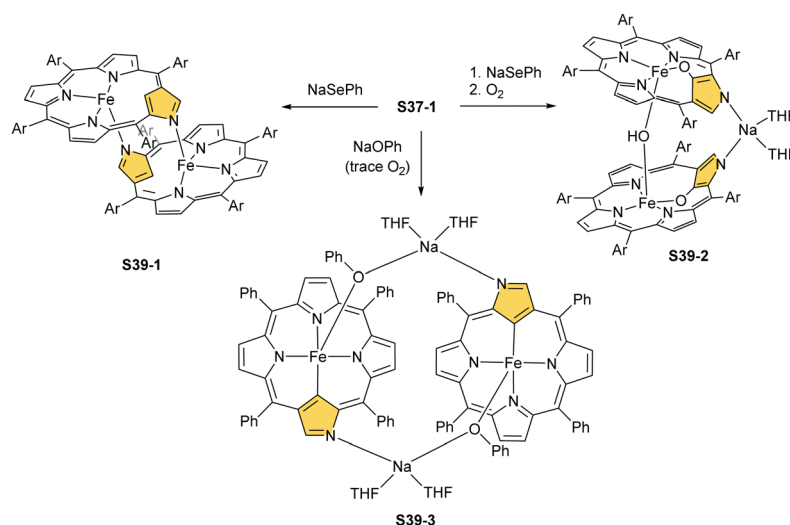
Fig. 12 Bridged dimeric iron NCP complexes. *meso*-Substituents not shown.

yields an air-sensitive product which, after exposure to air, transforms into a  $\mu$ -oxy-bridged iron(III) dimeric complex  $[(\text{Fe}^{\text{III}}\text{NCP})_2\text{O}](\text{BF}_4)_2$  **S38-4** (Fig. 12). Two antiferromagnetically coupled high-spin iron(III) centres are bridged by the oxygen dianion. However, there is no direct organometallic  $\sigma$ -bonding

as the distances for  $\text{C}(21)\cdots\text{Fe}$  contacts are 2.345(8) and 2.319(7) Å in both subunits.

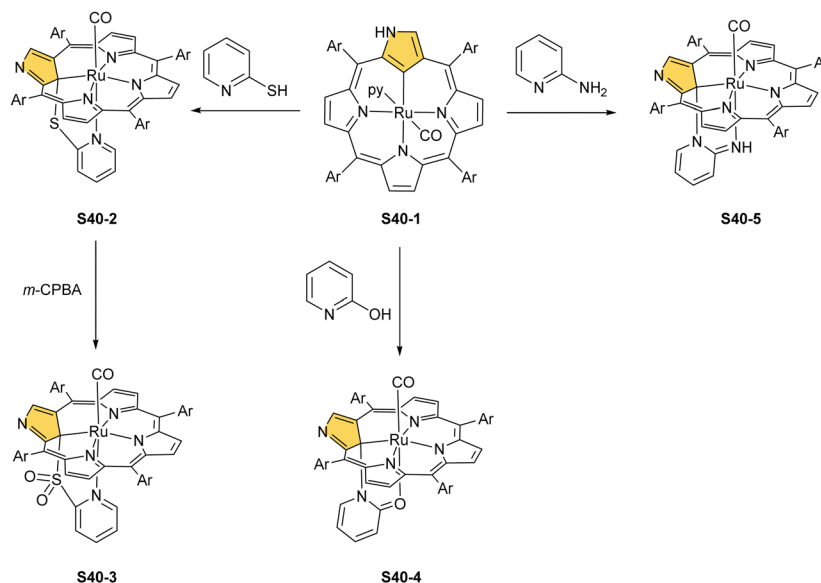
Over the years, other synthetic routes were successfully probed to construct the molecular system containing two iron N-confused porphyrin subunits. Thus, one can abstract the H(21) atom and axial bromide from bromoiron(II) NCP **S37-1** with sodium benzeneselenate.<sup>132</sup> This opens an opportunity to form a plain head-to-tail type  $[(\text{Fe}^{\text{II}}\text{NCP})_2]$  dimer **S39-1** (Scheme 39). Here, the outer N(2) and N(2)' nitrogen atoms act as the donors creating the typical iron(II)–N bonds with the iron centres form twin subunits in a similar fashion as previously encountered for the zinc(II)  $[(\text{Zn}^{\text{II}}\text{NCP})_2]$  analogue **S14-2**. The  $\text{C}(3)\text{N}(2)$  and  $\text{C}(3')\text{N}(2')$  vectors in **S39-1** point in opposite directions, which remains in contrast to the mutual arrangement of zinc(II) NCP or cadmium(II) NCP subunits in the respective dimers.<sup>78</sup>

**S39-1** is highly reactive towards dioxygen as its exposition to air results in the oxidation of iron(II) to iron(III) as well as in the oxygenation of C(21) positions. It eventually generates a diiron(III) species (**S39-2**). The fundamental dimeric arrangement was conserved, though the  $\mu$ -hydroxy bridge connecting two iron(III) ions is incorporated. The additional linkage is identified in the structure of **S39-2** as a  $\text{Na}(\text{THF})_2^+$  cation that coordinates N(2) and N(2)' atoms. The bond pattern of the oxygenated N-confused pyrrolic fragment of **S39-2** ( $\text{Fe}-\text{O}(21)$  1.957(4) Å,  $\text{Fe}-\text{C}(21)$  2.297(6) Å, and  $\text{C}(21)-\text{O}(21)$  1.336(6) Å) seems to reflect a framework of 21-hydroxy NCP. The reactivity of bromoiron(II) NCP **S37-1** was also tested in the presence of sodium phenolate under strictly anaerobic conditions.<sup>133</sup> A replacement of bromide with phenoxide is initially detected. Introducing trace amounts of dioxygen into the reaction mixture is sufficient to carry iron(II) to iron(III) one-electron oxidation. It is still insufficient for feasible oxygen incorporation into the  $\text{Fe}-\text{C}(21)$  bond or the formation of  $\mu$ -oxy ( $\mu$ -hydroxy) bridges. The formed complex **S39-3** captures each iron(III) centre in a square pyramid mode with a direct  $\text{Fe}-\text{C}(21)$  bond



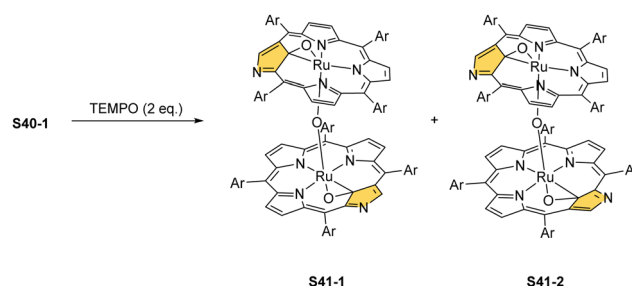
Scheme 39 Reactivity of iron(II) N-confused porphyrin **S37-1** with NaSePh and NaOPh.



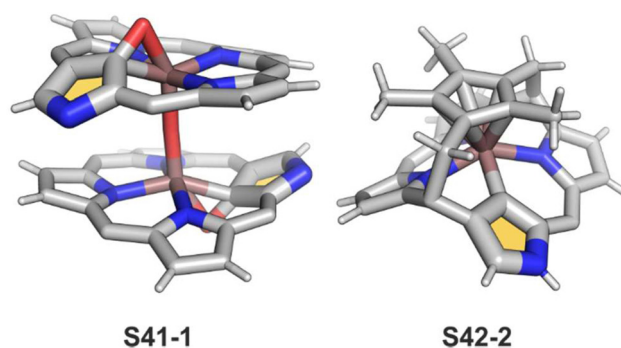
Scheme 40 Reactivity of ruthenium(II) N-confused porphyrin **S40-1**.

(1.950(5) Å; Fig. 12). Two  $\text{Fe}^{\text{III}}$ NCP subunits are symmetrically bridged with phenolate coordinated to the iron(III) centre as well as a sodium cation interacting with the phenolate oxygen atom and an N(2) atom of the second subunit.

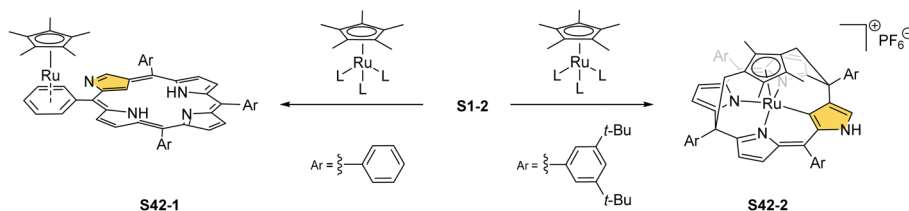
Substantial progress in ruthenium N-confused porphyrin chemistry has been recently noted. The formation of regular organometallic ruthenium(II) N-confused porphyrin **S40-1** (Scheme 40) was initially described. Insertion is performed in boiling chlorobenzene using triruthenium dodecacarbonyl  $[\text{Ru}_3(\text{CO})_{12}]$  as a metal source.<sup>33</sup> **S40-1** contains an axially coordinated carbonyl ligand and pyridine after its subsequent addition. The Ru–C(21) distance of 2.015(5) Å clearly shows direct bonding. The inner carbon is activated, as demonstrated in a reaction of **S40-1** with 2-mercaptopyridine. The reaction involves the formation of the covalent C(21)–S bond and trigonal to tetrahedral C(21) rehybridisation accompanied by pyridine side-arm coordination generating **S40-2**. The Ru–C(21) distance (2.118(3) Å) is still in a bonding range. The oxidation of **S40-2** with *m*-chloroperoxybenzoic acid yields the sulphone derivative **S40-3**, resembling the analogous cobalt N-confused porphyrin chemistry.<sup>134</sup> Also, 2-amino- and 2-hydroxypyridine react with **S40-1** generating coordinating side-arms.<sup>134</sup> Interestingly, in contrast to a mercapto derivative, they form a C(21)–N bond through a nitrogen atom from pyridine. The oxygen or nitrogen donors derived from the original 2-amine or 2-hydroxy substituents of pyridine coordinate to the ruthenium(II) centre in the typical side-arm geometry. In the case of the oxygen atom in **S40-4**, the C–O bond length is 1.264(4) Å, suggesting a double bond and dearomatization of a pyridine ring. A similar rearrangement has been detected in the case of **S40-5** in which the structural parameters of the side arm reflect the frame of pyridin-2-imine (C=NH bond: 1.305(3) Å). The characteristic of **S40-5**, the upfield relocated resonance of the NH hydrogen atom, has been unambiguously localised in the  $^1\text{H}$  NMR spectrum of **S40-5** at 0.16 ppm.

Scheme 41 Oxidation of ruthenium(II) N-confused porphyrin **S40-1**.

Oxidation of ruthenium(II) porphyrin **S40-1** using (2,2,6,6-tetramethylpiperidin-1-yl)oxyl (TEMPO) carried out under an argon atmosphere (in refluxing *o*-dichlorobenzene) affords two diamagnetic, isomeric ruthenium(IV) N-confused porphyrin  $\mu$ -oxy-bridged complexes **S41-1** (Scheme 41) and **S41-2**. They differ solely by alignments of the N(2)C(3) and N(2')C(3') vectors.<sup>135</sup> The C(21) environments in **S41-1** and **S41-2**, as determined by X-ray crystallography (Fig. 13), are only slightly tetrahedrally

Fig. 13 Ruthenium coordination motifs. Regular *meso*-substituents not shown.



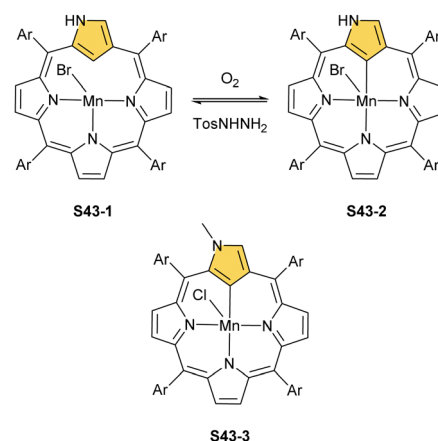


Scheme 42 N-confused porphyrins containing [RuCp\*] motifs.

distorted. The bond distances (e.g., in **S41-1** Ru–C(21) 2.121(7) Å, Ru–O 1.988(5) Å, C(21)–O 1.371(7) Å, C(4)–C(21) 1.462(7) Å, and C(1)–C(21) 1.461(8) Å) point a borderline situation between a direct bonding and the  $\eta^2$  interaction between the C=O moiety and the ruthenium(IV) centre resembling the relevant structural features of the respective iron(III) 21-oxo N-confused porphyrin **S37-4** or {Co(NO)}<sup>7</sup> 21-oxo NCP **S31-2**.

Complexes of a quite distinct molecular architecture are formed once [RuCp\*](CH<sub>3</sub>CN)<sub>3</sub>]PF<sub>6</sub> is used as a ruthenium source (Cp\* – pentamethylcyclopentadiene).<sup>136</sup> Mixing it with NCP and refluxing the dichloroethane solution result in N-confused porphyrin incorporating the [RuCp\*]  $\pi$ -coordinated *meso*-phenyl ring **S42-1** (Scheme 42). The process is regioselective as the *meso*-phenyl ring adjacent to N(2) is solely involved in  $\pi$ -coordination. The outer nitrogen donor seems instrumental in providing regioselectivity, presumably stabilising the intermediate form which directs the final step, i.e.,  $\pi$ -coordination. The protection of *meso*-aryls with bulky substituents (3,5-di-*tert*-butylphenyl rings) redirects the reaction to build the transient ruthenium(IV) sitting-atop structure. The ruthenium(IV) coordination forced the adjacency of Cp\* methyl groups and two *trans meso* carbon atoms [C(5) and C(15)] of the NCP skeleton. This imposed vicinity induced a peculiar reaction in which two methyl groups of Cp\* formed two regular covalent C–C bonds with proximal C(5) and C(15) *meso* carbon atoms. Eventually, the process results in sitting atop ruthenocenophane **S42-2**, described alternatively as ruthenium(IV) N-confused calix[4]pyrrole strapped with a cyclopentadienyl ligand (Fig. 13). Ruthenium(IV) coordinates all inner donor atoms, including C(21) (the Ru–C(21) distance: 2.065(4) Å).

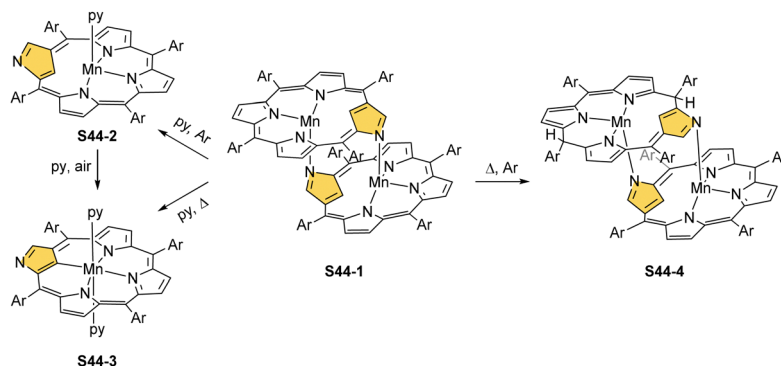
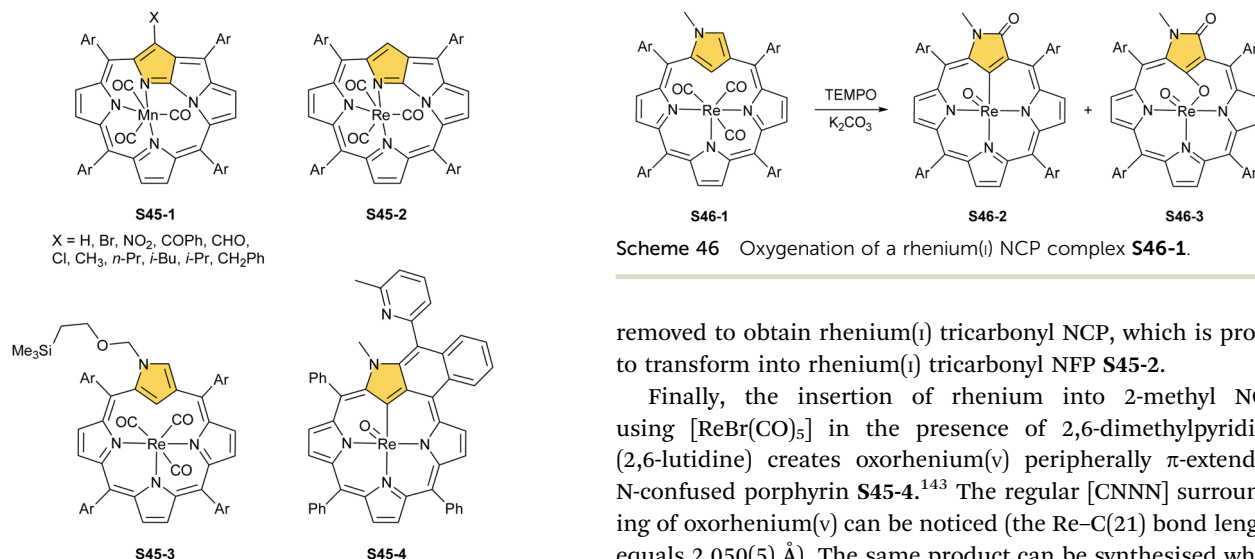
**Mn and Re.** Insertion of manganese(II) into NCP initiates similar processes as those described for iron NCP. A reaction between manganese(II) bromide and NCP (inert atmosphere) produces manganese(II) NCP **S43-1** (Scheme 43) which adopts the geometry detected for analogous iron(II) NCP **S37-1**. The manganese(II) centre is located in proximity to the inner C(21)–H unit (Mn–C 2.437(7) Å).<sup>137</sup> An exposure to dioxygen prompts one-electron oxidation to manganese(III) NCP **S43-2**, accompanied by the regular coordination of a trigonally hybridised anionic C(21) donor. The manganese(III) centre is located in an equatorial [CN<sub>3</sub>N] environment with bromide acting as an axial ligand. The structure of the macrocyclic ligand is related to the tautomer **S3-1** of NCP, preserving the hydrogen atom at the N(2) position. Interestingly, this oxidation is reversible and **S43-1** can be reinstated in the reduction of **S43-2** with *p*-toluenesulfonyl hydrazide.



Scheme 43 Manganese(II)/(III) complexes of N-confused porphyrin and 2-methyl N-confused porphyrin.

Manganese(II) NCP may also acquire a dimeric form in the absence of additional ligands contending for axial positions.<sup>138</sup> Thus, dimer **S44-1** (Scheme 44) is directly formed as a product of a reaction of NCP and [Mn<sub>2</sub>(CO)<sub>10</sub>] in toluene. Similar to other dimers, the fourth coordination site of the first [Mn(NCP)] building block is occupied by the N(2)' atom of the second one imposing the head-to-tail arrangement of subunits. Subsequently, dimer **S44-1** can be cleaved when a strong ligand, for example, pyridine, competes for the axial position to eventually form monomeric monopyridine species **S44-2**. The species **S44-1**, exposed to dioxygen, undergoes one-electron oxidation to produce **S44-3**. Manganese(II) to manganese(III) oxidation is accompanied by the formation of the regular [CN<sub>3</sub>N] donor set, similarly as described for **S43-2**. Organometallic manganese(III) N-confused porphyrin **S44-3** incorporates an equatorial trianionic ligand, which conserves features of the NCP tautomer **S1-2**. Two axial pyridine ligands complete the coordination sphere of manganese(III). The manganese(III) 2-methyl NCP (**S43-3**) is obtained directly in a reaction of 2-methyl NCP and manganese(II) acetate, followed by ligand exchange with sodium chloride.<sup>139</sup> A prolonged heating of dimeric **S44-1** with [Mn<sub>2</sub>(CO)<sub>10</sub>] leads to the ligand-centred reduction of a single subunit involving hydrogenation at C(10) and C(20) *meso* positions affording a heterogeneous dimanganese(II) ensemble **S44-4**. It is noteworthy that the opposite directionalities (*trans* vs. *cis*) of N(2)C(3) vectors have been identified for **S44-1** and **S44-4** in the solid-state structures.



Scheme 44 Reactivity of the manganese(II) NCP dimer **S44-1**.

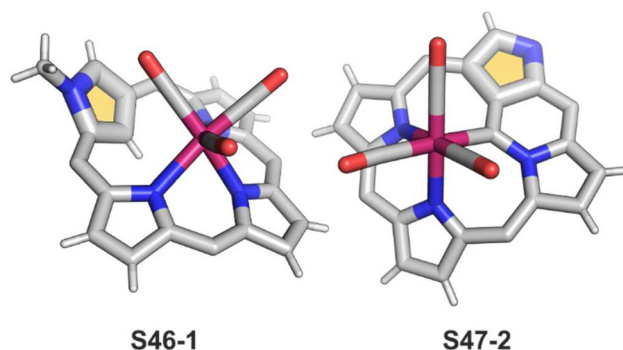
Scheme 45 Manganese(I) and rhenium(I)/(V) complexes of N-confused porphyrin derivatives.

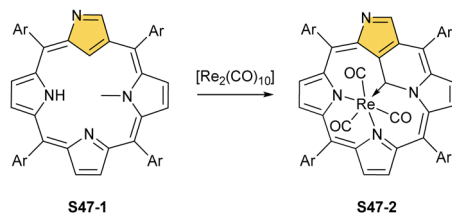
In a reaction of a manganese(I) source,  $[\text{MnBr}(\text{CO})_5]$ , and 21-substituted NCP (in the presence of  $\text{K}_2\text{CO}_3$ ), the manganese(I) N-fused porphyrin **S45-1** (Scheme 45) is synthesised instead of the expected regular manganese NCP.<sup>72</sup> NCP with electron-withdrawing C(21)-substituents like  $\text{NO}_2$  and Cl produces mostly not NFP but a manganese(II) dimeric complex **S44-1** with C(21)-substituents detached.

Similar reactivity, as reported for manganese(I) NCP, has been documented for manganese's heavier counterpart – rhenium. An attempt to insert rhenium into NCP using  $[\text{Re}_2(\text{CO})_{10}]$  results in the formation of the rhenium tricarbonyl complex bearing N-fused ligand **S45-2**.<sup>140</sup> Naturally, the protection of the N(2) position with a substituent prevents the N-fusion affording rhenium(I) tricarbonyl 2-substituted NCP **S45-3**.<sup>141,142</sup> The formed **S45-3** contains the octahedral rhenium(I) ion facially bound to three inner nitrogen atoms. Its coordination sphere is supplemented with three carbonyl ligands located on the opposite face. The C(21)–H fragment remained intact. When a suitable substituent is involved, N(2) protection can be readily

removed to obtain rhenium(I) tricarbonyl NCP, which is prone to transform into rhenium(I) tricarbonyl NFP **S45-2**.

Finally, the insertion of rhenium into 2-methyl NCP using  $[\text{ReBr}(\text{CO})_5]$  in the presence of 2,6-dimethylpyridine (2,6-lutidine) creates oxorhenium(V) peripherally  $\pi$ -extended N-confused porphyrin **S45-4**.<sup>143</sup> The regular [CNNN] surrounding of oxorhenium(V) can be noticed (the Re–C(21) bond length equals 2.050(5) Å). The same product can be synthesised when rhenium(I) tricarbonyl 2-methyl NCP **S46-1** (Scheme 46) (Fig. 14) reacts with  $[\text{ReBr}(\text{CO})_5]$  and 2,6-lutidine. The presence of 2,6-lutidine is essential because a fusion at the NCP perimeter occurs concomitantly to the rhenium(V) insertion. One of the methyl groups from 2,6-lutidine forms a C–C bond with the *ortho* carbon atom of *meso*-phenyl adjacent to C(3). Simultaneously, the same carbon atom forms the double bond with proximal C(3). The oxidation and oxygenation of initial

Fig. 14 Rhenium(I) NCP complexes. *meso*-Substituents not shown.



**Scheme 47** Rhenium(I) insertion into 22-methyl N-confused porphyrin **S47-1**.

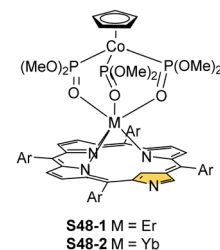
rhenium(I) to oxorhenium(V) were confirmed by X-ray crystallography.

The interesting oxygenation of **S46-1** occurs with suitable oxygen atom donors (*t*-BuOOH and TEMPO).<sup>144</sup> The tricarbonyl ruthenium(I) N(2)-methylated NCP complex acquires two or three oxygen atoms during oxygenation and transforms into **S46-2** and **S46-3**, respectively. Aside from oxorhenium centre formation, the attachment of the oxygen atom at C(3) affords a lactam unit (the lactam function is confirmed by the C=O bond length: 1.256(6) Å). Finally, the incorporation of the third oxygen atom, which eventually links rhenium(V) and C(21) atoms, finalises the process, as evident in the structure of **S46-3**. The Re–C(21) distance increases to 2.245(9) Å from 2.070(4) Å for **S46-2**. The C(21)–O(21) distance equal to 1.415(11) Å reflects the single bond character. Interestingly, interconversion between **S46-2** and **S46-3** can occur when one uses PPh<sub>3</sub> as a reductant and an oxygen atom scavenger and pyridine *N*-oxide as an oxidant.

Eventually, a different type of reactivity is induced when inner core methylated derivatives are explored.<sup>145</sup> The reaction of N(22)-methyl NCP **S47-1** (Scheme 47) and [Re<sub>2</sub>(CO)<sub>10</sub>] produces a single carbon bridge between the originally methyl-substituted site and an adjacent C(21) atom (aside from accompanied but predictable N-fusion). The bridge is then coordinated to the metal centre (**S47-2**). The bridging carbon atom acts as a carbene ligand, coordinated to the tricarbonyl rhenium(I) unit, also bound to the other two available inner nitrogen donors (Fig. 14). The Re–C bond length equals 2.140(5) Å. Its carbene character is confirmed by the characteristic <sup>13</sup>C NMR signal located at 196.4 ppm. The alternative insertion of rhenium(I) into 21-methyl NCP leads to a mixture of internally bridged rhenium(I) NCP-derivatives with a clear preference for the C(21)–N(24) fused one.

**Additional coordination motifs.** The previous sections provide a concise state-of-the-art of transition metal organometallic chemistry in NCP surroundings. One can readily notice that a few periodic table groups remain practically untouched by NCP coordination or organometallic chemistry. In this context, the lanthanides and lower actinides can be included in the class of prospective targets for future exploration. The opportunities in this area are clearly illustrated by lanthanide N-confused chemistry, which is evidently in its infancy.

In the unique for the field studies, it was demonstrated that erbium(III) and ytterbium(III) ions could form stable complexes with NCP.<sup>146,147</sup> Reactions of erbium(III) or ytterbium(III) amides

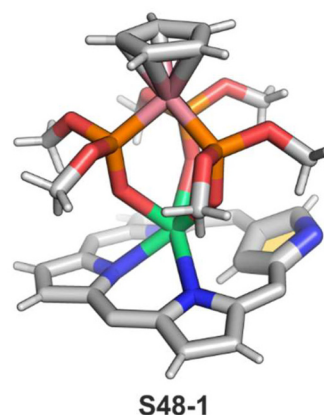


**Scheme 48** The unique erbium(III) and ytterbium(III) complexes of NCP derivatives.

(Ln(N(SiMe<sub>3</sub>)<sub>2</sub>)<sub>3</sub>·x[LiCl(THF)<sub>3</sub>]) with N-confused porphyrin in bis(methoxyethyl) ether are finalised by the isolation of the respective N-confused porphyrin complexes, **S48-1** (Scheme 48) and **S48-2**. Their stability is assured by the facial coordination of anionic tripodal cobaltocene decorated by three *P*-phosphonate arms. The stabilising interaction involves the coordination of three phosphoryl oxygen atoms located on a single face of a coordination polyhedron. The opposite face embraces three inner pyrrolic nitrogen atoms of NCP. In the case of **S48-1**, the η<sup>2</sup>-agostic interaction with the inner C(21)–H can be noticed with a Er···C(21) distance of 2.595(6) Å (Fig. 15).

N-Confused porphyrin was quite extensively probed as an appropriate macrocyclic setting for the coordination of main group metal ions and metalloids known for their small ionic radii, exemplified here by boron(III), phosphorus(V), and silicon(IV).

Thus, insertions of boron(III) or oxophosphorus(V) prompt the inversion of the N-confused pyrrole ring, followed by N-fusion, which creates the contracted three nitrogen [NNN] coordinating surrounding of N-fused porphyrin. Thus, the σ-phenyl boron(III) N-fused porphyrin **S49-1** (Scheme 49) cation and oxophosphorus(V) dihydro-N-fused porphyrin **S49-2** were identified.<sup>148,149</sup> Evidently, the apparent mismatch between the core of N-confused porphyrin and boron(III) or phosphorus(V) radii was instrumental for N-confused porphyrin to N-fused porphyrin conversions. Altogether, seemingly distant coordination centres boron(III) and phosphorus(V) and transition metal

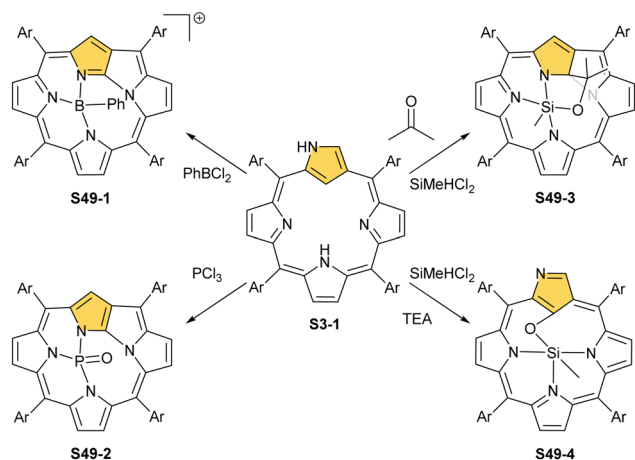


**S48-1**

**Fig. 15** Erbium double-decker NCP complex. *meso*-Substituents not shown.





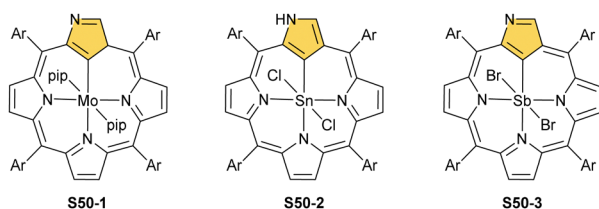


Scheme 49 Reactivity of N-confused porphyrin **S3-1** with boron(III), phosphorus(V), and silicon(IV) ions.

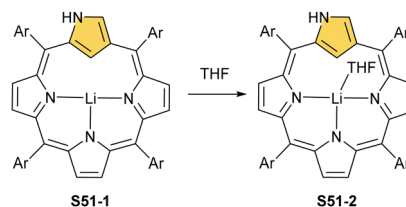
cations: rhenium(I) and manganese(I) enforce the identical NCP to the NFP rearrangement, fine-tuning the size of the macrocyclic core.

The similar values of the cationic radii of phosphorus(V) ( $r_{\text{cat}} = 0.38 \text{ \AA}$ ) and silicon(IV) ( $r_{\text{cat}} = 0.40 \text{ \AA}$ ) are consistent with the fact that the resembling types of NCP molecular rearrangements were discovered in the course of silicon(IV) insertions. Thus, the reaction of N-confused porphyrin and dichloromethylsilane in the presence of triethylamine and aldehydes of ketones results in the formation of the methylsilicon(IV) complex of a NFP derivative (**S49-3**). The novel macrocycle is substituted at the inner C(9) position with a hydroxyalkyl moiety derived from introduced aldehyde or ketone.<sup>150</sup> Interestingly, the fundamental NCP frame is preserved when the silicon(IV) insertion is carried out without even traces of aldehydes or ketones in the reaction mixture. Under these conditions, the methylsilicon(IV) 21-hydroxy NCP (**S49-4**) is solely isolated.

The other subgroup forms from regular complexes with NCP after C(21)H activation. The examples here are complexes with  $\text{Mo}^{\text{II}}$  and two axial piperidines (**S50-1**, Scheme 50),<sup>151</sup>  $\text{Sn}^{\text{IV}}$  with two axial chlorides (**S50-2**),<sup>152,153</sup> and  $\text{Sb}^{\text{V}}$  with two anions as well (**S50-3**).<sup>154,155</sup> Note that both  $\text{Sn}^{\text{IV}}$  and  $\text{Sb}^{\text{V}}$  have the same coordination environment and both complexes are neutral. This, once again, points to the exceptional flexibility of NCP in the stabilisation of different oxidation states.



Scheme 50 Molybdenum(III), tin(IV), and antimony(V) complexes of N-confused porphyrin.



Scheme 51 Coordination motifs of a lithium(I) N-confused porphyrin.

At present, the lithium N-confused porphyrin **S51-1** (Scheme 51) completes the set of main group N-confused porphyrins. A reaction of NCP or N(2)-methyl NCP with lithium bis(trimethylsilyl)amide results in the incorporation of lithium(I) in the carboxyporphyrinic crevice (**S51-1**).<sup>156</sup> Lithium(I) coordinates with three inner nitrogen atoms. The  $\text{Li}^{\text{I}} \cdots \text{C}(21)\text{-H}$  interaction is reflected by the  $\text{Li}^{\text{I}} \cdots \text{C}(21)$  distance which is equal to  $2.363(6) \text{ \AA}$ . It increases to  $2.482(4) \text{ \AA}$  after the axial coordination of the THF molecule (**S51-2**).

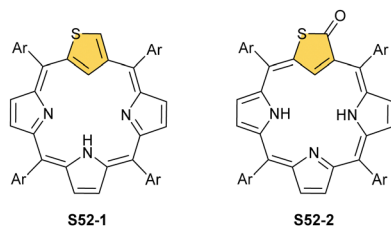
In summary, the vast abundance of organometallic motifs has been provided by N-confused porphyrin and spans from direct  $\sigma$ -bonds and  $\pi$ -coordination to weaker agostic interactions. Nonetheless, most of them are enforced and stabilised by macrocyclic confinement of the metal ion in the proximity of the carbon fragment.

## X-confused and other “peculiar” 21-carbaporphyrins

The N-confusion concept opened the route to the rich chemistry of N-confused porphyrin **S1-2** and subsequently to N-confused expanded porphyrins and heteroporphyrins.<sup>3,42,157</sup> The continuation of the story brings O-confusion and S-confusion concepts, affording 2-hetero-21-carbaporphyrins eventually.<sup>158–160</sup> In a macrocyclic environment, a heteroatom can function as a donor toward various metal ions, offering insight into the coordination properties of furan, thiophene, selenophene, or tellurophene.<sup>4,161</sup> The heteroatom confusion (X-confusion) concept was also successfully applied in constructing a nontrivial macrocyclic environment for organometallic chemistry.

The syntheses of 2-hetero-21-carbaporphyrins are more complex when compared to straightforward condensation affording **S1-2**. The appropriately prearranged building block including an X-confused heterocycle (furan or thiophene substituted at 2- and 4-positions) must be prepared for the final condensation. Thus, S-confused thiaporphyrin (2-thia-21-carbaporphyrin) **S52-1** (Scheme 52) is formed in the condensation of 2,4-bis(phenylhydroxymethyl)thiophene, pyrrole, and arylaldehyde catalysed with  $\text{BF}_3 \cdot \text{Et}_2\text{O}$ .<sup>158</sup> A prolonged oxidation using DDQ in excess results in C(3)-oxygenation and aromatic 2-thia-3-oxo-21-carbaporphyrin **S52-2**. Thus, the specific reactivity at the C(3) position has been detected. A direct comparison of N-confused porphyrin **S1-2** and S-confused thiaporphyrin **S52-1** concludes that the thia-derivative demonstrates the less malleable character of a coordination crevice.

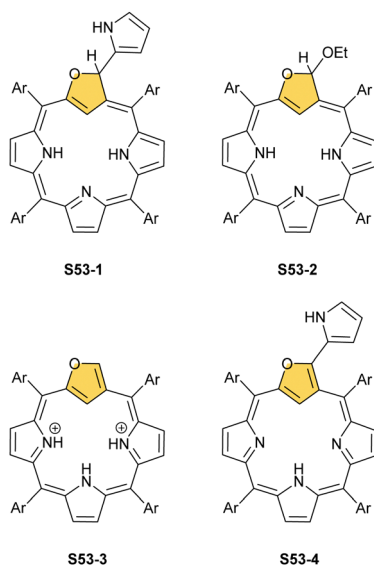




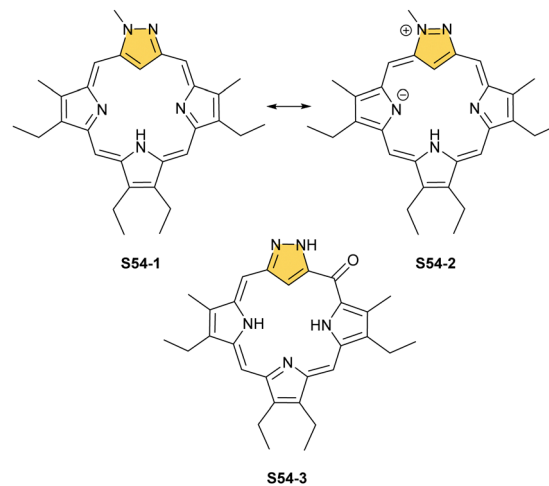
Scheme 52 S-confused thiaporphyrin **S52-1** and 3-oxo S-confused thiaporphyrin **S52-2**.

Only two dissociable hydrogen atoms are located in the cavity of **S52-1**, whereas the tautomeric equilibrium of **S1-2** allowed for switching between two or three such hydrogen atoms (see above). The oxygenation of **S52-1** provides the macrocycle **S52-2** with a coordination core prone to act as a trianionic ligand. The borderline macrocyclic aromaticity was detected for **S52-1**, whereas the evident aromatic behaviour was established for **S52-2** as documented by the appropriate chemical shift of the inner H(21) atom (**S52-1** 4.76 ppm and **S52-2** –5.31 ppm). Compared to the S-confusion procedure, the synthesis of O-confused oxaporphyrin remained a demanding task because of the peculiar furan activity. An acid-catalysed condensation of 2,4-bis(phenylhydroxymethyl)furan, pyrrole, and arylaldehyde readily yields the strongly aromatic macrocycle **S53-1**.<sup>159</sup> **S53-1** (Scheme 53) is structurally related to the hypothetical 3-dihydro-2-oxa-21-carbaporphyrin and contains an appended pyrrole ring linked to the tetrahedral C(3) atom.

Eventually, the condensation was purposely directed toward the formation of the 2-oxa-21-carbaporphyrin derivative **S53-2** without an appended pyrrole. However, the 3-ethoxy substituent was accommodated and turned out to be a “good” leaving group.<sup>160</sup> The careful titration of **S53-2** with trifluoroacetic acid (TFA) produced the true O-confused oxaporphyrin solely stabilised in its diprotonated form **S53-3**. The process is reversible,



Scheme 53 O-confused oxaporphyrinoids.



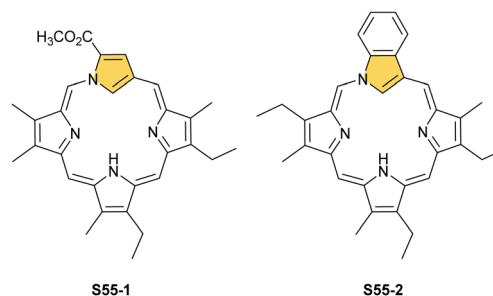
Scheme 54 Pyrazole-containing NCP analogues.

and **S53-2** can be rebuilt from **S53-3** simply by adding sodium ethoxide. An oxidised version of **S53-1**, that is, **S53-4**, structurally resembles the 3-(2'-pyrrolyl) N-confused porphyrin derivative, formed in the reaction of **S1-2** with pyrrole<sup>162</sup> and was identified in the form of metal complexes.<sup>163</sup>

Modifications at the C(3) position are reflected by pronounced changes in overall macrocyclic aromaticity. Thus, the borderline macrocyclic aromaticity was detected for **S53-3** and **S53-4** but the clear aromatic features were established for **S53-1** and **S53-2**. Two other original strategies to construct carbaporphyrinoids containing the [CNNN] core were explored, generating **S54-1** (Scheme 54) and neo-confused porphyrin **S55-1** (Scheme 55). **S54-1** forms when N-substituted pyrazole-3,5-dialdehyde is used in the typical condensation with tripyrrane.<sup>164</sup> As both outer positions (2 and 3) are now occupied with nitrogen atoms, the perimetral substitution cannot occur, yet the unprotected *meso* position is vulnerable to oxygenations (**S54-3**).<sup>165,166</sup>

The borderline aromaticity of **S54-1** is consistent with the H(21) NMR resonance located at 5.34 ppm. When an outer nitrogen atom is substituted by phenyl rather than methyl, the synthesis yields phlorin, which incorporates a tetrahedral C(5)H<sub>2</sub> *meso* bridge.

A prominent example of a 21-carbaporphyrin group is called neo-confused porphyrin and originally was synthesised as its



Scheme 55 Neo-confused porphyrin **S55-1** and its benzo-fused derivative **S55-2**.

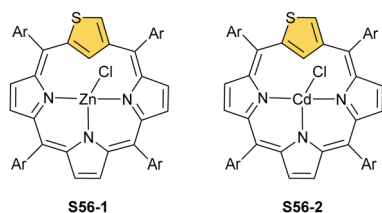
benzo-fused derivative **S55-2**<sup>167–169</sup> and subsequently, as intact neo-confused porphyrin **S55-1**.<sup>169</sup> Neo-confused porphyrin **S55-1**, similarly to N-confused porphyrin **S1-2**, is classified as a constitutional isomer of regular porphyrin which preserves its structural frame.<sup>41</sup> The neo-confused pyrrole ring is incorporated into a porphyrin scaffold at N(1) and C(3) positions. This particular connectivity allows for full  $\pi$ -conjugation and marked macrocyclic aromaticity as expressed in the chemical shifts of inner H(21) atoms 1.32 ppm (**S55-1**) and  $-0.74$  ppm (**S55-2**).<sup>167</sup>

### Organometallic chemistry

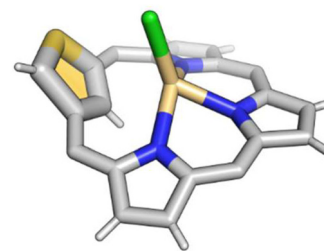
The coordination properties of X-confused heteroporphyrins were tested, albeit the scope of their investigation was significantly smaller compared to the extensive studies on N-confused porphyrin.

Inserting cadmium(II) and zinc(II) into S-confused thiaporphyrin **S52-1** results in the formation of the respective **S56-1** (Scheme 56) and **S56-2** complexes.<sup>170</sup> The macrocycle acts as a monoanionic ligand. Three nitrogen atoms and the C(21)H fragment of the S-confused thiophene are located at equatorial positions. The metal charge is compensated by the apical chloride coordination. The distinctive <sup>1</sup>H NMR resonances of the inner core H(21) atom, associated with the S-confused thiophene ring, are located at 1.71 and 1.86 ppm for **S56-2** and **S56-1**, respectively. The peculiar proximity of the S-confused thiophene fragment to the cadmium(II) ion induces direct scalar coupling between the spin-active nucleus of cadmium (<sup>111/113</sup>Cd) and the adjacent <sup>1</sup>H nucleus ( $J_{\text{CdH}} = 10.0$  Hz). The Cd...C(21)H interaction is clearly reflected by significant changes of C(21) chemical shifts: **S56-1** 92.9, **S56-2** 88.2 ppm vs. 123.7 ppm for **S52-1**. The molecular structure of **S56-2** confirmed the side-on cadmium...thiophene interaction with the close Cd...C(21) contact of 2.615(7) Å (Fig. 16).

O-Confused oxaporphyrin and its derivatives (**S53-1**, **S53-2**, and **S53-3**) applied as macrocyclic ligands toward selected metal ions (Zn/Cd/Ni/Cu<sup>2+</sup> and Cu/Ag<sup>3+</sup>) demonstrate the peculiar flexibility of its molecular and electronic structures firmly providing, however, the equatorial [CNNN] surrounding. It controls the subtle interplay between their structural flexibility, perimeter substitution, coordination, and aromaticity. The macrocyclic tuning is easily triggered by the addition/elimination of a nucleophile located at the C(3) position. The tetrahedral-trigonal rearrangements originating at the C(3) atom spread out their consequences to the whole macrocyclic scaffold.

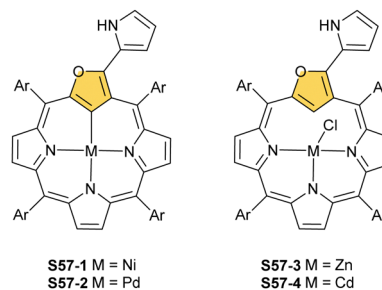


Scheme 56 Zinc(II) and cadmium(II) complexes of S-confused thiaporphyrin.



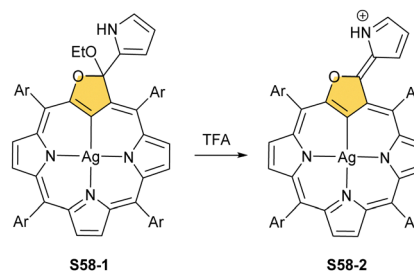
**S56-2**

Fig. 16 Agostic interactions in cadmium(II) SCP. *meso*-Substituents not shown.



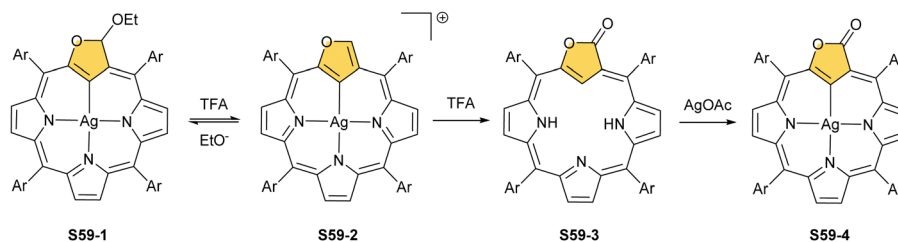
Scheme 57 Complexes of the O-confused oxaporphyrin derivative **S53-1**.

The reaction of **S53-1** with nickel(II) or palladium(II) chloride produces weakly aromatic **S57-1** (Scheme 57) and **S57-2**, respectively.<sup>159</sup> The structurally prearranged macrocycle **S53-4** affords **S57-1** as well. The molecular structure of **S57-1** shows a direct metal–carbon bond with a length of 1.892(4) Å. In contrast to nickel(II) or palladium(II), the insertion of zinc(II) or cadmium(II) into **S53-4** affords the side-on species **S57-3** and **S57-4** resembling the geometry of the thia analogue **S56-2**.<sup>163</sup> Thus, macrocycle **S53-4** acts as a monoanionic ligand. Compensation of the metal(II) charge requires axial chloride coordination. Coordination cores encountered for O-confused oxaporphyrins like **S53-1** are well-matched for stabilising higher oxidation states of metal ions. The dissociation of three inner protons (two NH and one C(21)H) leads to a trianionic equatorial surrounding. Thus, the reaction between silver(I) acetate and **S53-1** in acetonitrile in the presence of ethanol results in **S58-1**.<sup>159</sup> The tetrahedral geometry around the C(3) atom, required to preserve the aromaticity, is clearly demonstrated. The addition of TFA to **S58-1** (Scheme 58) yielded strongly aromatic **S58-2** *via* the elimination of the ethoxy group.



Scheme 58 Protonation of the silver(III) O-confused oxaporphyrin derivative **S58-1**.

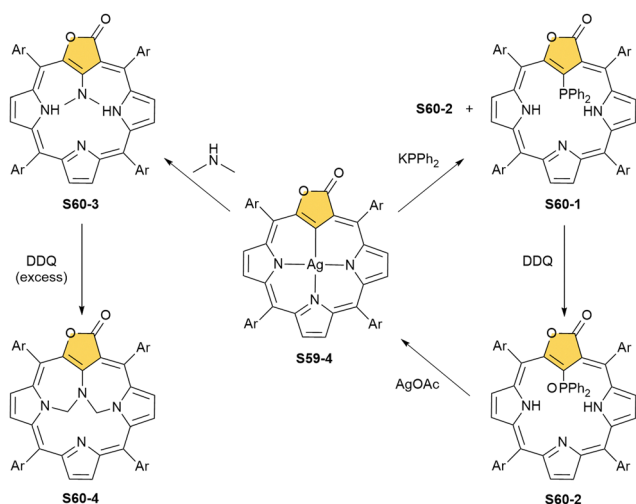


Scheme 59 Reactivity of the silver(III) O-confused oxaporphyrin derivative **S59-1**.

A reaction between the 3-ethoxy-substituted O-confused oxaporphyrin and silver(I) acetate produces the respective  $\text{Ag}^{\text{III}}$  complex **S59-1**.<sup>160</sup> An addition of TFA to **S59-1** (Scheme 59) generates weakly aromatic silver(III) “true” O-confused oxaporphyrin **S59-2** formed by the elimination of the ethoxy group. The subsequent intramolecular oxidation of **S59-2**, accompanied by water C(3)-addition and two-electron-reduced silver(I) extrusion, affords carbaporpholactone **S59-3**, the aromatic 21-carbaporphyrinoid. **S59-3** acts as a trianionic ligand capable of again accommodating silver(III) (**S59-4**; the Ag–C(21) bond of 2.013(5) Å).

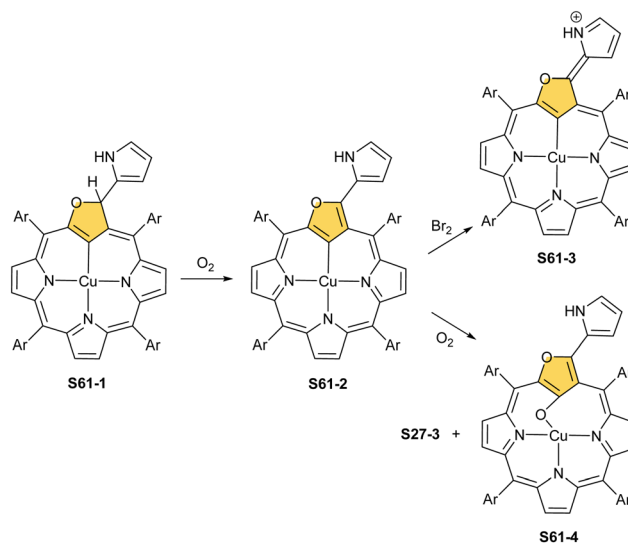
Silver(III) carbaporpholactone **S59-4** can be treated with potassium diphenylphosphide yielding the mixture of two derivatives with diphenylphosphanyl **S60-1** (Scheme 60) or diphenylphosphoryl **S60-2** moieties attached at the C(21) position.<sup>26</sup> The coordination of the highly oxidised silver(III) and C(21)H activation are prerequisite factors for phosphorylation, as **S59-3** is inactive toward potassium diphenylphosphide under similar conditions. The subsequent oxidation with DDQ produces exclusively **S60-2**, and the insertion of silver(I) into **S60-2** recovers **S59-4**.

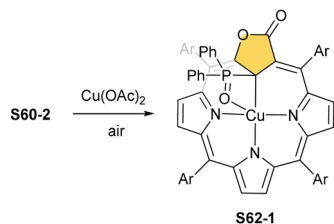
The reaction of dimethylamine and **S59-4** reveals analogous regioselectivity of substitution.<sup>101</sup> The process results in the formation of **S60-3**. Stepwise oxidation of the dimethylamine derivative leads finally to the internally bridged carbaporpholactone **S60-4**, which incorporates the [5.7.5.7.5] pentacyclic ring into its macrocyclic scaffold.

Scheme 60 Reactivity of silver(III) 21-carbaporpholactone **S59-4**.

O-confused oxaporphyrins with an appended pyrrole ring (**S53-1** and **S53-4**) and carbaporpholactone **S59-4** create unique macrocyclic surroundings to form organocopper(II) or alternatively organocopper(III) compounds. The reaction of copper(II) acetate and **S53-1** under mild conditions results in the quantitative formation of the organocopper(III) compound **S61-1** (Scheme 61), which preserves the scaffold of maternal **S53-1**.<sup>171</sup> A straightforward insertion of copper(II) into **S53-4** quantitatively produces paramagnetic organocopper(II) species **S61-2**, which conserves the geometry of starting **S53-4**. The transformation of **S61-1** in the course of the reaction with dioxygen, which includes the oxidation of macrocycle and the reduction of copper(III) to copper(II), generates **S61-2** as well. The one-electron oxidation of **S61-2** forms organocopper(III) species **S61-3** resembling the analogous silver(III) molecule **S58-2**.

The electron paramagnetic resonance spectroscopic features of **S61-2** correspond to a copper(II) oxidation state. The crystallographic analysis of **S61-2** revealed the practically planar structure and confirmed the formation of a direct  $\text{Cu}^{\text{II}}\text{--C}$  bond (1.939(4) Å) in which C(21) acts similarly to an  $\text{sp}^2$   $\sigma$ -carbanion. The degradation of **S61-2** in a reaction with dioxygen yields known from NCP chemistry copper(II) tripyrrinone **S27-3**. This process is accompanied by regioselective oxygenation at the inner C(21) position to form complex **S61-4**.

Scheme 61 Reactivity of copper(III) O-confused oxaporphyrin derivative **S61-1**.



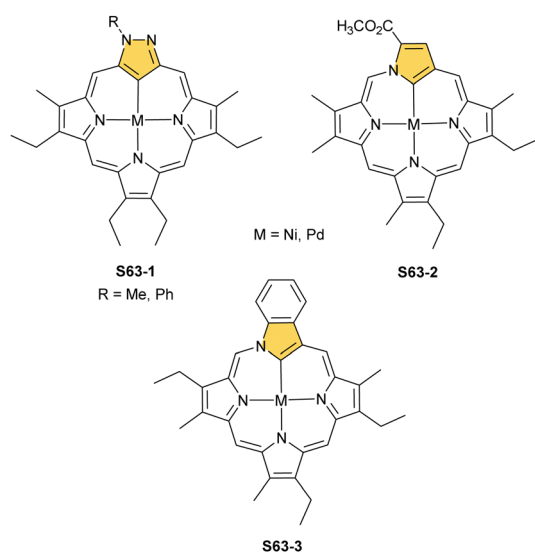
Scheme 62 Synthesis of copper(II) 21-carbaporpholactone derivative **S62-1**.

The reaction of copper(II) acetate with **S60-2** under mild conditions affords **S62-1** (Scheme 62).<sup>26</sup> The EPR spectrum recorded for **S62-1** reveals typical features associated with the copper(II) electronic state resembling copper(II) N-confused porphyrin and copper(II) 21-carbaporpholactone derivatives. The coordination environment of copper(II) forms a square pyramid with the equatorial positions occupied by the cavity donors [CNNN] and an oxygen atom located apically. The Cu–C(21) bond length equals 2.232(2) Å. The furanone is sharply tipped out of the [CNNN] plane, allowing the coordination to the copper(II) ion through the  $sp^3$ -hybridised C(21) atom.

The coordination chemistry of pyrazole containing 21-carbaporphyrin **S54-1**, neo-confused porphyrin **S55-1**, and benzo-fused **S55-2** was explored in the scope limited solely to nickel(II) and palladium(II).

Treatment of **S54-1** with either nickel(II) or palladium(II) leads to regular 21-carbaporphyrin-like complexes with an organometallic C(21)–M<sup>II</sup> bond. Insertion into a phlorin variant ends up with an appropriate 21-carbaporphyrin complex **S63-1** (Scheme 63) as well.<sup>164</sup>

A similar organometallic potential was demonstrated for neo-confused porphyrins, like **S55-1** and **S55-2** producing



Scheme 63 Nickel(II) and palladium(II) complexes of the pyrazole-containing NCP analogue, neo-confused porphyrin, and its benzo-fused derivative.

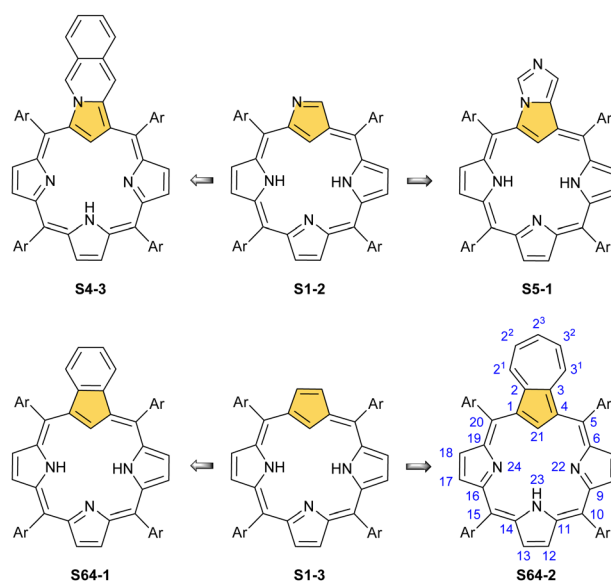
typical for 21-carbaporphyrins planar **S63-2** and **S63-3** complexes.<sup>167,172</sup>

## Azuliporphyrin and benzocarbaporphyrin

At this stage, it is essential to recall that the leitmotif macrocycles of this review have to preserve the fundamental skeleton of porphyrin or heteroporphyrin, clearly incorporating a 21-carbaporphyrin-like [CNNN] coordination core. Accordingly, they encompass X-confused (**S2-1**, **S52-1**, and **S53-3**) or neo-confused (**S63-2**) five-membered rings. The presented data analysis clearly reveals that this class can be readily extended by applying the fusion concept. Namely, the fusion of the five-, six-, or seven-membered rings to the already transformed five-membered ring conserves the major porphyrinic core, markedly modifying the overall properties of the resulting carbaporphyrin. In this manner, a collection of 21-carbaporphyrinoids have been impressively enriched, as shown in Scheme 64, demonstrating the relationship between N-confused porphyrin **S1-2** and its fused derivatives (**S4-3** and **S5-1**). A similar fusion-type relationship was described above for neo-confused porphyrin **S55-1** and benzo-fused neo-confused porphyrin **S55-2**.

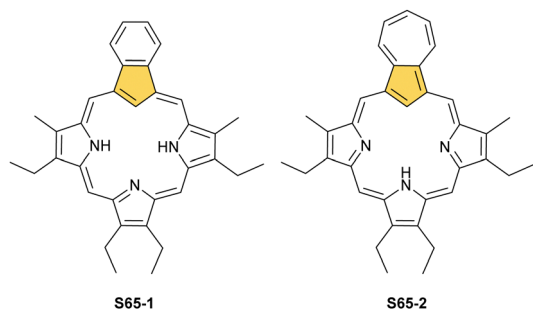
A fusion approach, illustrated above, performs perfectly well when applied to a regular *meso*-tetraaryl-21-carbaporphyrin **S1-3**. Namely, the fusions of six- or seven-membered rings assemble benzocarbaporphyrin **S64-1** or azuliporphyrin **S64-2**, respectively.

Retrospectively,  $\beta$ -alkylated benzocarbaporphyrin **S65-1** (Scheme 65) belongs to the group of macrocycles synthesised just after N-confused porphyrin, which played a founding role in launching a carbaporphyrinoid field. Serendipitously, in



Scheme 64 N-confused porphyrin **S1-2** with its fused derivatives, and 21-carbaporphyrin **S1-3** with its fused derivatives.





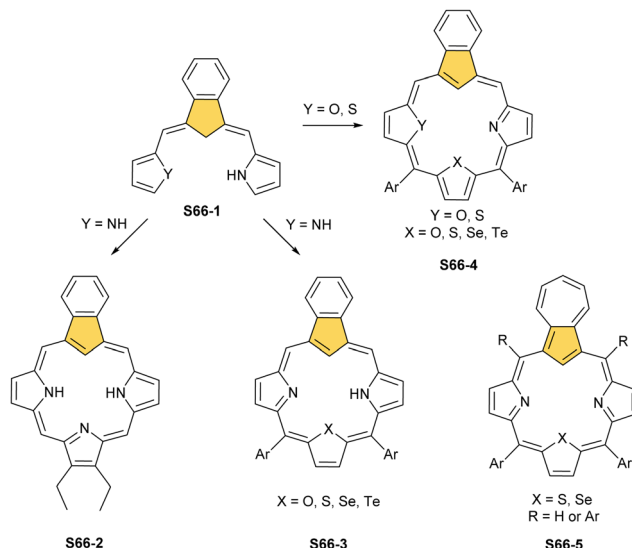
Scheme 65  $\beta$ -Alkylated benzocarbaporphyrin **S65-1** and  $\beta$ -alkylated azuliporphyrin **S65-2**.

their effort to form azuliporphyrin **S65-2**, Berlin *et al.* identified  $\beta$ -alkylated benzocarbaporphyrin **S65-1**.<sup>173</sup> It occurs that the applied reaction conditions induced a peculiar transformation of the initially formed azuliporphyrin **S65-2** into benzocarbaporphyrin **S65-1** as firmly proven in the course further investigations by Lash.<sup>174</sup> This discovery led to optimising the synthetic pathway leading to **S65-1**. Under base-catalysed conditions, azuliporphyrin **S65-2** reacts with *tert*-butyl hydroperoxide yielding benzocarbaporphyrin **S65-1** and its formyl-substituted derivative.

Subsequently, the “3+1” methodology, by which porphyrinoid systems are constructed from a tripyrrane and a cyclic dialdehyde, *i.e.*, azulene-1,3-dicarbaldehyde, was successfully applied to generate  $\beta$ -alkylated azuliporphyrin **S65-1**.<sup>174</sup> An alternative [3+1] strategy using the azulene analogue of the tripyrranes was developed to form  $\beta$ -substituted azuliporphyrins.<sup>175–177</sup> The related [3+1] methodology procedure affords 10,15-diaaryl-23-thia and 23-selenaazuliporphyrins (**S66-5**, R = H).<sup>178</sup> Finally, *meso*-tetraaryl-23-thiaazuliporphyrin forms in a reaction of plain azulene, arylaldehyde, and thia-tripyrane (**S66-5**, R = Ar).<sup>179</sup>

Benzocarbaporphyrin **S66-2** and its 23-heteroanalogue **S66-3** are directly synthesised starting from carbatripyrrin **S66-1**, as shown in Scheme 66.<sup>175,180</sup> Diheterocarbaporphyrins **S66-4** can be obtained following a similar synthetic approach.<sup>180,181</sup>

Eventually, a one-pot Rothemund-type synthesis of *meso*-tetraarylazuliporphyrin **S64-2** was developed. Thus, azulene, pyrrole, and arylaldehyde were shown to react under typical Lindsey conditions with a boron trifluoride etherate catalyst to form *meso*-tetraarylazuliporphyrin **S64-2** up to 20% yield.<sup>182,183</sup> Treatment of **S64-2** with *tert*-butyl hydroperoxide results (similarly as for **S65-2**) in the contraction to a fused benzene ring yielding *meso*-tetraarylbenzocarbaporphyrin **S64-1** and its 2<sup>1</sup>- or 2<sup>2</sup>-formyl-substituted derivatives.<sup>182,183</sup> The contraction of the seven-membered ring and Rothemund-like condensation are feasible because of the specific electronic structure of azulene. Azulene is more nucleophilic on its five-membered ring – leading to its ability to undergo a macrocyclic condensation reaction similarly to pyrrole. On the other hand, the seven-membered ring is more electrophilic, thus, prone to nucleophile attacks. It leads to a ring contraction and the formation of benzocarbaporphyrin and its derivatives with a formyl group



Scheme 66 Synthesis of 23-hetero-, 22,23-dihetero- and regular benzocarbaporphyrins from carbatripyrrin **S66-1**. Respective 23-heteroazuliporphyrin **S66-5**.

(formed from the extruded carbon atom) located on a fused benzo-ring.

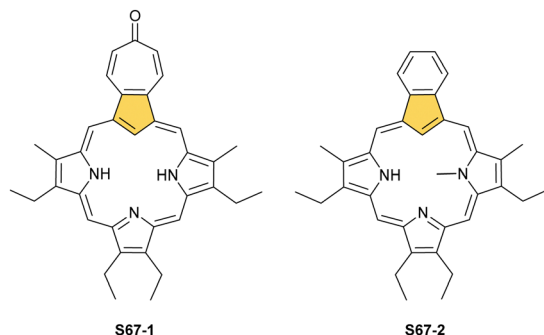
These relationships between **S64-1/S64-2** and **S65-1/S65-2** as well as the intrinsic properties of azuliporphyrin itself are important for encountered coordination abilities in both types of carbaporphyrinoids. Generally, benzocarbaporphyrins **S64-1/S65-1** demonstrate the spectroscopic and structural features of aromatic porphyrinoids, as confirmed with a H(21) chemical shift of  $-5.3$  ppm for a *meso*-substituted derivative.<sup>182</sup> In contrast to **S64-1/S65-1**, azuliporphyrins **S64-2/S65-2** provide a case of borderline aromaticity,<sup>182,184,185</sup> with a formally disrupted  $\pi$ -delocalization pathway. The resonance contributors of **S64-2/S65-2** with charge separation favouring the positive charge accumulation over the seven-membered ring are responsible for the residual aromatic features. This is apparent after the protonation of **S64-2**. The inner H(21) shifts from 3.3 to  $-0.5$  ppm.<sup>182</sup>

Analysing the potential coordination properties, one can notice that **S64-1/S65-1** and **S64-2/S65-2** complementarily resemble tautomers of N-confused porphyrins – **S1-2** and **S3-1**. Therefore, benzocarbaporphyrins **S64-1/S65-1** can act as trianionic macrocyclic ligands (C(21)H, N(22)H, and N(24)H dissociable protons), whereas azuliporphyrins **S64-2/S65-2** acquire the dianionic form (C(21)H and N(23)H dissociable protons). An adjustment of the anionic charge of the core delivers a substantial driving force for the contraction of the azulene fragment to suitably stabilise specific coordination motifs.<sup>179,186</sup> The total anionic charge of a macrocyclic crevice can be rationally modified *via* replacing one or more pyrrole rings with a heterocycle, *e.g.* thiophene, incorporating a heteroatom instead of an NH (see Scheme 66).<sup>179,180,187,188</sup>

Tropone-fused carbaporphyrin **S67-1** (Scheme 67) was generated in the typical procedure originally aimed to form 2<sup>3</sup>-methoxyazuliporphyrin.<sup>189</sup> The process involves a classical







Scheme 67 Tropone-fused carbaporphyrin **S67-1** and 22-methyl-benzocarbaporphyrin **S67-2**.

[3+1] condensation of methoxyazulitripyrrane and pyrrole dialdehyde. Presumably, the spontaneous demethylation affords the transient 2<sup>3</sup>-hydroxyazuliporphyrin, which transforms into isomeric tropone-fused carbaporphyrin **S67-1**. The molecule preserves the structural frame of azuliporphyrin but acts as a trianionic aromatic ligand resembling benzocarbaporphyrin, including its aromatic  $\pi$ -delocalization pathway.

It is essential to note that the nature of the coordination cavity can be modified by appropriate inner core substitution. The cavity of azuliporphyrin was significantly altered when 2-substituted azulene was used for condensation. 21-Alkyl-azuliporphyrin lacks removable H(21) in the cavity, suffering as well from the imposed increased crowdedness.<sup>177</sup>

In the case of **S64-1/S65-1**, the inner C(21) position was modified in a reaction with FeCl<sub>3</sub> in methanol.<sup>190</sup> The conditions lead to the dimethoxy substitution of the inner carbon atom. The direct inner core alkylation was also explored as the controlling means. Alkyl iodide mixed with **S65-1** in a base presence results in preferential N(22) alkylation yielding 22-methyl-benzocarbaporphyrin **S67-2**.<sup>191</sup>

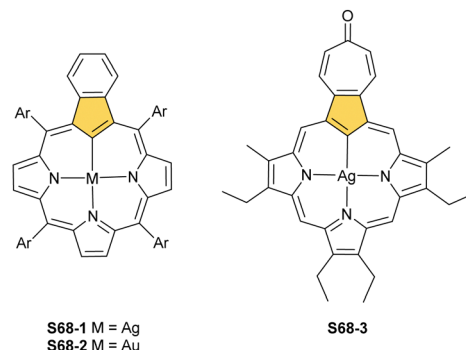
The coordination environments of mentioned benzocarbaporphyrinoids make them natural platforms for performing fascinating organometallic transformations.

### Coordination of fused 21-carbaporphyrins

An occurrence of a C(21) atom in the inner cavity of benzocarbaporphyrins **S65-1** and **S64-1** or azuliporphyrins **S65-2** and **S64-2** is crucial for the arrangement of suitable [CNNN] surroundings.

Consistent with their prearranged cores, the coordination of “classical” coordination probes, *i.e.*, metal(II) cations, is favoured by azuliporphyrins, whereas the coordination of metal(III) cations seems to be preferred by benzocarbaporphyrins.

Thus, benzocarbaporphyrin treated with silver(I) acetate efficiently forms silver(III) benzocarbaporphyrin **S68-1** (Scheme 68),<sup>192</sup> compared to unsuccessful trials with trifluoroacetate salt.<sup>193</sup> Silver(III) benzocarbaporphyrin **S68-1** reproduces the essential structural features of analogous silver(III) N-confused porphyrin **S25-1**, including the formation of a direct Ag–C(21) bond. A similar procedure affords gold(III) benzocarbaporphyrin **S68-2**. Gold(I) iodide acts poorly as a gold source;

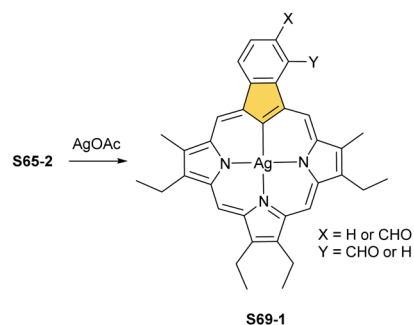


Scheme 68 Silver(III) and gold(III) complexes of benzocarbaporphyrin and silver(III) tropone-fused carbaporphyrin.

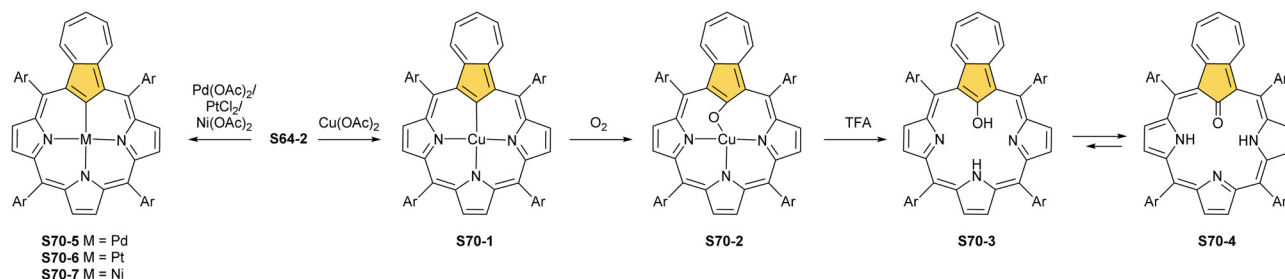
thus, gold(III) acetate is preferred. Interestingly, a *meso*-substituted derivative **S64-1** occurred to be superior when compared to  $\beta$ -substituted derivatives due to the side reactivity of **S65-1**, which was not observed in the course of silver(III) insertions. The same organometallic silver(III) environment can be achieved using a benzo homologue of **S65-1**, *i.e.*, naphtho[2,3-*b*]carbaporphyrin.<sup>194</sup> A respective complex could also be obtained for another 3H macrocycle yielding silver(III) tropone-fused carbaporphyrin **S68-3**.<sup>189</sup>

In attempts to insert silver(III) ions into azuliporphyrin **S65-2**, the profound transformation of the original carbaporphyrinoid scaffold was discovered (Scheme 69). Thus, silver(III) benzocarbaporphyrin **S69-1** and its formyl-substituted derivatives were unambiguously identified in this process.<sup>186</sup> Presumably, initial coordination of a silver(III) ion within **S65-2** induces contraction of the seven-membered ring, forming eventually a benzocarbaporphyrin framework which could naturally stabilise a tricationic centre. It was speculated that the silver(III) species mediates the activation and attack of an active oxygen species on the azulene ring. Several insertion trials into **S65-2** using various gold sources did not give any insertion or insertion and contraction products.

A similar dioxygen activation, as reported for silver species, could be expected for its lighter counterpart – copper. In this case, however, the activation occurs during the treatment of azuliporphyrin **S64-2** with copper(II) acetate.<sup>195</sup> The product isolated in the reaction contains an oxygen atom inserted between the metal centre and the C(21) atom (**S70-2**).



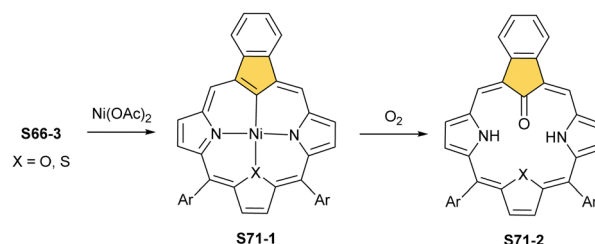
Scheme 69 Silver(III) benzocarbaporphyrin **S69-1** and its formyl-substituted derivatives.



Scheme 70 Synthesis of azuliporphyrin complexes with various metal(II) cations.

The electronic structure of **S64-2/S65-2** strongly disfavours the  $C(sp^3)$  configuration of the inner C(21) atom in contrast to those of **S64-1/S65-1** and N-confused porphyrin **S1-2**. The oxygenated ligand trapped in **S70-2** acquires a structure related to 21-hydroxyazuliporphyrin as suggested by the close to phenolic-like C(21)–O(21) bond distance of 1.302(3) Å. The incorporated oxygen bridge pushes the C(21) atom away from the metal centre (C(21)···Cu distance is 2.474(2) Å) and the azulene fragment is significantly canted with respect to the porphyrin mean [18]annulene plane. Considering an affinity of the metal(II) cation to azuliporphyrin, it is justified to assume that the formation of a regular complex of  $Cu^{II}$  with an organometallic bond precedes the formation of **S70-2**. Such a hypothesis was tested and indeed, under strictly anaerobic conditions, without an excess of the copper(II) source, appropriate species **S70-1** (Scheme 70) is obtained.<sup>196</sup> This elusive, very reactive form, trapped by EPR spectroscopy, transforms into **S70-2** as soon as exposed to dioxygen, reflecting the incorporation of an oxygen atom into the extremely sensitive  $Cu^{II}$ –C(21) bond. The acidic demetallation of **S70-2** afforded 21-hydroxyazuliporphyrin **S70-3**, but in solution, its oxo tautomer **S70-4** (identified in the solid state – C(21)=O 1.268(3) Å) prevails.<sup>197</sup> Subsequently, **S70-4** was used as a dianionic macrocyclic ligand for other metal ions, for example, nickel(II), palladium(II), and platinum(II).<sup>197</sup> As discussed above, regular azuliporphyrins form typical [CNNN] organometallic complexes with various metal(II) cations. Thus, a reaction with metal(II) acetate or chloride (in the case of platinum) in DMF provides the stable complexes of respective ions [e.g., **S70-5** for palladium(II)].<sup>198</sup> The  $M^{II}$ –C(21) distances of 1.896(3) Å for nickel(II) and 1.980(3) Å for palladium(II) clearly indicate the successful deprotonation and formation of an organometallic bond.

23-Heterobenzocarbazoporphyrin **S66-3** possesses the same number of dissociable inner protons as regular azuliporphyrin **S64-2/S65-2** and is expected to preferentially accommodate metal(II) cations. The nickel(II) and palladium(II) reactivities are similar, provided that the reaction with the former is conducted under anaerobic conditions.<sup>199</sup> The heating of the obtained complex **S71-1** (Scheme 71) under aerobic conditions leads to the oxygenation of the inner C(21) atom and demetallation of the macrocycle to give a 23-hetero-21-oxobenzocarbazoporphyrin **S71-2**. 23-Tellurabenzocarbazoporphyrin also forms a stable palladium(II) complex, in contrast to the stability of the macrocycle

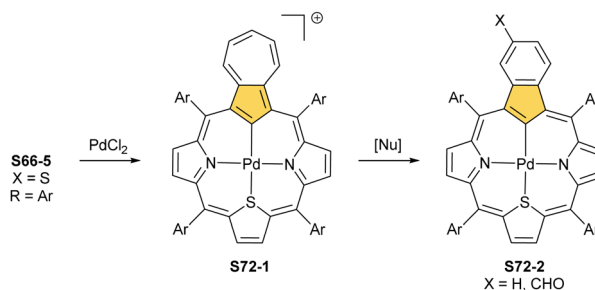


Scheme 71 Synthesis of nickel(II) 23-heterobenzocarbazoporphyrin and its reactivity with dioxygen.

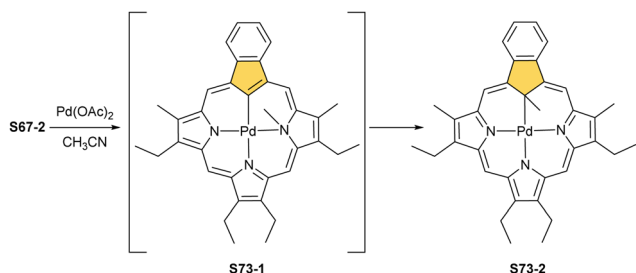
itself.<sup>180</sup> In it, the tellurophene ring is reactive towards dioxygen forming a derivative with a hydroxyl group attached (forming an internal Te–OH motif) resembling 21-telluraporphyrin reactivity.<sup>200</sup>

Interestingly, palladium(II) 23-thiabenzocarbazoporphyrin **S72-2** can also be obtained when 23-thiaazuliporphyrin with one inner proton [H(21)] is used in the insertion reaction.<sup>179</sup> The primarily obtained  $Pd^{II}$  complex (**S72-1**) (Scheme 72) acquires square-planar geometry and is cationic because of the charge imbalance. This enforces the participation of resonance contributors with charge accumulated over the seven-membered ring, rendering it prone to nucleophilic attacks and, consequently, contraction.

An interesting transformation occurs during palladium(II) insertion into N(22)-methylated benzocarbazoporphyrin **S67-2**. When heated briefly with palladium(II) acetate in acetonitrile, the ligand produces an expected insertion product (**S73-1**) (Scheme 73), yet as a minor fraction.<sup>201</sup> The major product was identified as palladium(II) 21-methylbenzocarbazoporphyrin **S73-2** (Fig. 17), which forms from initially generated **S73-1**.



Scheme 72 Synthesis of palladium(II) 23-heteroazuliporphyrin and its nucleophile-induced contraction.



Scheme 73 Methyl group migration after palladium insertion into methylated benzocarbaporphyrin **S67-2**.

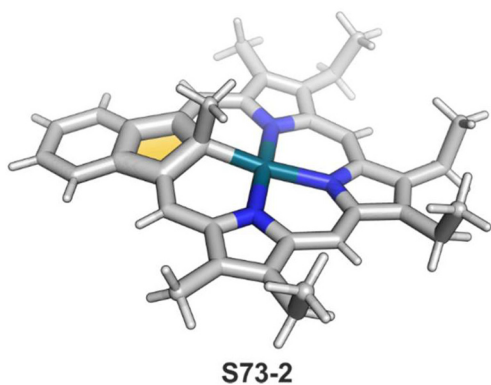
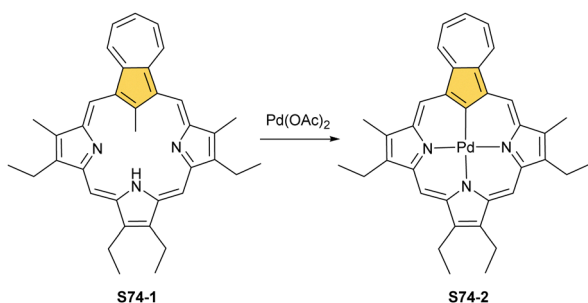


Fig. 17 Palladium(II) C(21)-methylated benzocarbaporphyrin.



Scheme 74 Palladium(II) insertion into 21-methylazuliporphyrin.

Thus, N(22)-methyl migrates to the inner C(21) atom and creates the C(sp<sup>3</sup>) donor centre eventually, as reflected by the

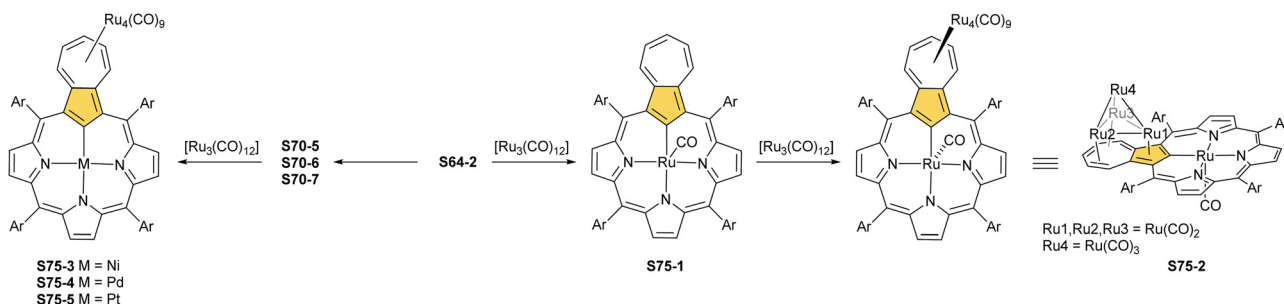
C(21) characteristic chemical shift of 45.3 ppm in <sup>13</sup>C NMR spectra. A similar transformation occurs for 23-methylbenzocarbaporphyrin, yet the process is significantly slower, suggesting the increased number of methyl relocation steps which are required for the passage to **S73-2**.<sup>191</sup>

21-Methylazuliporphyrin **S74-1** (Scheme 74) was treated with palladium(II) acetate affording solely the product of C-demethylation **S74-2**, synthesised previously in regular insertion into azuliporphyrin **S65-2**.<sup>177</sup> The inner core charge of transient palladium(II) 21-methylazuliporphyrin is not sufficient to stabilise divalent metal ions and the C(21) atom could not adopt the necessary C(sp<sup>3</sup>) hybridisation.

As shown for several metal(II) cations, the [C<sub>4</sub>NNN] coordination cavity of azuliporphyrins facilitates the generation of M–C σ-bonding. Significantly, it was encountered that the azulene moiety in the metal(II) azuliporphyrin provides a specific, suitable π-surface which reveals a distinct affinity to accommodate ruthenium(0) clusters, including Ru<sub>4</sub>(CO)<sub>9</sub>. Azulene incorporated into the azuliporphyrin **S64-2** scaffold constitutes an independent organometallic centre.<sup>35</sup> Two conceptually different organometallic motifs are merged in a unique three-dimensional architecture. It was documented that these particular coordination abilities of azulene introduced into a carbaporphyrinoid frame are preserved in other suitable systems producing a series of bimetallic complexes [M(**S64-2**)(Ru<sub>4</sub>(CO)<sub>9</sub>)], in which M = Ni, Pd, Pt, Ru, or Co.<sup>35,196</sup>

A reaction between [Ru<sub>3</sub>(CO)<sub>12</sub>] and azuliporphyrin **S64-2** leads primarily to the insertion of a ruthenium(II) ion into the [C<sub>4</sub>NNN] cavity to yield ruthenium(II) azuliporphyrin **S75-1** (Scheme 75), which involves the formation of a direct Ru–C(21) bond. The reaction does not stop there and, in the presence of an excess of [Ru<sub>3</sub>(CO)<sub>12</sub>], hybrid **S75-2** forms (Fig. 18). The formed Ru<sub>4</sub>(CO)<sub>9</sub> cluster possesses a tetrahedral ruthenium scaffold and coordinates to both the 5-membered and 7-membered rings of the azulene moiety through the three basal ruthenium atoms (Ru1, Ru2, and Ru3).

The coordination can be correlated with significantly upfield-shifted proton and carbon signals (H(2<sup>3</sup>) shifts for 4.80 ppm). The molecular structure shows a significant bending of the azulene moiety to efficiently accommodate the cluster, while the Ru<sup>II</sup>–C(21) distance remains in a regular binding range (2.017(6) Å for **S75-1** with sixth, axial N,N'-dimethylaminopyridine ligand and 2.039(9) Å for **S75-2**). Besides intriguing organometallic chemistry, **S75-2** demonstrates the



Scheme 75 Reactivity of azuliporphyrin **S64-2** and its metal(II) complexes with [Ru<sub>3</sub>(CO)<sub>12</sub>].



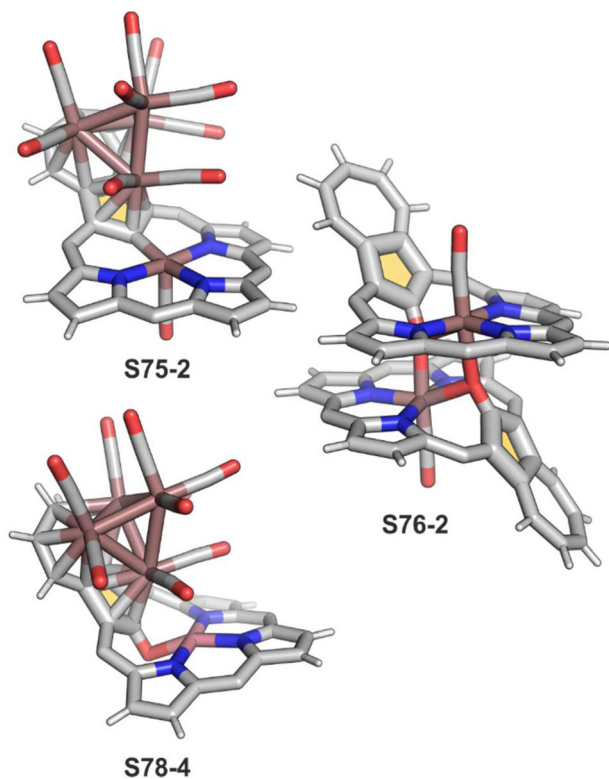
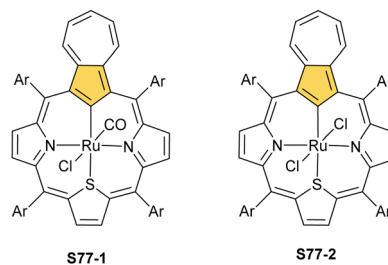


Fig. 18 Azulene- and cavity-ruthenium-coordinated azuliporphyrins. meso-Substituents not shown.

special geometric features enabling the forced proximity of metal ions: the ruthenium(II) centre located in the [C<sub>4</sub>NNN] cavity and the ruthenium(0) atom coordinating the five-membered ring (Ru1). Their contact is much shorter than the van der Waals radius sum (the Ru<sup>II</sup>...Ru<sup>0</sup> distance in **S75-2** is 3.1596(18) Å vs. 2.9–2.7 Å within the Ru<sub>4</sub> cluster), indicating possible intermetallic interactions. If at least one axial position of a coordination centre is unoccupied, then the other hybrids may potentially form. Accordingly, a series of bimetallic complexes **S75-3**, **S75-4**, **S75-5**, and **S78-2** were synthesised, taking as substrates regular nickel(II), palladium(II), platinum(II), and cobalt(II) azuliporphyrins.

Regular ruthenium(II) azuliporphyrin **S75-1** demonstrates an additional reactivity as well. The Ru–C(21) bond is quite stable, yet in time, in the presence of dioxygen, especially in a heated solution, **S75-1** transforms into **S76-1** (Scheme 76) at the oxygenated C(21) position.<sup>202</sup> The formed complex exists in



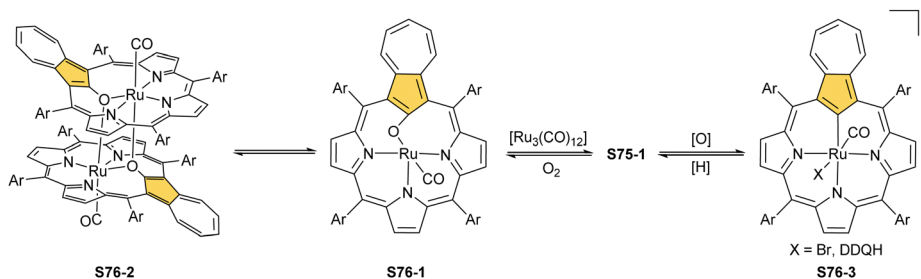
Scheme 77 Ruthenium(II) 23-thiaazuliporphyrin **S77-1** and ruthenium(III) 23-thiaazuliporphyrin **S77-2**.

equilibrium with its dimer **S76-2** in solution (Fig. 18), as long as no potential axial ligand (*e.g.*, pyridine) is present. The C(21)···Ru distance increases to 2.523(13) Å in a complex with a sixth axial *n*-butanol ligand and the length of a seemingly single C–O bond is 1.314(16) Å.

The oxygen bridge of **S76-1** or **S76-2** can be removed in reduction with [Ru<sub>3</sub>(CO)<sub>12</sub>] to recover **S75-1**. On the other hand, **S75-1** can get one-electron oxidised to an organoradical **S76-3** with spin density noticeably distributed over the azulene's seven-membered ring.

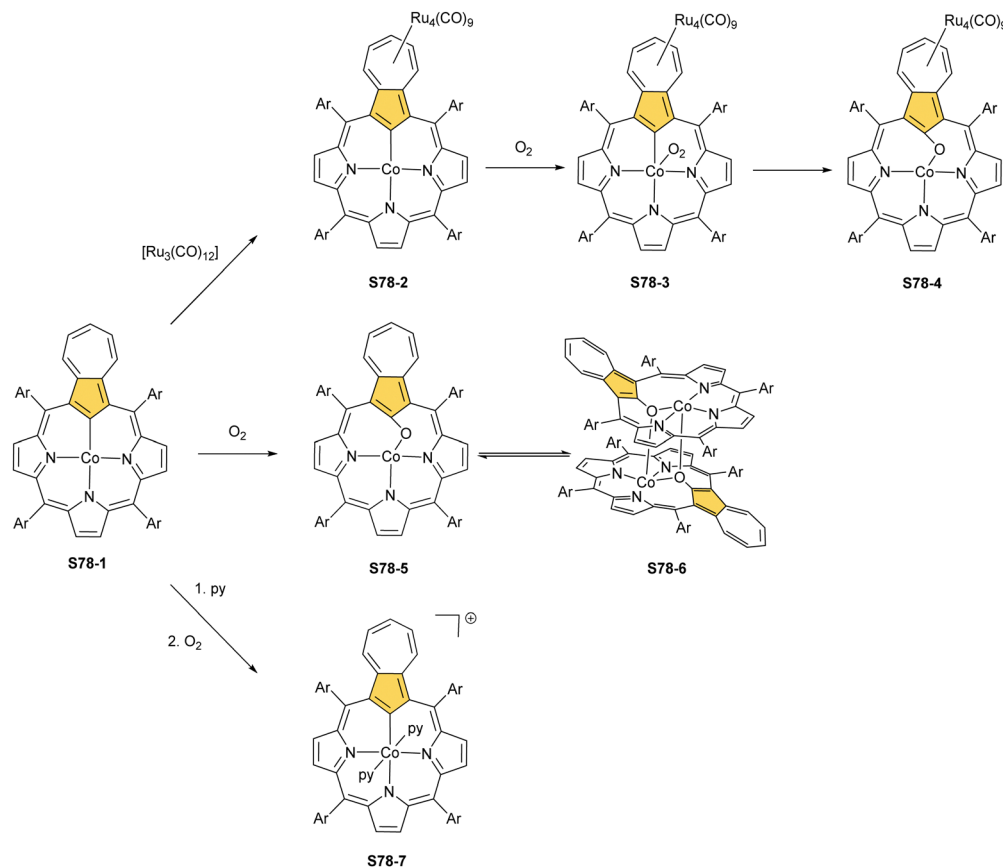
Ruthenium(II) 23-thiaazuliporphyrin **S77-1** (Scheme 77) can neither form a cluster nor a radical since the sixth coordination site is occupied with a chloride ligand.<sup>179</sup> It can be obtained from a reaction with a range of ruthenium sources, including [RuCl<sub>2</sub>X]<sub>2</sub>, in which X is an additional π-ligand (cyclooctadiene (cod) or *p*-cymene). This implies the formation of the axial carbonyl ligand, present in the final product, during the insertion reaction. Yet, an attempt to synthesise the complex from different ruthenium compounds resulted, at times, in a second product, an alternative one-electron oxidised possibility – a ruthenium(III) complex with two axial chlorides (**S77-2**).

Regular cobalt(II) azuliporphyrin **S78-1** (Scheme 78) forms smoothly in a reaction of azuliporphyrin **S64-2** and cobalt(II) salts.<sup>196</sup> The complete insertion occurs, inferring the activation of the C(21)–H bond and the formation of a new one, Co<sup>II</sup>–C(21), with a length of 1.930(2) Å. Treatment of **S78-1** with triruthenium dodecacarbonyl [Ru<sub>3</sub>(CO)<sub>12</sub>] yields the paramagnetic Co–Ru<sub>4</sub> hybrid **S78-2**. Interestingly, this low-spin cobalt(II) complex can coordinate a dioxygen molecule (**S78-3**), which intramolecularly oxygenates the organometallic Co–C(21) bond, forming **S78-4**.



Scheme 76 Reactivity of ruthenium(II) azuliporphyrin **S75-1**.



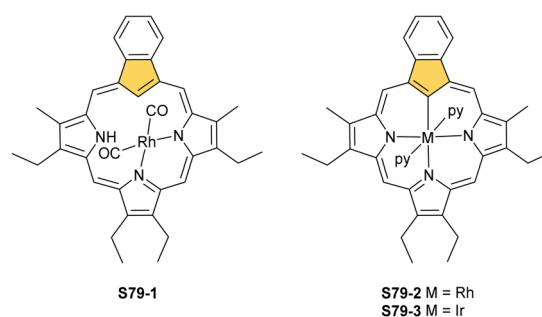
Scheme 78 Reactivity of cobalt(II) azuliporphyrin **S78-1**.

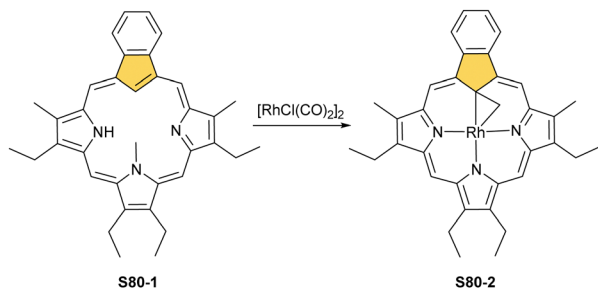
Due to the incorporation of the oxygen bridge in **S78-4**, the azulene moiety is even more deflected from the porphyrin plane, which forces even closer contact between metal centres, compared to **S78-2**, with a  $\text{Co}^{\text{II}} \cdots \text{Ru}^0$  distance of 2.9799(12) Å (Fig. 18). Meanwhile, the  $\text{Co} \cdots \text{C}(21)$  distance measures 2.364(8) Å. The  $\text{C}(21)\text{--O}$  bond length is 1.288(8) Å, situating it on a border between the single and double bonds. Perhaps, it is one of the reasons for the relatively close distance of the metal centre to the C(21) atom. The low-spin cobalt(II) species **S78-4** coordinates a dioxygen molecule but without any further reactivity observed. **S78-1** gets oxygenated even faster (probably a cluster in **S78-2** performs a sterically protective role) to form **S78-5**, which can dimerise (**S78-6**), similarly to the respective ruthenium(II) complex (**S76-1** into **S76-2**). The  $\text{C}(21)\text{--O}$  distance is 1.303(4) Å and the  $\text{Co}^{\text{II}} \cdots \text{C}(21)$  separation equals 2.730(4) Å, far greater than in **S78-1**, but it is also significantly more distant than in a hybrid complex **S78-4** (2.363(7) Å). Monomeric **S78-5** and, in particular, dimeric **S78-6** reveal spectroscopic features that clearly indicate the high-spin cobalt(II) ground electronic state.

This observation provides proof of a significant alteration of the overall electronic structure of Co–Ru hybrids in comparison to regular cobalt(II) azuliporphyrin. Dimer **S78-6** is readily cleaved into monomeric subunits by pyridine addition which competes for the axial position. The addition of pyridine to **S78-1** under strictly anaerobic conditions followed by exposure to

dioxygen results eventually in one-electron cobalt(II) to cobalt(III) oxidation and diamagnetic organocobalt(III) **S78-7** is formed. Analogously to a cationic  $\text{Pd}^{\text{II}}$  complex **S72-1**, **S78-7** demonstrates increased aromaticity due to its cationic nature.

A similar complex forms in the insertion of the heavier congener of cobalt–rhodium. At first, a reaction of benzocarporphyrin with  $[\text{RhCl}(\text{CO})_2]_2$  yields a rhodium(I) complex **S79-1** (Scheme 79).<sup>203</sup> This asymmetric species binds the  $\text{Rh}(\text{CO})_2$  moiety through N(22) and N(23) in the typical side-on fashion. It does not have a direct  $\text{Rh}\text{--C}(21)$  bond and the relevant distance equals 3.1775(12) Å. When **S79-1** is heated in pyridine, oxidation to rhodium(III) occurs with parallel incorporation of

Scheme 79 Rhodium(I)/(III) and iridium(III) complexes of  $\beta$ -alkylated benzocarporphyrin.



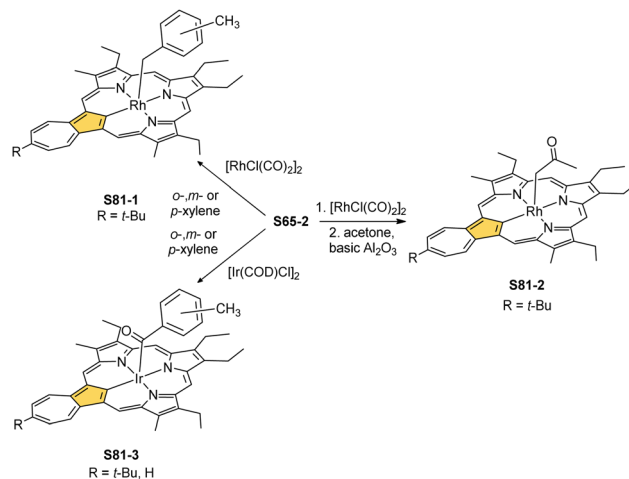
**Scheme 80** Rhodium insertion into 23-methylbenzocarbaporphyrin **S80-1**, yielding rhodium(III) 21-methylbenzocarbaporphyrin with a rhodacyclopropane motif **S80-2**.

rhodium(III) into the [CNNN] crevice of **S79-2**. This naturally narrows the Rh–C(21) distance to 1.988(2) Å. The analogous iridium(III) benzocarbaporphyrin **S79-3** was produced *via* the treatment of **S65-1** with an appropriate iridium(I) source. The same reactivity was also observed for naphthocarbaporphyrin.<sup>204</sup> Internally methylated benzocarbaporphyrin was tested in the search for the organometallic environment of rhodium(III).<sup>191</sup>

When 23-methylbenzocarbaporphyrin **S80-1** (Scheme 80) is heated in toluene with the rhodium(I) source, a methyl group migration occurs, resembling the palladium(II) 22-methylbenzocarbaporphyrin **S73-1** behaviour. Finally, the methyl group lands at the C(21) position, yielding transient rhodium(III) 21-methylbenzocarbaporphyrin perfectly prearranged for the next step in this peculiar process. Thus, the rhodium(III) in the structurally forced adjacency to C(21)–Me activates one of the C–H methyl bonds and forms a rhodacyclopropane motif of **S80-2**. The methylene bridge enforces a rehybridisation of the C(21) atom. The coordination of the methylene group does not replace but rather supplements the C(21) atom coordination. Both Rh–C(21) and Rh–C<sub>Me</sub> distances are similar, being slightly longer for the in-plane bond to C(21) (2.1329(11) Å *vs.* 1.9932(11) Å to C<sub>Me</sub>). This specific C–H activation leads to a neutral complex stabilising rhodium(III) in the crevice.

Rhodium insertion into **S62-2** can bring another yet related product during prolonged heating with xylene isomers.<sup>205</sup> Regardless of the xylene isomer, the insertion is accompanied by activation of xylene methyl groups, followed by axial coordination, yielding **S81-1** (Scheme 81 and Fig. 19). This allows for Rh<sup>III</sup> stabilisation within azuliporphyrin with two starting inner protons. The distance from Rh<sup>III</sup> to C(21) (1.966(3) Å) is similar to the one from the methylene group in the axial position (2.073(4) Å). Interestingly, a similar procedure with toluene failed to produce an analogue of **S81-1** (presumably because of a too-low boiling point of toluene when compared to xylene).

Yet, activating a methyl group in acetone is possible when the initial insertion is carried out in acetonitrile and the formed rhodium azuliporphyrin is directly transferred into a mixture of acetone and toluene to afford **S81-2**, especially under basic conditions. The treatment of azuliporphyrin **S65-2** with  $[\text{IrCl}(\text{COD})]_2$  in xylenes leads to solvent activation as well. The



**Scheme 81** Rhodium and iridium insertion into  $\beta$ -alkylated benzocarbaporphyrin in xylene isomers or acetone/toluene mixture.

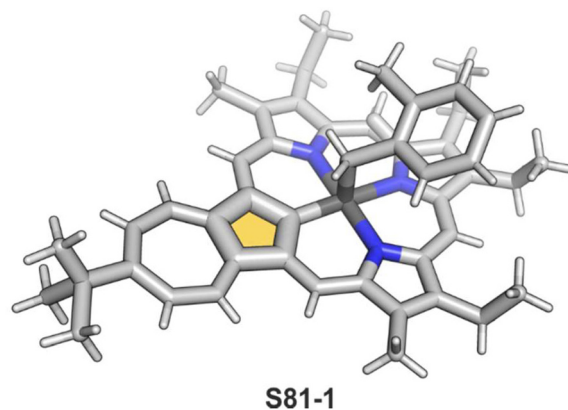


**Fig. 19** Axial and equatorial organometallic rhodium(III) complexes of azuliporphyrin.

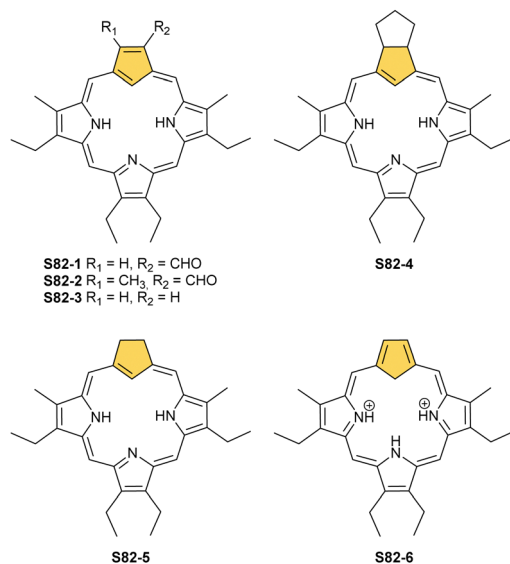
solely isolated iridium(III) azuliporphyrin **S81-3** incorporates the axially coordinated methylbenzoyl ligand presumably formed by the oxygenation of the originally linked  $\sigma$ -methylbenzyl unit. Here, again, both organometallic bonds are of similar distance (Ir–C(21): 1.985(7) Å and Ir–C(=O): 1.981(7) Å). A similar insertion trial conducted in toluene did not provide any metalated derivative.

## Fundamental 21-carbaporphyrin

The exploration of carbaporphyrin chemistry, reported in the previous sections, brought us to the most fundamental motif one could imagine to be explored in organometallic chemistry encompassed in a porphyrinic framework, namely 21-carbaporphyrin (**S1-3**). Here, one of the inner nitrogen atoms is simply replaced with a carbon atom.

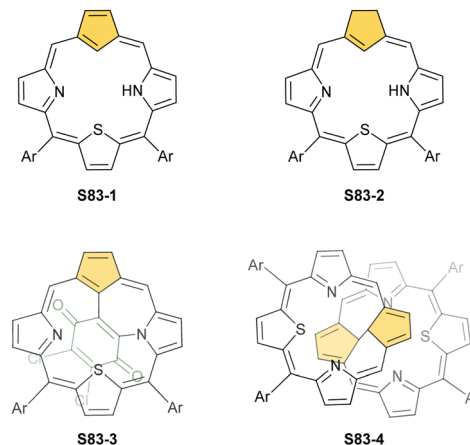
21-Carbaporphyrin, sometimes called true carbaporphyrin, was first reported as a  $\beta$ -substituted derivative. In fact, the publication occurred soon after N-confused porphyrin, but till present, this subfield remains to be extensively investigated.



Scheme 82  $\beta$ -Alkylated 21-carbaporphyrinoids.

This state may be related to demanding synthetic pathways which afford **S82-1/S82-2/S82-3** (Scheme 82), or **S1-3**. Thus, the first 21-carbaporphyrin **S82-1/S82-2** was reported in 1996 by Berlin.<sup>206</sup> The reaction of triformylcyclopentadiene with tripyrrane in the presence of HBr/glacial acetic acid as the catalyst gives 2-formyl-21-carbaporphyrins **S82-1** and **S82-2** in 7.8% and 6.5% yields, respectively. The synthesis and characterisation of **S82-1** were refined in 1997 by Lash and Hayes.<sup>207</sup>

Macrocycle **S82-1** (and other similar derivatives) is fully aromatic, as clearly indicated by the  $-7.23$  ppm chemical shift of the inner H(21) atom. The preliminary metallations with zinc(II) and nickel(II) were described as unsuccessful.<sup>206</sup> Another molecule reported in a path to 21-carbaporphyrins is 21-carbachlorin isolated initially as the derivative, which incorporates an additional fused five-membered ring **S82-4**.<sup>208</sup> A version with a non-substituted five-membered ring (**S82-5**) was also reached after the suitable carbocycle substrate redesign.<sup>209</sup> **S82-5** is formed in the [3+1] MacDonald condensation using 3-ethoxymethylenecyclopentene-1-carbaldehyde and tripyrrane catalysed by TFA. The subsequent oxidation with aqueous ferric chloride solution results in **S82-5** with an 11–16% yield. The subsequent careful oxidation of **S82-5** with one equivalent of DDQ affords  $\beta$ -alkylated-21-carbaporphyrin **S82-3** with a remarkable outcome (70%). The facile diprotonation of **S82-5** produces a dication **S82-6**, which accommodates the additional protons at the single available pyrrolic nitrogen atom and – noticeably – at the rehybridised tetrahedral C(21) atom. The dication preserves the strong diatropic character of maternal **S82-3**, as reflected by the  $^1\text{H}$  chemical shift of C(21)H<sub>2</sub> ( $-8.27$  ppm). A 21-chlorinated derivative of **S82-5** has also been obtained.<sup>210</sup> In this case, the subsequent oxidation with DDQ results in dechlorinated **S82-3** and its derivatives in which  $R_1$  and/or  $R_2$  get substituted with chlorine atoms (2-chloro- or 2,3-dichloro-21-carbaporphyrins). In general,  $\beta$ -alkylated 21-carbaporphyrins **S82-1/S82-2/S82-3** bear some resemblance to widely used octaethylporphyrin.



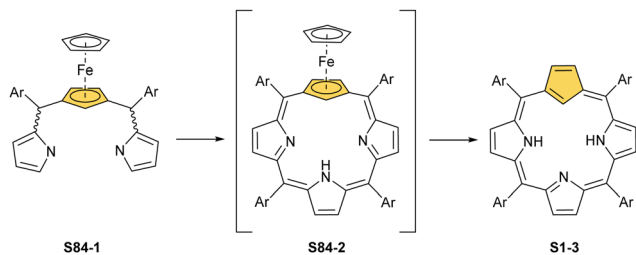
Scheme 83 21-Carba-23-thiaporphyrin derivatives.

A significant synthetic effort was also devoted to creating *meso*-substituted 21-carbaporphyrins, which resemble, at least in their general scaffolds, extensively explored *meso*-tetraarylporphyrins. Chronologically, this area has been initialised by the synthesis of 10,15-dimesityl-21-carba-23-thiaporphyrin **S83-1** (Scheme 83), and its reduced congener **S83-2**.<sup>211</sup> The synthesis of carbachlorin **S83-2** involves the one-pot reaction of the mixture of the carba analogues of tripyrrane with 2,5-bis(mesitylhydroxymethyl)thiophene catalysed by  $\text{BF}_3 \cdot \text{Et}_2\text{O}$ , eventually followed by oxidation with *p*-chloranil (tetrachloro-1,4-benzoquinone). The subsequent careful oxidation of **S83-2** with only one equivalent of DDQ at room temperature gives **S83-1** with a 25% yield. The intriguing minor side-product **S83-3**, which incorporates a chloranil-derived fragment linked to the C(21) and N(22) atoms, was isolated as well. The macrocycles are aromatic, as reflected by the H(21) chemical shifts of  $-5.16$  and  $-4.79$  ppm for **S83-2** and **S83-1**, respectively.

In separate studies, another oxidation product was recognised, namely the C(21)–C(21') bridged dimer **S83-4**.<sup>212</sup> Bis(carbathiaporphyrin) **S83-4** was obtained with 46% yield by oxidation of **S83-1** with DDQ. The two-electron reduction of **S83-4** with zinc dust results in splitting the C(21)–C(21') bond, recovering the monomer **S83-1**. The reactivity of the incorporated cyclopentadiene ring has been noted. For instance, the outer rim [C(2), C(3)] fragment reacts with hydrochloride or hydrobromide, yielding doubly halogenated 21-carbachlorins. Similarly, oxygenation products were identified, which form during the protonation of a molecule with *ca.* 10 eq. of TFA.

The rational synthesis of *meso*-tetraaryl-21-carbaporphyrin **S1-3** was eventually reported.<sup>213</sup> As cyclopentadiene tends to be unstable and reactive, a tripyrrane derivative used in condensation contains a 1,3-ferrocenyl unit **S84-1** (Scheme 84). Thus, incorporating a cyclopentadiene moiety into the *meso*-tetraarylporphyrin framework results in **S1-3** with a suggested transient formation of ferrocenylporphyrins like **S84-2**. The molecular design of **S1-3** preserves all essential virtues of the original tetrapyrrolic architecture of *meso*-tetraarylporphyrin, including the perfect match between the ionic radii of an



Scheme 84 Synthesis of *meso*-tetraaryl-21-carbaporphyrin.

inserted metal and the size of the macrocyclic [C<sub>4</sub>NNN] core, as well as steric protection provided by thoughtfully chosen *meso*-aryl substituents. The molecule is aromatic, similar to  $\beta$ -substituted analogues **S82-1/S82-2/S82-3**. The characteristic H(21) chemical shift of aromatic **S1-3** equals  $-5.86$  ppm and changes to  $-6.26$  ppm after the formation of dication. Diprotonation of **S1-3** is accompanied by C(21)-centred protonation and the formation of a methylenic C(21)H<sub>2</sub> unit.

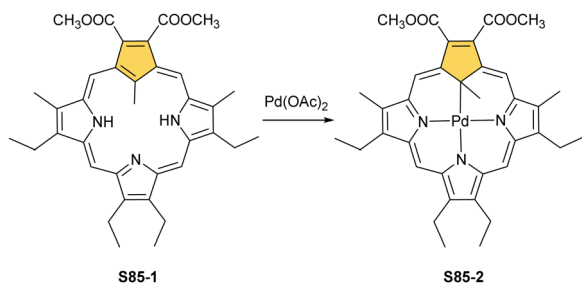
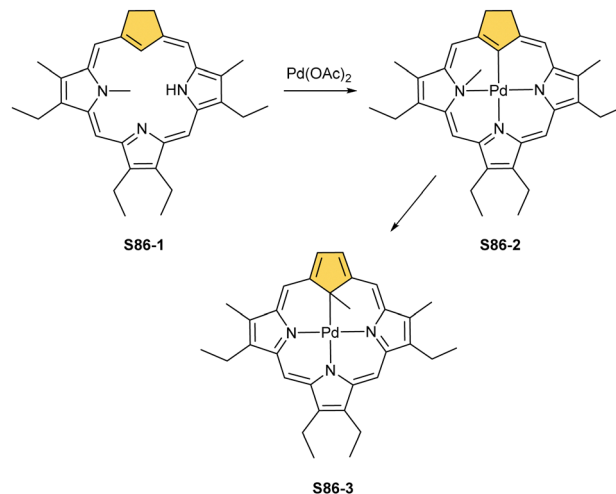
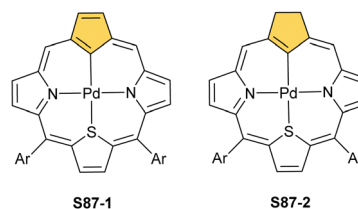
### Organometallic chemistry of 21-carbaporphyrins

**Insertion route.** One can readily notice that the coordination chemistry of 21-carbaporphyrins **S82-3** and **S1-3** consistently follows that previously presented for N-confused porphyrin or benzocarbaporphyrin analogues.

Palladium(II) seems to be a metal cation of choice to initially test the coordination properties of carbaporphyrinoids, including 21-carbaporphyrins.

The feasible rearrangements have been well illustrated, focusing on inner core methylated  $\beta$ -substituted 21-methyl-21-carbaporphyrin **S85-1** (Scheme 85) and 22-methyl-21-carbachlorin **S86-1** (Scheme 86). The insertion of palladium(II) into **S85-1** yields neutral **S85-2**.<sup>209,214</sup> The coordination enforced rehybridisation of the C(21) atom from a trigonal one to a tetrahedral one. The insertion of a palladium(II) ion into **S86-1** initially produces palladium(II) N(22)-methylated 21-carbachlorin **S86-2**. The insertion requires the inner C(21)–H bond activation. The subsequent step-wise migration of the methyl group, accompanied by oxidation, affords palladium(II) C(21)-methylated carbaporphyrin **S86-3**.<sup>209</sup>

21-Carba-23-thiaporphyrin **S83-1** and its counterpart **S83-2** are predestined to act as macrocyclic dianionic ligands because of a sulphur atom.<sup>211</sup> Both carbaporphyrinoids form palladium(II) complexes **S87-1** (Scheme 87) and **S87-2**. However,

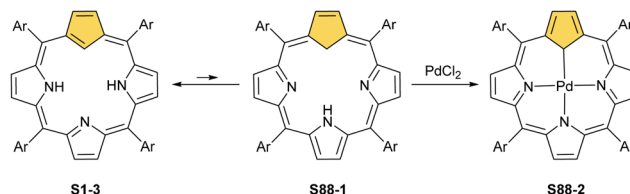
Scheme 85 Palladium insertion into  $\beta$ -substituted 21-methyl-21-carbaporphyrin **S85-1**.Scheme 86 Methyl group migration after palladium insertion into N(22)-methylated 21-carbachlorin **S86-1**.

Scheme 87 Palladium(II) complexes of 21-carba-23-thiaporphyrin and 21-carba-23-thiachlorin.

in these cases, in contrast to **S86-3** and **S85-2**, the organometallic bond is formed between the palladium(II) and  $sp^2$ -hybridised inner carbon centres.

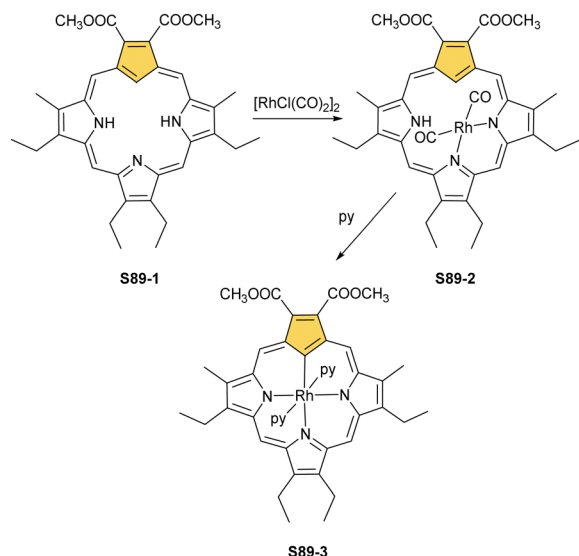
The typical palladium(II) insertion is effective for **S1-3** as well, forming complex **S88-2** (Scheme 88).<sup>213</sup> The coordination of palladium(II) stabilises the macrocyclic scaffold of the tautomer with  $sp^3$ -hybridised C(21), prone to act as a dianionic ligand. Silver(III), gold(III), and nickel(II) complexes of  $\beta$ -substituted carbaporphyrins and their C(21)- or N(22)-methylated derivatives were also reported.<sup>214</sup>

A reaction of **S89-1** (Scheme 89) with  $[\text{RhCl}(\text{CO})_2]_2$  brings, at first, the side-on rhodium(I) complex **S89-2** with two inner adjacent nitrogen atoms solely engaged in coordination.<sup>204</sup> **S89-2** can be heated in pyridine solution and be efficiently transformed into regular rhodium(III) 21-carbaporphyrin **S89-3**, acquiring the classical [C<sub>4</sub>NNN] binding surroundings.



Scheme 88 Synthesis of palladium(II) 21-carbaporphyrin.

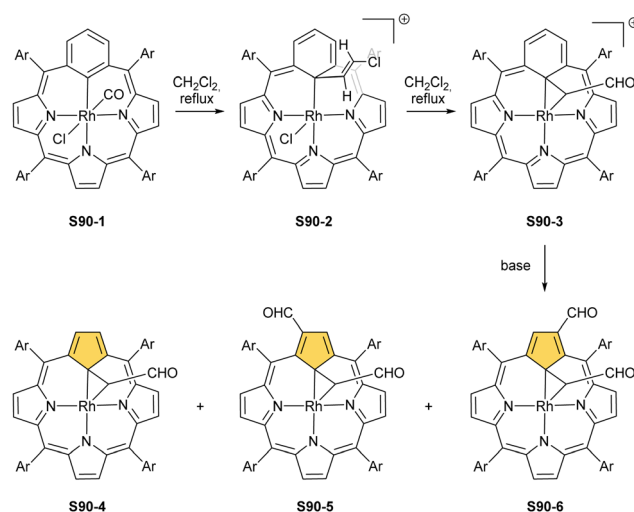




**Scheme 89** Synthesis of the rhodium(i) and rhodium(III) complexes of the  $\beta$ -substituted 21-carbaporphyrin derivative.

**Contraction routes.** The rational synthetic route to form *meso*-tetraaryl-21-carbaporphyrin **S1-3** was elaborated in 2019. In the rather peculiar and reversed course of typical synthetic routes, **S1-3** was trapped eight years earlier, acting as an organometallic macrocyclic ligand.<sup>27</sup> The molecule can be solely created and isolated in the presence of selected transition metal cations as metal(*n*) 21-carbaporphyrin. In general, the palladium(II), rhodium(III), and gold(III) ions stimulate contractions of *p*-phenylene in 5,10,15-20-tetraaryl-*p*-benziporphyrin or *m*-phenylene in 5,10,15-20-tetraaryl-*m*-benziporphyrins to cyclopentadiene yielding the very first complexes of **S1-3**. Evidently, this approach is far from general and is limited to certain transition metals. In addition, the demetallation of such complexes was unsuccessful.

Somewhat analogously to already described rearrangements of azuliporphyrin **S64-2/S65-2** into benzocarbaporphyrin **S64-1/S65-1**, *meso*-tetraaryl-*m*-benziporphyrin or the inner carbon-alkylated derivative undergo an extrusion of one of the *m*-phenylene outer carbon atoms, when coordinated with rhodium(III) or gold(III) ions.<sup>28,215,216</sup> In the first step, the reaction with  $[\text{RhCl}(\text{CO})_2]_2$  affords nonaromatic rhodium(III) *m*-benziporphyrin **S90-1** (Scheme 90) with a typical equatorial [C<sub>4</sub>NNN] surrounding of central metal ion to be accompanied by axially coordinated chloride and carbonyl ligands.<sup>28</sup> This species, when exposed to dichloromethane on a silica gel column under oxidative conditions, transforms into aromatic rhodium(III) *m*-benziporphyrin **S90-3**, which incorporates the rhodacyclopropane motif substituted with a formyl group. **S90-1** converts into **S90-3** during prolonged reflux in dichloromethane through an initial formation of **S90-2** containing a 2-chlorovinyl moiety generated from the solvent. **S90-2** and **S90-3**, when mixed with basic alumina, are immediately transformed into a mixture of rhodium(III) 21-carbaporphyrins **S90-4**, **S90-5**, and **S90-6**. The C(sp<sup>3</sup>) centre in **S90-4** binds to the Rh<sup>III</sup> ion



**Scheme 90** Reactivity of rhodium(III) *meta*-benziporphyrin **S90-1**.

(Rh–C(21), 2.116(7) Å) and, simultaneously, a carbon atom from a CHCHO substituent (Rh–C, 2.060(9) Å) forming a rhodacyclopropane motif (Fig. 20).

Consequently, the rhodium(III) and gold(III)-triggered transformations of a *m*-phenylene ring embedded in 22-alkyl-*m*-benziporphyrins were explored.<sup>215,216</sup> When **S91-1** (Scheme 91) is mixed with basic alumina or treated with selected basic reagents in solution (triethylamine, 2,4,6-trimethylpyridine), it quickly converts into a mixture of rhodium(III) 21-( $\mu$ -ethylidene)-21-carbaporphyrins **S91-2** and two diastereomers of rhodium(III) 2-formyl-21-( $\mu$ -ethylidene)-21-carbaporphyrin.

An exposure of **S91-2** to hydrogen chloride potentially results in the formation of rhodium(III) 21-ethylcarbaporphyrin **S91-3**. The thermodynamically reversible protonation is centred at the  $\mu$ -ethylidene substituent in **S91-2**. The protonation/deprotonation is convoluted with the cleavage/reformation of rhodacyclopropane. Subsequent two-electron oxidation of cationic **S91-3**

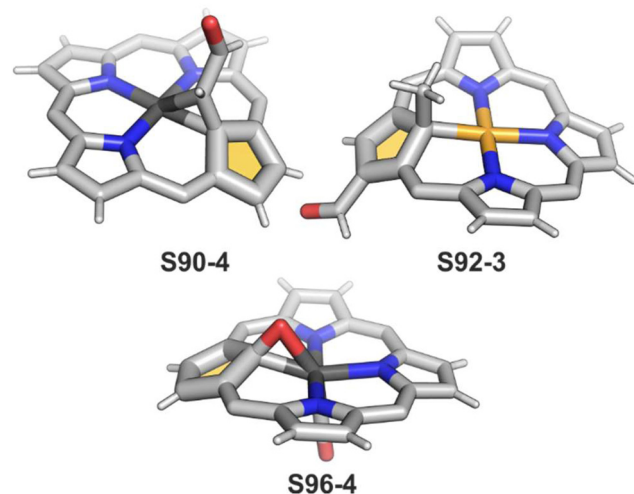
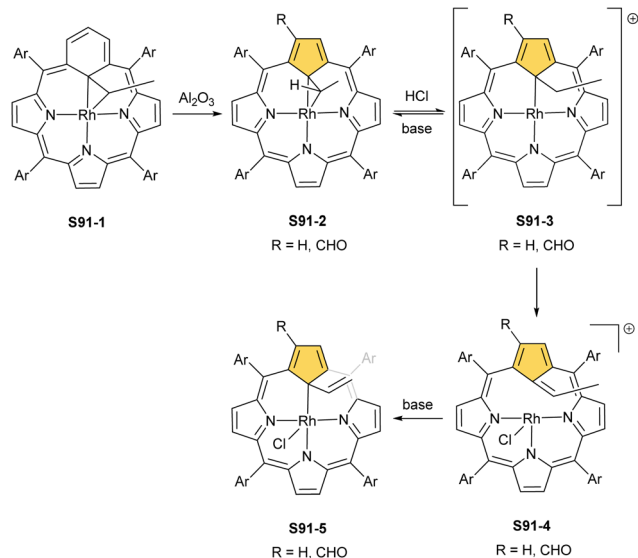


**Fig. 20** Contraction-derived carbaporphyrin complexes. *meso*-Substituents not shown.



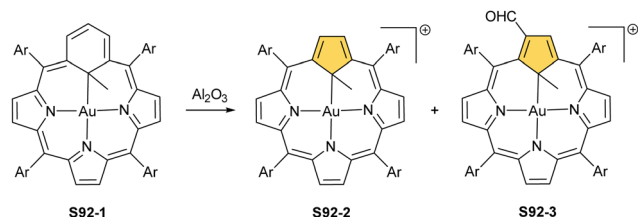


Scheme 91 Contraction of rhodium(III) 22-(μ-ethylidene)-*m*-benziporphyrin **S91-1**.

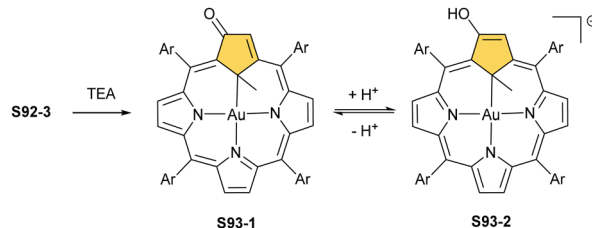
yields **S91-4**, which formally incorporates the 6-methylfulvene motif into the 21-carbaporphyrin frame. The side-on interaction between rhodium(III) and the C(21)=C(25) double bond of fulvene was suggested. The situation changes after adding a nitrogen base (e.g., Et<sub>3</sub>N) to the solution of **S91-4** as it activates isomerisation to rhodium(III) 21-vinylcarbaporphyrin **S91-5**.

Treatment of 22-methyl-*m*-benziporphyrin with sodium tetrachloroaurate(III) in dichloromethane results in quantitative transformation into gold(III) 22-methyl-*m*-benziporphyrin **S92-1** (Scheme 92). This species is chemically unstable and readily converts into a mixture of gold(III) 21-methyl-21-carbaporphyrins **S92-2** and **S92-3**.<sup>215</sup> In striking contrast, the insertion of gold(III) to regular *m*-benziporphyrin, carried out under similar conditions, produced solely unreactive gold(III) *m*-benziporphyrin. Thus, the inner alkylation of *m*-phenylene is a prerequisite for initiating the contraction.

As gold(III) coordination preferences differ from rhodium(III), the methyl group is not involved in direct binding with the gold(III) centre in **S92-1** or products of contraction (**S92-2** and **S92-3**). The feature is clearly indicated by the Au...C<sub>methyl</sub> distance of 2.868(13) Å as compared to that of 2.073(11) Å for Au–C(21) determined for gold(III) 2-formyl-21-methyl-carbaporphyrins **S92-3** (Fig. 20). The presence of the formyl group at the perimeter of **S92-3** allows for its peculiar transformation. In the presence of Et<sub>3</sub>N, the 2-formyl group in **S92-3** is



Scheme 92 Contraction of gold(III) 22-methyl-*m*-benziporphyrin **S92-1**.

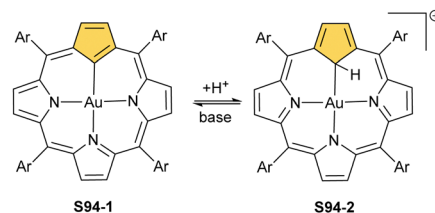


Scheme 93 Reactivity of gold(III) 2-formyl-21-methyl-21-carbaporphyrin **S92-3**.

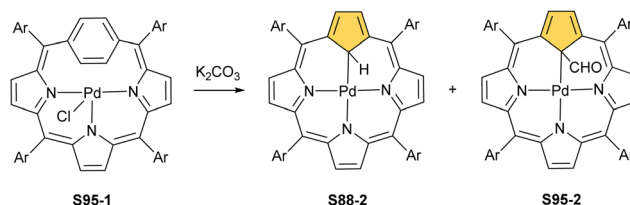
substituted by the hydroxyl one. It forms cationic gold(III) 2-hydroxy-21-methyl-21-carbaporphyrin **S93-2**, eventually affording **S93-1** (Scheme 93) under basic conditions. **S93-1** is only weakly aromatic, as shown by the <sup>1</sup>H NMR pattern. With the addition of acid, the equilibrium shifts towards **S93-2**, which regains the marked macrocyclic aromaticity.

It is possible to induce the contraction of a differently introduced benzene ring, namely the one in *para*-benziporphyrin, through gold coordination.<sup>217</sup> An extrusion of the external carbon atom has been suggested in the case of *m*-benziporphyrin contraction. In the case of isomeric *p*-benziporphyrin, an alternative route of contraction has been encountered. Namely, the inner carbon atom of *p*-phenylene, which directly interacts with a coordinating metal ion, is, in due course, extruded.<sup>217,218</sup> The gold(III)-stimulated contraction of *p*-phenylene to cyclopentadiene can be encountered in a reaction of *p*-benziporphyrin with sodium tetrachloroaurate(III) and potassium carbonate in dichloromethane.<sup>217</sup> The macrocycle in the gold(III) complex **S94-1** (Scheme 94) after contraction acts as trianionic ligand. The [CN<sub>3</sub>N] equatorial surrounding was detected for **S92-3** as well, albeit the enforced by *C*-methylation geometry around C(21) is tetrahedral. It is noteworthy that **S94-1** experiences the reversible protonation centred at the inner C(21) atom with the formation of a less aromatic cationic derivative **S94-2**.

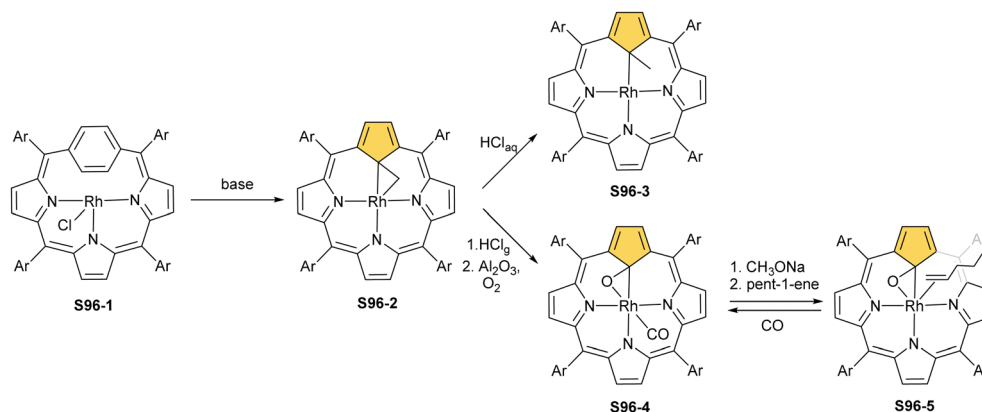
Treatment of *p*-benziporphyrin with palladium(II) chloride in acetonitrile yields **S95-1** (Scheme 95). In the presence of



Scheme 94 Protonation of gold(III) 21-carbaporphyrin **S94-1**.



Scheme 95 Contraction of palladium(II) *p*-benziporphyrin **S95-1**.



Scheme 96 Contraction of rhodium(III) *p*-benziporphyrin **S96-1**.

potassium carbonate, this species transforms into palladium(II) 21-carbaporphyrin **S88-2** and palladium(II) 21-formyl-21-carbaporphyrin **S95-2**.<sup>27</sup> The molecular structure of **S95-2** shows the conventional square-planar coordination environment of the palladium(II) centre with the relatively short Pd...C(formyl) distance (2.531(2) Å). The Pd–C(21) distance of 2.084(2) Å clearly reflects the  $\sigma$ -bonding interaction.

It is also important to note that the fused benzoanalogue of *meso*-tetraaryl-*p*-benziporphyrin, *i.e.*, *meso*-tetraaryl-1,4-naphthiporphyrin, when exposed to the coordination of palladium(II) or gold(III), undergoes the contraction of the inner phenylene ring to appropriate palladium(II) or gold(III) benzocarbaporphyrin complexes.<sup>217,218</sup> It additionally reconfirms contraction centred at the inner carbon atom forced to interact with metal centres, as opposed to contractions in *m*-benziporphyrins.

Eventually, rhodium(III) coordination was reported to induce the contraction of *p*-benziporphyrin.<sup>219</sup> Once again, similar to palladium(II) or gold(III) chemistry, rhodium(III) *p*-benziporphyrin **S96-1** (Scheme 96), when heated under basic conditions, contracts smoothly to rhodium(III) 21-methylene-21-carbaporphyrin as the major aromatic product (**S96-2**). The molecule incorporates a rhodacyclopropane motif also identified in the products of rhodium(III) 22-alkylated *m*-benziporphyrin contractions.

The bound methylene bridge can be reversibly protonated, affording the 21-methylated derivative **S96-3**. **S96-2** undergoes oxygenation when acidified with gaseous HCl and transferred onto basic alumina. The oxygenation leads to rhodium(III) 21-oxo-21-carbaporphyrin **S96-4**, with the metal ion interacting with both atoms from the C(21)–O(21) fragment. Thus, **S96-4** gains an oxygen bridge between C(21) and Rh atoms without breaking the organometallic bond (Fig. 20). The respective distances are 2.099(2) Å [Rh–C(21)], 2.035(2) Å [Rh–O(21)], and 1.343(6) Å [C(21)–O(21)]. Additionally, the methylene bridge gets oxidised as well, forming an axially coordinated carbonyl group. Also, the rhodium(III) centre in **S96-4** coordinates to a double bond acquiring a mixed  $\sigma/\pi$  organometallic coordination (**S96-5**). It occurs when the centre is deprived of the carbonyl group in a reaction with methanolate and then exposed to an alkene, *e.g.*, 1-pentene.

To summarise, we showed the richness of organometallic interactions between the metal centre and the inner carbon atom of monocarbaporphyrins. A selection of more common motifs is presented in Table 1.

## Many-carbon tetraphyrin and related systems

In previous sections, an overview of various monocarbaporphyrins, completed with *meso*-tetraaryl-21-carbaporphyrin, was presented. In particular, the utility as platforms for macrocyclic organometallic chemistry was addressed. Over recent years, a dynamic development of monocarbaporphyrinoid organic chemistry has been seen that resulted in the availability of an impressive portfolio of ligands, mainly with a [CNNN] donor set. Consequently, a promising direction of expansion is expected to present di-, tri-, and tetracarbabporphyrins.

This way, one can establish a playground to explore the novel aspects of the chemistry of fundamental nature. This will include specific metal binding modes and intermediaries between the regular bond and the van der Waals interaction. The distinctive macrocyclic environment creates a long-sought chance to trap unique organometallic intermediates, typically postulated in the catalytic process, shedding some light on their real nature. The basic strategies to construct multicarbaporphyrins are directly derived from monocarbaporphyrin chemistry taking advantage of well-elaborated syntheses, which initially allowed for the incorporation of a single carbocyclic building block.

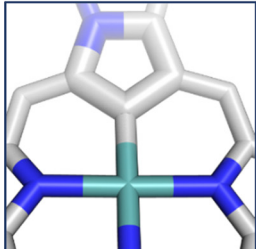
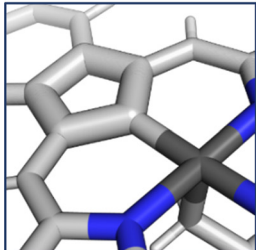
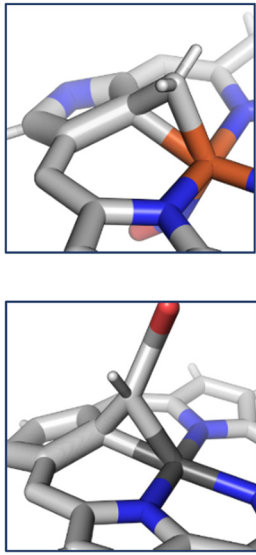
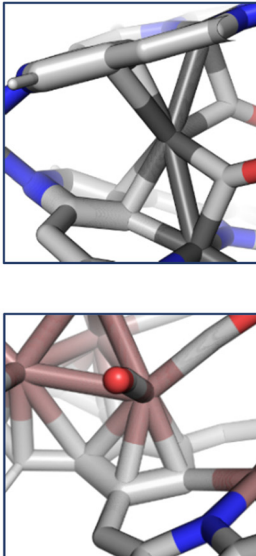
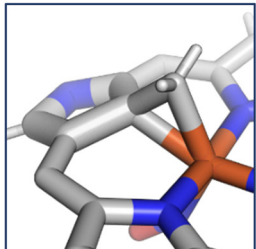
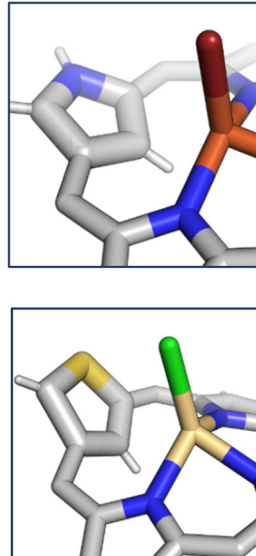
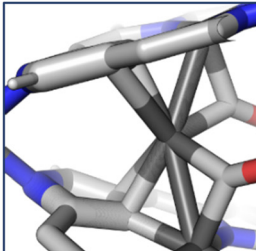
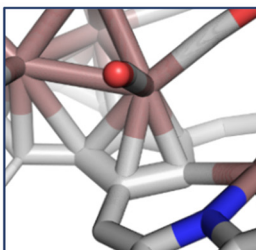
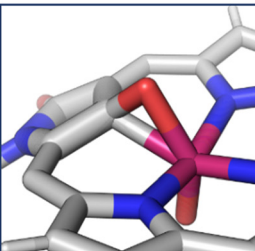
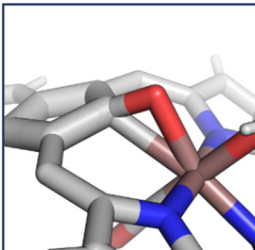
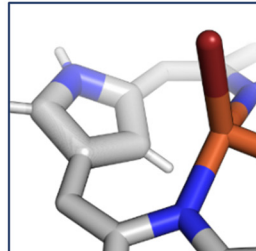
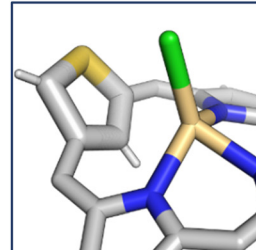
### N-confusion

The N-confusion adopted to more than one pyrrolic ring seemed to be the strategy to be explored while aiming for multicarbaporphyrins. The probabilities of double or triple N-confusion in a simple condensation seem unlikely for statistical reasons.

Construction of the [CCNN] frame was preceded by forming a predesigned building block, *i.e.*, N-confused dipyrromethane



**Table 1** The most common coordination motifs identified in monocarba porphyrins

Type of $M\cdots C$ interaction	$\sigma$ -bonding $C(sp^2)-M$	$\sigma$ -bonding $C(sp^3)-M$	$\eta^2$ -bonding $C-C\cdots M^*$
$M\cdots C$ distance	2.002(6) Å (Ag, <b>S26-2</b> ) 1.969(4) Å (Rh, <b>S81-1</b> )	2.046(4) Å (Co, <b>S31-1</b> ) 2.092(12) Å (Au, <b>S92-3</b> )	1.974(3) Å, 2.103(3) Å (Fe, <b>S38-3</b> ) 2.060(9) Å, 2.116(7) Å (Rh, <b>S90-6</b> )
Geometry	 	 	 
Type of $M\cdots C$ interaction	$\pi$ -bonding $C(sp^2)-M^{**}$	Through $\mu$ -oxo bridge	Agostic interaction $C-H\cdots M$
$M\cdots C$ distance	2.213(4) Å (Rh, <b>S35-1</b> ) 2.204(10) Å (Ru, <b>S75-2</b> )	2.245(9) Å (Re, <b>S46-3</b> ) 2.523(13) Å (Ru, <b>S76-1</b> )	2.361(10) Å (Fe, <b>S37-1</b> ) 2.623(6) Å (Cd, <b>S56-2</b> )
Geometry	 	 	 

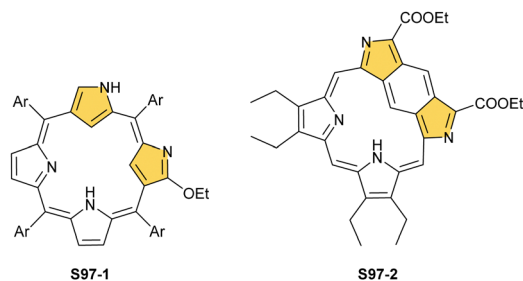
\*Italics for the distance to substituent's carbon. \*\*The closest contact [in both cases it is C(21)].

and further condensation with an aldehyde. Such an approach yields *cis*-doubly N-confused porphyrin **S97-1**.<sup>220</sup> Additionally, as the reaction is conducted in chloroform stabilised with ethanol, an outer position on one of the inverted rings becomes

substituted with an ethoxy group. In total, the macrocycle has three inner dissociable protons in the cavity. Macrocycle **S97-1** (Scheme 97) is only borderline aromatic as the delocalisation pathway has a formal disruption. It results in a relatively small





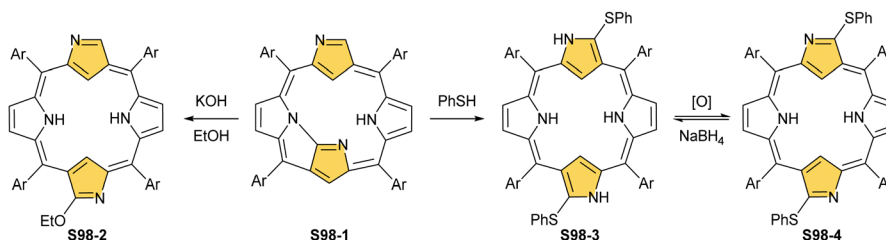


**Scheme 97** *cis*-Doubly N-confused porphyrin **S97-1** and benzene-fused doubly N-confused porphyrin **S97-2**.

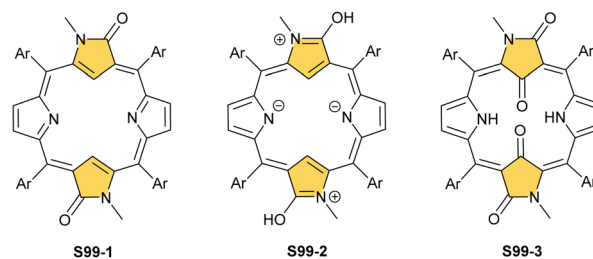
upfield relocation of the inner H(21) and H(22) atoms, with chemical shifts of 3.52 and 3.22 ppm, respectively.

The specific core modification of *cis*-doubly N-confused porphyrin (the isomeric frame as compared to **S97-1**, please notice the alternative location of outer nitrogen atoms) was presented recently.<sup>221</sup> It took the shape of a methine bridge between the inner carbon atoms (**S97-2**). The complete macrocycle possesses a shrunk cavity with a motif similar to the already presented in the chemistry of NCP, which led to N-heterocyclic carbene embedded in an NCP framework (**S47-2**).<sup>145</sup> The bridge also imposes a different  $\pi$ -delocalization pathway, and that the molecule is more aromatic than the unbridged congener, as the chemical shift of the inner bridge proton equals  $-1.85$  ppm.

Another possible variation is introducing N-confused pyrrole rings in the mutual translocation. Thus, *trans*-doubly N-confused porphyrin **S98-2** was obtained in a self-condensation of N-confused dipyrromethene carbinol.<sup>222</sup> In this reaction, N-confused N-fused porphyrin **S98-1** (Scheme 98) forms at first and later transforms into **S98-2** under basic conditions in an alcohol environment. The process is accompanied by ethoxylation of the outer carbon atom. The formed **S98-2** is strongly aromatic in contrast to its *cis* counterpart, **S97-1**. The inner CH protons [H(21) and H(23)] resonate at  $-4.34$  and  $-4.36$  ppm, respectively. An attempt to open a semi-fused macrocycle with thiophenol instead of alcohol results in more complex chemistry. It affords a substitution of the outer N-confused pyrrole carbon atoms of both rings, generating **S98-3**.<sup>223</sup> It is reduced when compared to **S98-2**. Its electronic structure varies significantly from the aromatic counterpart, as the  $\pi$ -delocalization pathway is interrupted, so the inner CH protons resonate at 8.29 ppm. It can be reversibly oxidised to an aromatic form **S98-4** (the diagnostic CH signal relocates to  $-4.05$  ppm).



**Scheme 98** Reactivity of N-confused N-fused porphyrin **S98-1**.



**Scheme 99** *trans*-Doubly N-confused porphyrin derivatives.

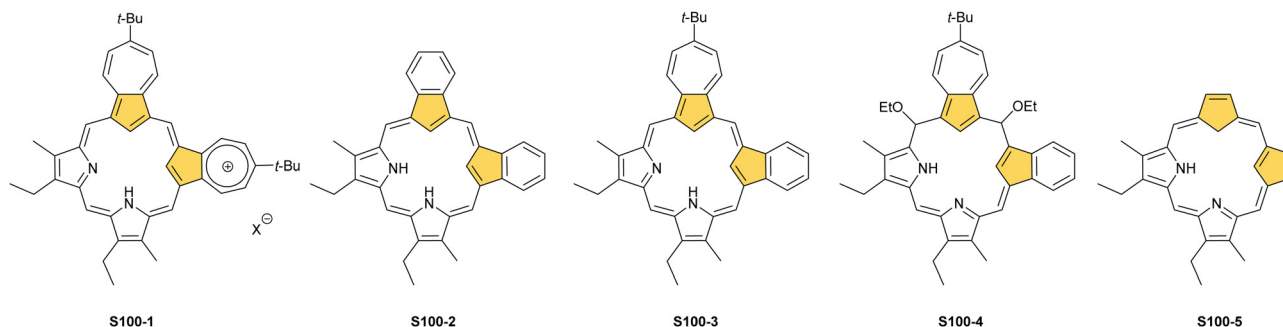
Another approach was applied to obtain *trans*-doubly N-confused porphyrin with two oxo substituents on outer carbon atoms.<sup>224</sup> **S99-1** (Scheme 99) can be efficiently obtained in condensation of *N*-methylated building units, N-confused tripyrrane and N-confused dicarbinol (condensation [3+1]), followed by oxidation in which lactam functionalities are formed. The molecule possesses the  $16\pi$ -electron delocalisation pathway, leading to its antiaromaticity. This is depicted with a chemical shift of inner protons equal to 12.98 ppm. After two-electron reduction with  $\text{NaBH}_4$ , one gets an aromatic macrocycle (**S99-2**; the contributor with separated charges is shown), with inner protons at  $-1.88$  ppm. By using DDQ instead of chloranil for oxidation, the tetraoxygenated product **S99-3** is formed instead of **S99-1**.<sup>225</sup>

### Incorporation of five-membered rings – cyclopentadiene and fused derivatives

Simple building blocks, including those incorporating azulene, indene, or cyclopentadiene, were used as the rewarding units to construct *cis*- or *trans*-dicarbaporphyrins. A first example is  $\beta$ -substituted *cis*-diazuliporphyrins **S100-1** (Scheme 100) which also accounts for the first case of mesoionic porphyrinoid.<sup>226</sup> A diazulene precursor is condensed with dipyrromethene. The compound has been isolated in the solid state as monoprotonated hydrochloride or hydrobromide salts. In solution, the isolated species also exists in a cationic form, and the inner CH atoms resonate at  $-0.05$  ppm (bromide as a counterion).

Similarly, *cis*-dibenzocarbaporphyrin **S100-2** is obtained from a diindene precursor and dipyrromethane.<sup>227</sup> The porphyrinoid is fully aromatic (the H(21), H(22) chemical shift locates at  $-6.24$  ppm) and contains four inner protons. Protons from nitrogen atoms can be removed using 1,8-diazabicyclo[5.4.0]undec-7-ene (DBU) to form macrocyclic dianions. The alternative stepwise



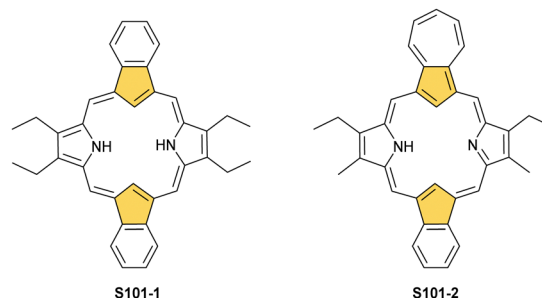
Scheme 100  $\beta$ -Substituted *cis*-dicarbaporphyrins.

protonation is centred at the inner carbon atoms, which requires their trigonal to tetrahedral rehybridisation.

Eventually, the azulene-benzocarpa hybrid **S100-3** was produced, preceded by azulene and indene coupling to form a building unit for [2+2] condensation.<sup>228,229</sup> Its aromaticity is hampered by azulene. Still, the inner H(21) and H(22) atoms demonstrate the upfield relocation (chemical shifts equal 1.6 and 3.5 ppm). The protonation of **S100-3** promotes their further upfield repositioning, similar to azuliporphyrins. Structurally, the cavity of **S100-3** contains three removable protons, *i.e.*, the intermediate situation between *cis*-diazuli **S100-1**, which could stabilise dication in its neutral state, and *cis*-dibenzocarpa **S100-2** analogues. **S100-3** reacts with silver(I) acetate in ethanol, yet the expected silver(III) coordination does not occur and instead two ethoxy groups are added at *meso* positions flanking azulene to form nonaromatic **S100-4**.<sup>229</sup>

*cis*-Dicarbaporphyrin, which incorporates two five-membered carbocycles, seemed to be logically targeted as the next step. The procedure resembles that applied for **S100-1** and **S100-2** starting, however, using dicyclopentadienemethane.<sup>230</sup> Peculiar dicarbaporphyrin **S100-5**, which contains an internal methylene group, was isolated (Fig. 21). Still, **S100-5** is fully aromatic (H(21) and H(22) shifts are  $-6.68$  and  $-4.03$  ppm) and, despite one deprotonated nitrogen atom, the cavity possesses four protons. This way, all kinds of environments occur by varying the carbon-providing units.

The translocation of the respective carbocyclic rings afforded a separate subclass of dicarbaporphyrins. The elaborate procedures usually involve a condensation of activated azulene or indene fragments with two units containing pyrrole

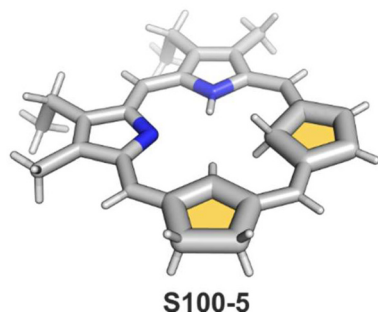
Scheme 101  $\beta$ -Substituted *trans*-dicarbaporphyrins.

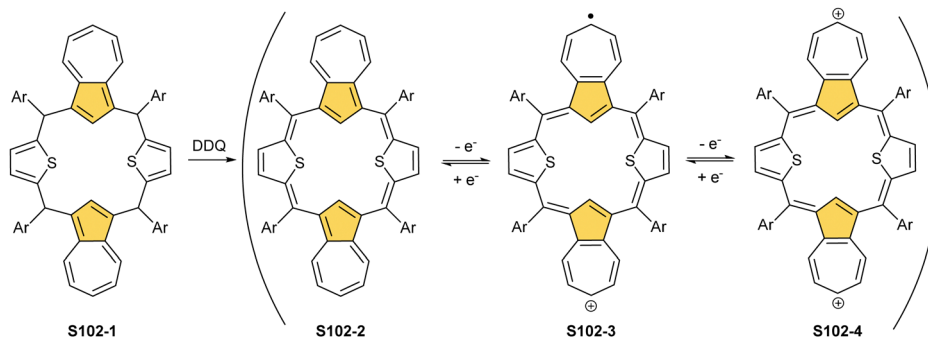
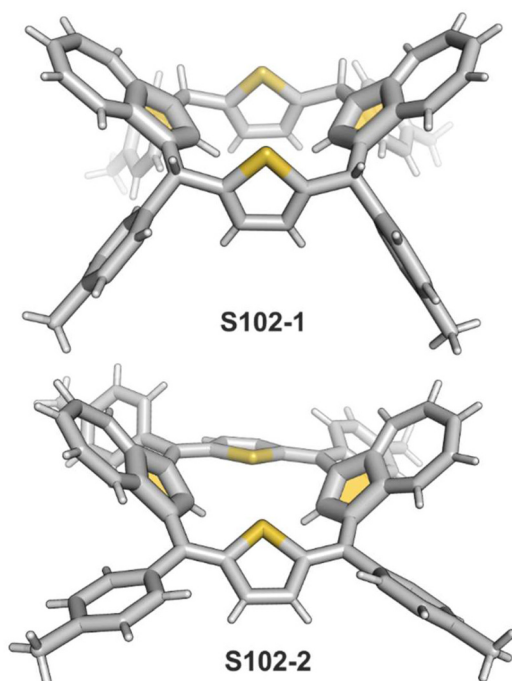
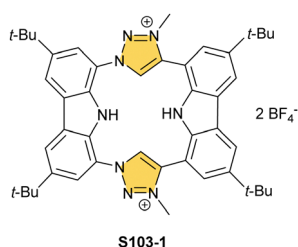
or a heterocycle. Due to less directional synthesis, the yields are sometimes lower than for the respective *cis* analogues. The first dicarbaporphyrinoid with two opposite benzocarpa moieties (**S101-1**, Scheme 101) was reported as early as 1999.<sup>231</sup> The properties of **S101-1** resemble those reported for *cis*-dibenzocarbaporphyrin **S100-2**. The inner protons resonate at  $-5.7$  ppm, reflecting strong diatropicity. The macrocycle is somewhat less stable in solution than 22,24-dioxa<sup>232</sup> and the *cis* analogues.

Azulene-based tripyrrane condensed with an indene derivative gives mixed azulene-indene porphyrinoid **S101-2**.<sup>233</sup> The macrocycle is aromatic as its *cis* counterpart **S100-3** with inner H(21) and H(23) signals detected below 2 ppm.

Diazuliporphyrinoids can be formed in a reaction of azulene and heterocycle-based dicarbinols.<sup>234–236</sup> The condensation leads to the formation of diazuliporphyrinogen, *e.g.*, **S102-1** (Scheme 102 and Fig. 22). **S102-1** is naturally nonaromatic and more flexible than the target porphyrin. The oxidation of **S102-1** with controlled amounts of DDQ yields mixtures of the porphyrin analogue **S102-2** (Fig. 22), its radical cation **S102-3**, and dication **S102-4**. These three species constitute a peculiar multi-electron redox system. The neutral form **S102-2** is not aromatic as indicated with a H(21), H(23) chemical shift of 7.02 ppm. On the other hand, dication **S102-4** reveals a significant degree of diatropicity (the H(21), H(23) signal shifts to 1.48 ppm) evidently related to the accumulation of the positive charge over the seven-membered ring. Similar reactivity was observed for dioxa-,<sup>235</sup> diselena-, and ditelluraderivatives.<sup>236</sup>

Finally, a molecule bridging the features of porphyrinoids and the final, presented in this section group of potential

Fig. 21 Dicarbaporphyrinoids with C(sp<sup>2</sup>) and C(sp<sup>3</sup>) in the cavity.

Scheme 102 Reactivity of diazulporphyrinogen **S102-1**.Fig. 22 Diazulporphyrinoids. *meso*-Substituents preserved to show changes in conformation after oxidation.Scheme 103 Carbazole-triazolydene porphyrin **S103-1**.

ligands – macrocyclic polycarbenes – was described.<sup>237</sup> Macrocycle **S103-1** (Scheme 103) is obtained in a click-reaction between alkyne-disubstituted carbazole and a diazide derivative, followed by the *N*-methylation of two formed triazole rings

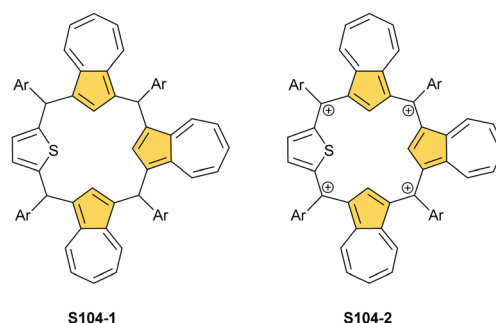
with trimethyloxonium tetrafluoroborate. The final dication (**S103-1**) is colourless, indicating carbazole-centred aromaticity rather than the presence of any macrocyclic ring current as typical for porphyrins.

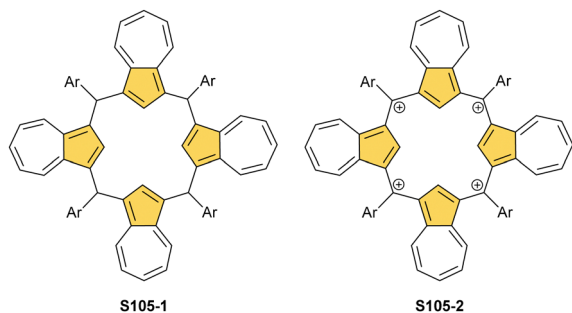
### Tri- and tetracarbamacrocycles

Macrocycles preserving some structural features of the regular porphyrin that contain more than two inner carbon atoms are really scarce. Over the years, quatyrim,<sup>238</sup> a porphyrin with four inner carbon atoms, has been a target structure and remains to be synthesised. Still, there are a few examples of tri- or tetracarbamacrocydes that can potentially serve as multiorganometallic macrocyclic ligands.

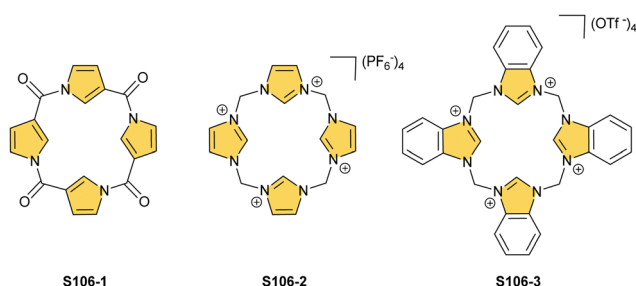
A reaction of thiophene-based biscarbinol with arylaldehyde and azulene catalysed by  $\text{BF}_3 \cdot \text{Et}_2\text{O}$  yields azulporphyrinogen-type isomeric structures exemplified by **S104-1** (Scheme 104), containing sulphur and three carbon atoms in the core.<sup>239</sup> The subsequent oxidation with DDQ produces a rare organic tetracation **S104-2** with four  $\text{C}(\text{sp}^2)$  *meso* bridges. The positive charge is preferentially located at the *meso* carbon atoms. Significantly, the macrocyclic  $\pi$ -delocalization is absent, and the macrocycle is nonplanar. **S104-2** is quite susceptible to nucleophilic attacks centred at *meso* positions.

A simple condensation of azulene with arylaldehyde (1 : 1 molar ratio) affords *meso*-tetraaryl-tetraazulporphyrinogen **S105-1** (Scheme 105) as a mixture of stereoisomers,<sup>240,241</sup> similar as with paraformaldehyde (which produces the unsubstituted derivative – calix[4]azulene).<sup>240</sup> Oxidation of **S105-1** leads to a tetracation **S105-2**, resembling **S104-2**, with no

Scheme 104 Triazulporphyrinogens **S104-1** and **S104-2**.



Scheme 105 Tetraazuliporphyrinogen **S105-1** and oxidised **S105-2**.



Scheme 106 Tetra(neo-confused) porphyrin-like macrocycles.

indication of macrocyclic aromaticity (inner protons resonate at 11.34 ppm).

Another interesting macrocycle, described soon after NCP, can be generated by the flash vacuum thermolysis of an appropriately designed pyridine derivative (e.g., 3-diazo-4-hydroxypyridine).<sup>242</sup> It transforms into 3-carbonyl-3H-pyrrole that tetramerizes forming **S106-1** (Scheme 106). The macrocycle could be viewed as the tetra(neo-confused) porphyrin, but due to carbonyl moieties at *meso* positions, there is no macrocyclic aromaticity present (inner protons resonate at 8.78 ppm). The synthesis of the poorer soluble tetrabenzohomologue of **S106-1** was also described.

An original group of macrocycles containing a [CCCC] set of donors that reveal the high coordination potential have been presented in the literature. Our attention will be focused on a subset with the evidently porphyrin-like framework. Their electronic structure is principally different from that classified as typical for carbaporphyrinoids. They have a molecular structure containing four N-heterocyclic carbene (NHC) donors. However, the high structural similarity of molecular skeletons to so far described porphyrinoids and porphyrinogens in particular, straightforward and efficient syntheses, and the essential flexibility of frameworks bring a promise of interesting organometallic chemistry. The synthesis involves bridging two bisimidazolmethanes to obtain the final tetracationic species **S106-2**.<sup>243,244</sup> Benzohomologue **S106-3** was obtained following a similar procedure.<sup>245</sup> Naturally, the fundamental framework has various modifications, including heteroatoms like boron at *meso* positions to decrease the overall charge and tune the molecular properties.<sup>246–249</sup> These macrocycles also

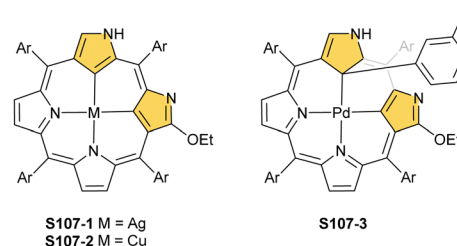
have exciting organometallic chemistry, e.g., with actinides,<sup>250</sup> iron,<sup>247</sup> or chromium.<sup>251</sup> The all-carba ligands (**S106-2** and **S106-3**) allow following the organometallic reactivity in more polar solvents than that in the case of neutral porphyrin complexes. Additionally, anion exchange can be applied to tune the solubility of complexes in different organic media.<sup>243,244</sup>

### Organometallic chemistry of di-, tri-, and tetracarba porphyrinoids

Although several examples of di-, tri-, and tetracarba porphyrinoids have been described in a previous section, only a handful of coordination examples exist in the literature, which remains in contrast to monocarba analogues. It indicates that the field is still in its infancy and that novel, exciting possibilities to stabilise extraordinary organometallic motifs still await exploration.

Starting from *cis*-doubly N-confused porphyrin **S97-1**, in contrast to NCP, it stabilises  $M^{III}$  complexes with both silver and copper.<sup>220</sup> Silver(III) complex **S107-1** (Scheme 107) forms after stirring the ligand with silver(I) acetate, while the stable copper(III) square-planar coordination (**S107-2**) is provided after stirring with copper(II) acetate. The lengths of organometallic bonds in both molecules are within standard ranges, i.e., 1.987(8) and 2.011(8) Å for  $Ag^{III}-C$  and 1.939(3) and 1.934(4) Å for  $Cu^{III}-C$ . The treatment of **S97-1** with palladium(II) acetate in refluxing toluene afforded palladium(II) dicarbaporphyrin **S107-3**.<sup>252</sup> Its formation is clearly associated with toluene activation as the *p*-tolyl or *m*-tolyl moiety has been attached in **S107-3** to one of the inner carbon atoms (Fig. 23). Such *C*-substitution has been detected with benzene in a mixture with toluene or *m*-xylene as well. It is noteworthy that the new C(21)–C(aryl) bond is formed directly to the phenyl ring and not the potentially more reactive methyl group. The C–Pd distances vary significantly between the coordination of tetrahedrally distorted C(21) (2.202(9) Å) and the regular  $C(sp^2)$  (1.971(15) Å) inner carbon atom.

*trans*-Doubly N-confused porphyrin **S98-3** containing four inner dissociable protons may potentially act as a tetraanionic ligand but behaves very similarly to the *cis* isomer **S97-1**. Namely, a reaction with copper(II) acetate results in copper(III) insertion with one inverted pyrrole unit accommodating an outer proton on the outer nitrogen atom.<sup>222</sup> This points to a degree of flexibility of such ligands resembling NCP. A similar outcome of silver(III) or copper(III) of coordination (**S108-1** and **S108-2**, Scheme 108) was observed in a reaction with



Scheme 107 *cis*-Doubly N-confused porphyrin complexes.





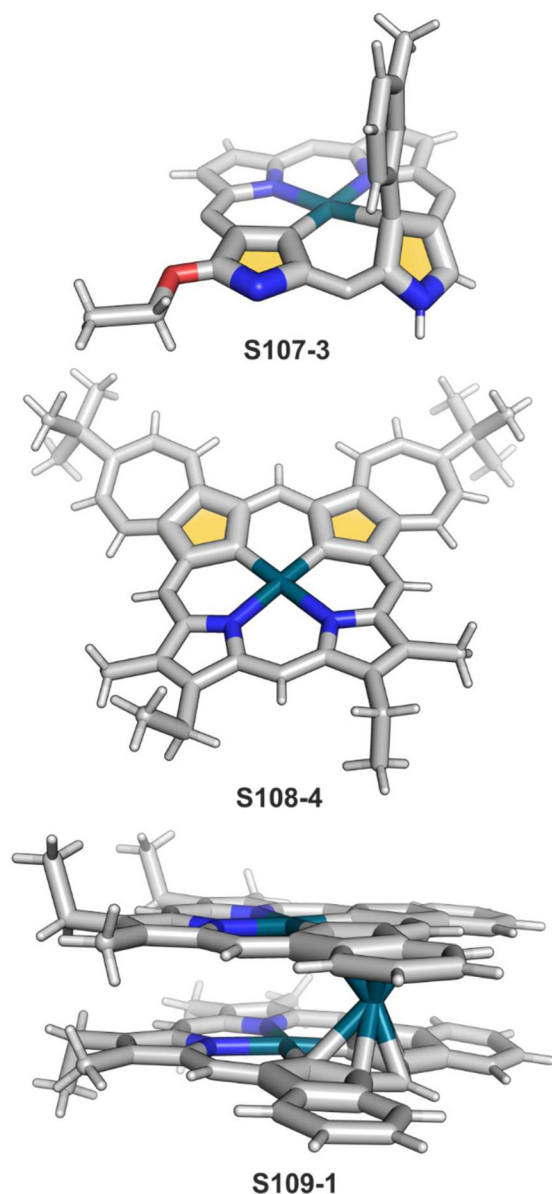
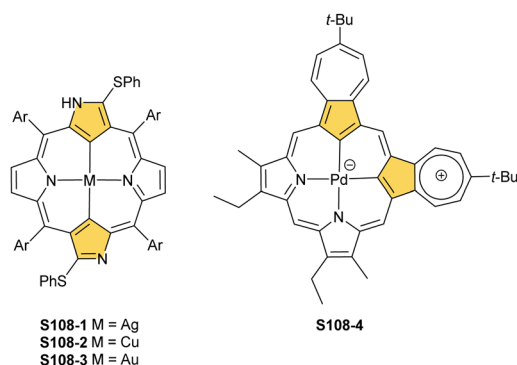
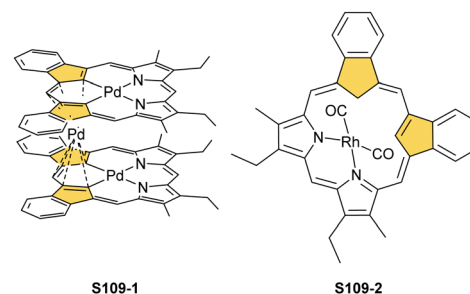


Fig. 23 Palladium coordination motifs for dicarbaporphyrins. *meso*-Substituents in **S107-3** not shown.



Scheme 108 Trans-Doubly N-confused porphyrin complexes and the palladium(II) *cis*-diazuliporphyrin derivative.



Scheme 109 *cis*-Dibenzocarbaporphyrin complexes.

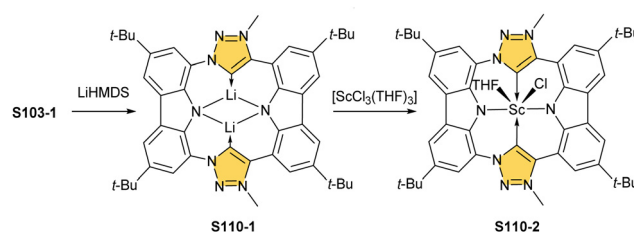
isophlorin **S98-3** and its aromatic counterpart **S98-4**.<sup>223,253</sup> A reaction of **S98-3** with  $[\text{AuCl}(\text{S}(\text{CH}_3)_2)_2]$  yields an analogous gold(III) complex (**S108-3**), yet to conduct gold(III) insertion, preceding bromination of inner CH positions is necessary.<sup>253</sup>

*cis*-Diazuliporphyrin **S100-1**, after deprotonation, is dianionic. Thus, it is a suitable platform to accommodate a palladium(II) ion. After a reaction of diazuliporphyrin bromide **S100-1** with a palladium source, the neutral complex **S108-4** is formed,<sup>226</sup> which continues to have a mesoionic electronic structure as the free ligand has (Fig. 23).

The dibenzocarpa analogue (**S100-2**) reacts with palladium(II) acetate under similar conditions, yet the product is strikingly different.<sup>227</sup> The formed species acquires the dianionic nature as four inner protons are removed after complete palladium(II) coordination. Eventually, the process affords a stable  $[\text{Pd}_3\text{L}_2]$  dimer (**S109-1**) (Scheme 109) with two inserted palladium(II) cations and one palladium(IV) playing the bridging role (Fig. 23). The palladium(IV) centre links two subunits *via* effective  $\pi$ -coordination interactions. The inner Pd<sup>II</sup>–C(21) distances are typical (*ca.* 2.0 Å), while the closest contacts with palladium(IV) forming the  $\eta^5$  motif with each unit are in a range of 2.223(9) to 2.515(8) Å.

Coordination to a rhodium(I) ion requires the rehybridisation of one of the inner carbon atoms to provide the environment with one deprotonated inner nitrogen atom.<sup>204</sup> This is how two coordinated nitrogen atoms secure the neutrality of the formed complex **S109-2**. Two uncoordinated C(21) and C(22) carbon atoms are confirmed to possess different  $\text{sp}^2$  and  $\text{sp}^3$  hybridisations.

The mentioned porphyrin–carbene hybrid (**S103-1**) gets activated by deprotonation with lithium bis(trimethylsilyl)amide to form a dilithium complex **S110-1** (Scheme 110).<sup>237</sup> It can be transmetalated with scandium(III) using a trichloride source.

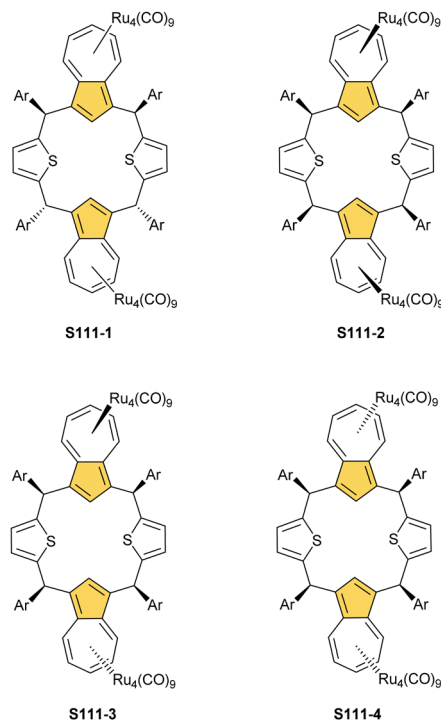


Scheme 110 Dilithium carbene complex of carbazole-triazolydene porphyrin **S110-1** and its transmetalation.

The formed complex **S110-2** possesses apically attached chloride and a THF molecule at the same macrocyclic side. To probe any possible macrocyclic ring currents, the ligands on the scandium(III) centre have been replaced with a cyclopentadienyl anion (from LiCp), but no upfield shift of the Cp resonances was detected in the  $^1\text{H}$  NMR spectrum.

Let us remain with nonaromatic *trans*-dicarbaporphyrinoids in which the only known coordination of ruthenium was encountered for azuliporphyrinogens, including dithiadiazuliporphyrinogen **S102-1**.<sup>254</sup>

Reactions of **S102-1** with  $[\text{Ru}_3(\text{CO})_{12}]$  result in the formation of ruthenium  $\pi$ -bound clusters, similarly, as reported for azuliporphyrin **S64-2**. In this case, though, the cavity persists in being unoccupied. The complex is formed purely due to azulene  $\pi$ -coordination. As there are two azulene moieties, both participate, and each accommodates identical  $\text{Ru}_4(\text{CO})_9$  units forming **S111-1** (Scheme 111). Otherwise, a transient cluster  $\text{Ru}_2(\text{CO})_5$  may be attached, providing that there is not enough of the ruthenium(0) source accessible or the reaction time is too short. Interestingly, the number of products is determined by the conformation of parental dithiaporphyrinogen **S102-1**. The one having all four *meso* substituents at the same side of the macrocyclic frame yields three isomeric complexes varying by clusters attached to different sides of azulene surfaces (**S111-2** to **S111-4**) heavily influencing the overall molecular conformation (Fig. 24). The tri- (**S104-1**) and tetraazuliporphyrinogen (**S105-1**) also provide **S111-2**-like complexes with one (**S112-1**, Scheme 112) or two (**S112-2**) azulene fragments remaining unbound.



**Scheme 111** Diazuliporphyrinogens with azulene rings coordinated with tetraruthenium clusters.

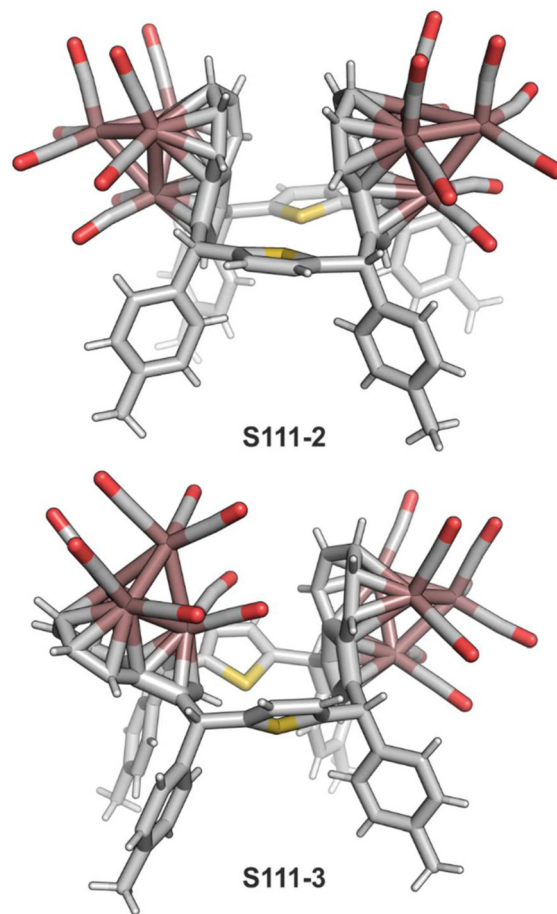
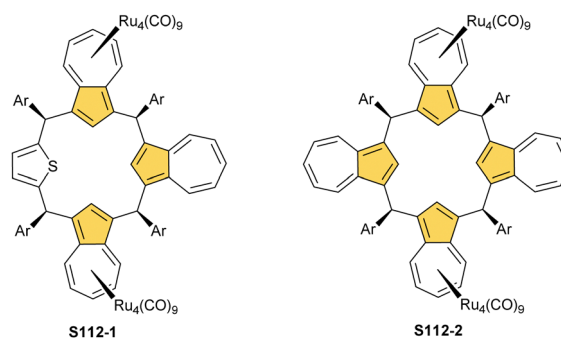


**Fig. 24** Diazuliporphyrinogens  $\pi$ -coordinated with ruthenium clusters. *meso*-Substituents preserved.

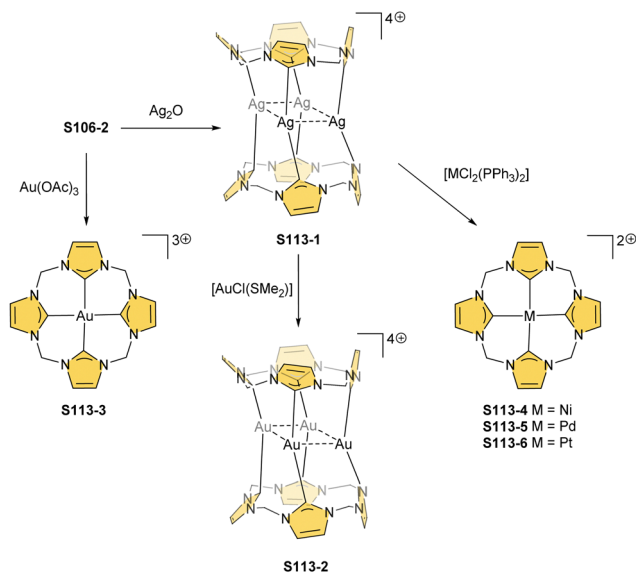


**Scheme 112** Triazuliporphyrinogen and tetraazuliporphyrinogen with ruthenium clusters.

N-Heterocyclic carbene macrocycles **S106-2** and **S106-3** with porphyrinogen topology present quite rich organometallic chemistry taking advantage of the unique [CCCC] core and the peculiar conformational flexibility.

Starting from **S106-2**, this species reacts easily with  $\text{Ag}_2\text{O}$  in acetonitrile to form  $[\text{Ag}_4\text{L}_2]^{4+}$  **S113-1** (Scheme 113).<sup>255</sup> Four silver(I) ions, which prefer a linear coordination mode, form a  $\text{Ag}_4$  square motif in which each cation is bound with NHC from

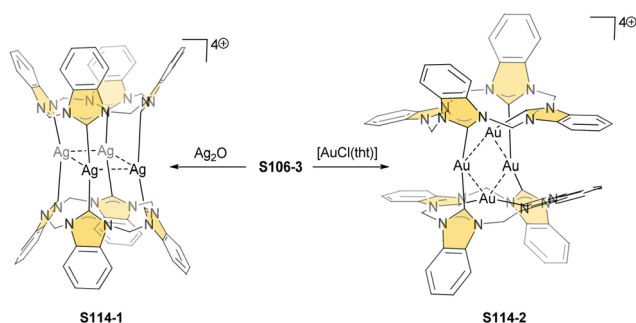




Scheme 113 Carbene silver and gold complexes with calix[4]imidazolium.

the top and bottom rings. To reach such an arrangement, a conformationally flexible molecule **S106-2** has oriented all four five-membered rings perpendicularly to the  $\text{N}_8$  mean plane. The average  $\text{Ag}-\text{C}$  distance is *ca.* 2.09 Å, whereas the  $\text{Ag} \cdots \text{Ag}$  contacts are *ca.* 3.21 Å. The benzimidazole-containing derivative **S106-3** was also probed.<sup>245</sup> **S114-1** (Scheme 114) acquired the identical conformation to **S113-1** with respective average distances being *ca.* 2.11 Å for  $\text{Ag}-\text{C}$  and around 3.00 Å for  $\text{Ag} \cdots \text{Ag}$ . Silver(I) species **S113-1** may also serve as a nontrivial substrate for transmetalation. Accordingly, a reaction of **S113-1** with  $[\text{AuCl}(\text{S}(\text{CH}_3)_2)]$  results in a replacement of  $\text{Ag}^{\text{I}}$  for  $\text{Au}^{\text{I}}$  to create **S113-2** with the preserved dimolecular frame of **S113-1**.<sup>255</sup> Here, metallophilic interactions are also prominent as the  $\text{Au} \cdots \text{Au}$  contact equals 3.1482(5) Å and the  $\text{Au}-\text{C}$  bond lengths are around 2.03 Å (Fig. 25).

Transmetalation of **S114-1** does not provide a related and expected gold(I) product. Interestingly, the direct treatment of **S106-3** with chloro(tetrahydrothiophene)gold(I) generates  $[\text{Au}_4\text{L}_2]^{4+}$  **S114-2** with the same stoichiometry as in **S113-2**, although structurally significantly different (Fig. 25).<sup>245</sup> The



Scheme 114 Coordination of benzo-fused calix[4]imidazolium with silver and gold salts.

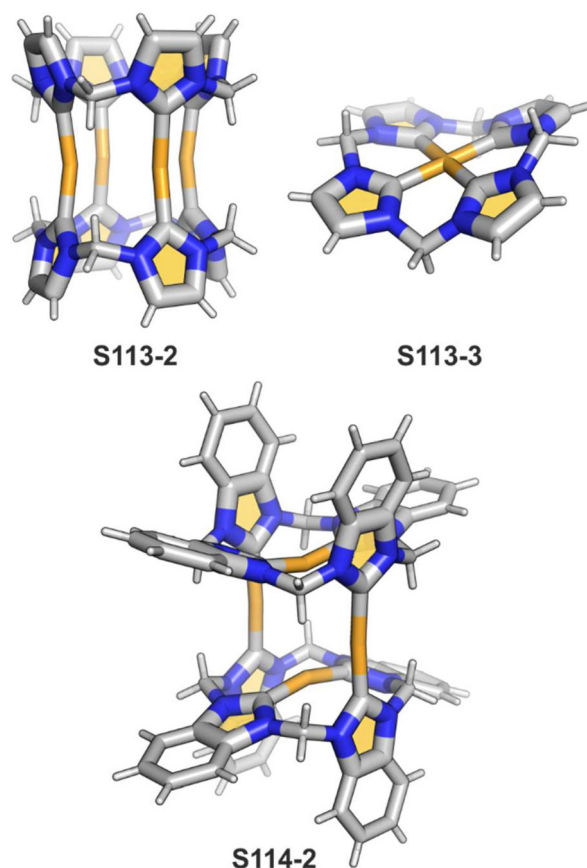


Fig. 25 Carbene gold complexes.

X-ray-determined molecular structure of **S114-2** clearly shows two gold(I) cation ions coordinating to two *trans* 'in-plane' benzimidazoles ( $\text{Au}-\text{C}$ : 2.03 Å), while two other gold(I) cations link rings perpendicular to the mean plane ( $\text{Au}-\text{C}$ : 2.02 Å) affording the dimer. Eventually, **S106-2** was also directly reacted with gold(III) acetate and provided a mononuclear, regular complex with four  $\text{Au}-\text{C}$  bonds in a planar arrangement (**S113-3**; Fig. 25).<sup>245</sup> The bonds are, on average, 1.99 Å long, a bit shorter than determined in the respective gold(I) complex **S113-2**.

An attempt of transmetalation of **S113-1** with  $[\text{MCl}_2(\text{PPh}_3)_2]$ , in which  $\text{M} = \text{Ni}$ ,  $\text{Pd}$ ,  $\text{Pt}$ , was elaborated as an effective route to generate respective mononuclear complexes **S113-4**, **S113-5**, and **S113-6**.<sup>255</sup> As typical for low-spin nickel(II) porphyrins, the incorporation of nickel(II) into **S106-2** leads to the most deformed structure of **S113-4**. At the same time, the larger congeners **S113-5** and **S113-6** remain relatively planar. The bond length range for  $\text{Ni}-\text{C}$  is between 1.851(3) and 1.886(3) Å, while for  $\text{Pd}^{\text{II}}$  and  $\text{Pt}^{\text{II}}$ , it is slightly below 2.00 Å.

The direct metallation of **S106-2** with iron(II) occurs in a reaction with  $[\text{Fe}(\text{N}(\text{Si}(\text{CH}_3)_3)_2)_2]$ .<sup>244</sup> It opens a route to interesting coordination chemistry on its own.<sup>256–258</sup> The formed tetracarbene dicationic complex **S115-1** (Scheme 115) demonstrates the features of the diamagnetic low-spin iron(II) electronic state (the  $\text{Fe}-\text{C}$  distances of *ca.* 1.91 Å). The iron(II) centre coordinates axially two acetonitrile ligands apart from four



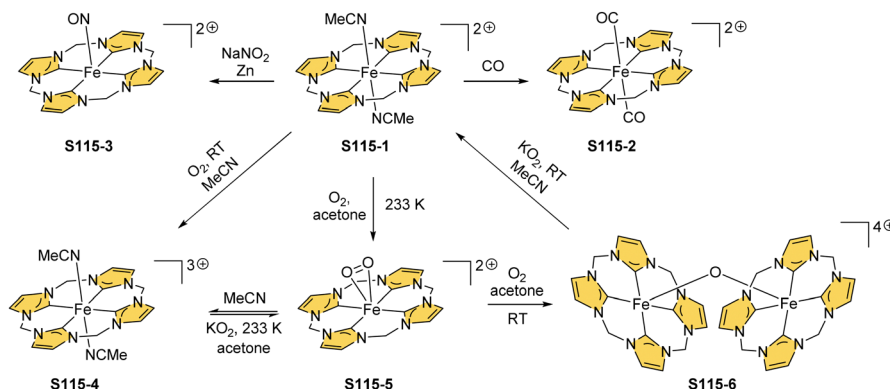
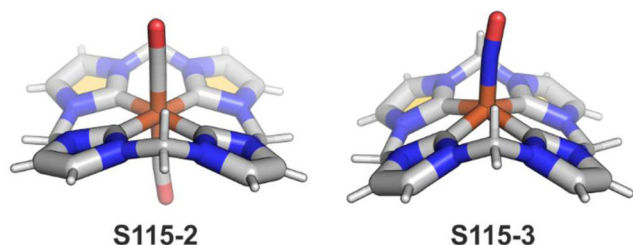
Scheme 115 Reactivity of iron(II) calix[4]imidazolium **S115-1**.

Fig. 26 Iron tetracarbenes complexes with calix[4]imidazolium.

equatorial carbon donors. The molecules can be exchanged for DMSO and, interestingly, also for two carbonyl ligands forming **S115-2**, yet the distances from the centre to the inner carbon atoms remain unaltered (Fig. 26). A reaction of **S115-1** with *in situ* formed nitric oxide results in pentacoordinate **S115-3** and slightly longer Fe–C bonds (*ca.* 1.95 Å; Fig. 26). Despite the {Fe(NO)}<sup>7</sup> electronic structure, a diamagnetic-like <sup>1</sup>H NMR spectrum is observed together with a characteristic EPR signal. **S115-1** can be efficiently oxidised to the iron(III) complex **S115-4** by mixing it with thianthrenyl hexafluorophosphate.<sup>259</sup> This involves only slight variations in the coordination environment with Fe–C distances close to 1.95 Å.

The oxidation of **S115-1** also occurs in acetonitrile exposed to dioxygen.<sup>258</sup> When a solvent is switched to acetone, and the reaction occurs at low temperature, a diamagnetic form with activated dioxygen (**S115-5**) can be detected and even isolated. This species can be alternatively generated by treating **S115-4** with KO<sub>2</sub>. By elevating the temperature to ambient conditions, **S115-5** transforms into the μ-oxydimer **S115-6** (Fig. 27). The Fe–C bonds are, on average, 1.95 Å long, as in **S115-4**, while the Fe–O distance is 1.7322(7) Å. The dimer, in turn, can be split and reduced back to **S115-1** with a range of agents, including KO<sub>2</sub> in acetonitrile. Further iron carbene oxidative reactivity was explored, yet with ligands beyond porphyrin-like geometry.<sup>260,261</sup>

Another dioxygen-activating centre can be successfully introduced into **S106-2** in a reaction with CoCl<sub>2</sub> yielding **S116-1** (Scheme 116).<sup>262</sup> In the solid state, the cobalt tetracarbenes complex **S116-1** acquires a single axial acetonitrile ligand. The Co<sup>II</sup>–C distances are in a range of 1.889(2) to 1.901(2) Å. After

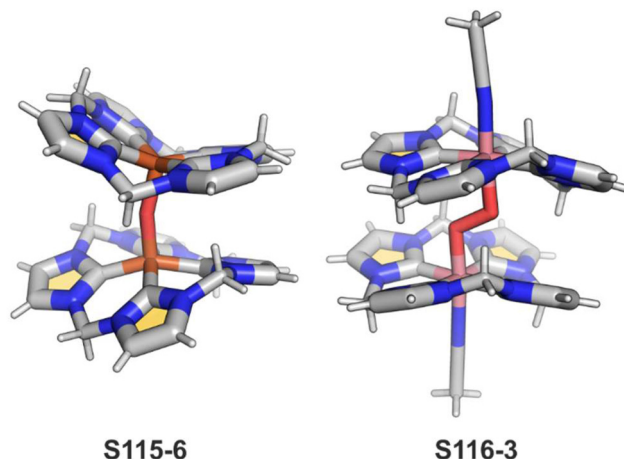
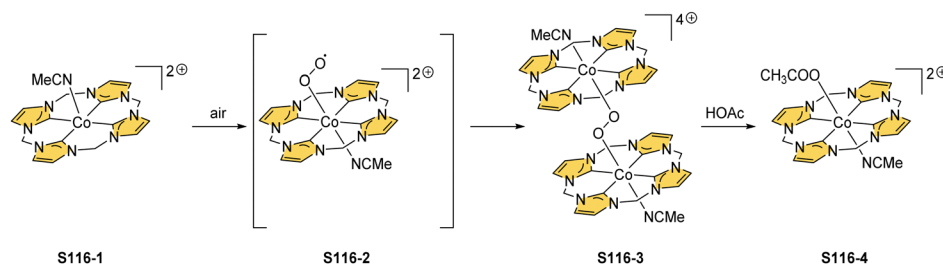
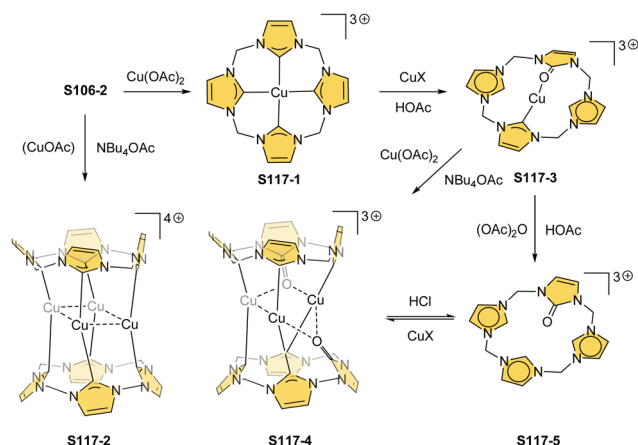


Fig. 27 μ-Oxy(peroxy)-bridged carbene complexes.

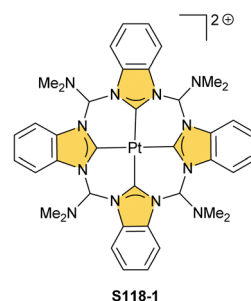
exposure to air, the solution **S116-1** undergoes a colour change, forming a diamagnetic compound. The X-ray-determined molecular structure reflects the formation of the μ-peroxy dicobalt(III) species **S116-3** (Fig. 27). It was confirmed that the transformation proceeds through a reactive superoxy intermediate **S116-2**. Finally, after mixing **S116-3** with acetic acid, the mononuclear Co<sup>III</sup> complex **S116-4** is recovered.

The insertion of copper(II) opens a route to interesting redox chemistry as well. **S106-2** treated with copper(II) acetate in DMSO affords the copper(III) complex **S117-1** (Scheme 117) structurally analogous to the gold(III) derivative **S113-3**.<sup>263</sup> Alternatively, the reaction of **S106-2** with copper(I) acetate leads to a dimeric counterpart of the respective dimeric silver(I) **S113-1** or gold(I) **S113-2** species with four copper(I) cations bridging two macrocyclic units (**S117-2**). Interestingly, **S106-2** mixed with copper(II) acetate and a base (tetrabutylammonium acetate) yields a completely different product **S117-4** in high yields. The reaction is shown to proceed through a copper(I) species (**S117-3**). Both macrocycles in **S117-4** have one of the inner positions oxygenated (Fig. 28); thus, three, not four, copper(I) cations provide stabilising C–Cu–C links. **S117-4** is also significantly more resistant to oxygenation. The demetallation of



Scheme 116 Reactivity of cobalt(III) calix[4]imidazolium **S116-1**.

Scheme 117 Reactivity of calix[4]imidazolium with copper(I)/(II) ions.

Scheme 118 Platinum(II) tetracarbene dicationic complex **S118-1**.

do not meet all outlined initially criteria. Namely, the requirement to contain four five-membered rings and/or four *meso*-carbon bridges is not accomplished. However, their structural similarity to the already presented molecules and specific properties secured their place in the review.

### N-confused calix[4]phyrins

The first subgroup contains N-confused porphyrinoids with one or two *meso* bridges possessing hybridisation C(sp<sup>3</sup>), a clear reference to the nonaromatic macrocycles presented above.

Calix[4]phyrin with one C(sp<sup>3</sup>) bridge substituted with two methyl groups is obtained when condensation leading to NCP gets enriched with acetone.<sup>265</sup> This produces **S119-1** (Scheme 119) with the oxygenated C(3) atom in 3% aside from also formed NCP. The macrocycle acquires a 2H cavity and a lactam moiety at the confused pyrrole ring. Expectedly, **S119-1** proved to be a suitable ligand for nickel(II) (**S119-2**) and, significantly, copper(II) (**S119-3**) forming a direct and stable organometallic bond (1.905(4) and 2.007(4) Å, respectively). In further explorations,<sup>266</sup> the chlorozinc(II) centre was also formed in a reaction of **S119-1** with Zn(CH<sub>3</sub>COO)<sub>2</sub> followed by the saturation of the mixture with NaCl (**S119-4**). Here, the

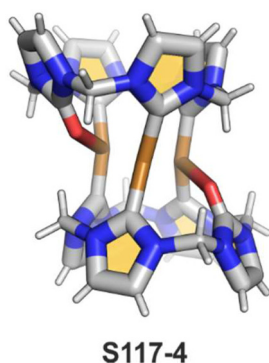


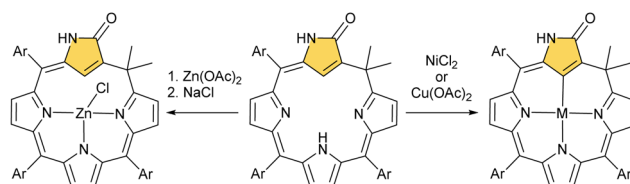
Fig. 28 Copper carbene complex with inner-C position oxygenated.

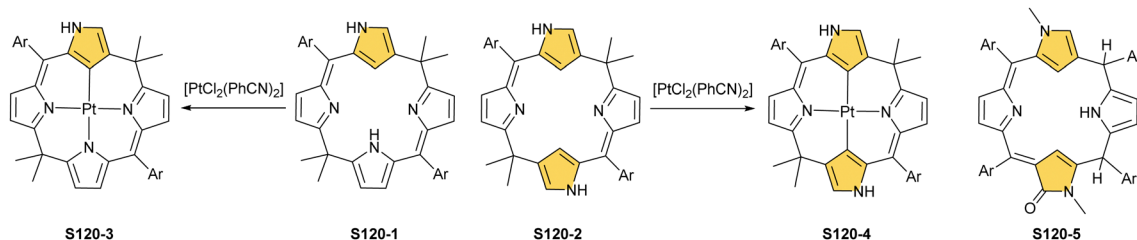
**S117-4** with acid produces the oxygenated macrocycle **S117-5**. Surprisingly, the oxygen atom originates from the acetate anion rather than water or dioxygen, as proven by <sup>18</sup>O labelling.

For the sake of completeness, it remains to mention that the *meso*-dimethylamino-substituted derivatives of the platinum(II) tetracarbene dicationic complex **S118-1** (Scheme 118) were also reported.<sup>264</sup> This species forms using a template approach.

## Beyond carbaporphyrin(1.1.1.1)

In the last section, selected macrocycles, which are arbitrarily chosen as being representative of the further developments in the carbaporphyrinoid field, will be described. Formally, they

Scheme 119 Complexes of the N-confused calix[4]phyrin derivative **S119-1**.



Scheme 120 Complexes of N-confused calix[4]pyrrole derivatives **S120-1** and **S120-2** and porphodimethene **S120-5**.

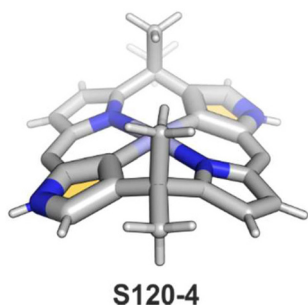


Fig. 29 Platinum(II) dicarbocalix[4]pyrrole. *meso*-Aryls not shown.

$\text{Zn} \cdots \text{C}(21)$  distance increases to 2.67(1) Å from 2.41–2.53 Å for zinc(II) complexes with NCP (**S14-2** and **S14-3**).

Calix[4]pyrrole complexes have more intensive infrared absorption than the respective NCP derivatives, which was also noted in the study of macrocycles with two  $\text{C}(\text{sp}^3)$  *meso* bridges and one or two N-confused rings.<sup>267</sup> The macrocycles are formed in a condensation of substituted N-confused dipyrromethene. Both macrocycles, **S120-1** (Scheme 120) and **S120-2**, possess a 2H cavity that was matched with the platinum(II) centre in a reaction with  $[\text{PtCl}_2(\text{PhCN})_2]$ . Interestingly, only **S120-4** (with two N-confused pyrroles) shows a significant degree of nonplanarity (Fig. 29). Yet both, **S120-3** and **S120-4**, stabilise organometallic bonds with an average distance of 2.00 Å. Another, not fully oxidised example – porphodimethene **S120-5** possesses two adjacent *meso* bridges  $\text{C}(\text{sp}^3)$ -hybridised.<sup>268</sup> This ligand stabilises  $\text{Cu}^{\text{III}}$  and  $\text{Ni}^{\text{II}}$  metal centres.

There are also known singly and doubly N-confused macrocycles with all four *meso* bridges  $\text{sp}^3$ -hybridised called calix[4]pyrroles, yet their main application so far was sensing and anion recognition.<sup>269–271</sup>

## Carbacorroles

Another subgroup contains carbaporphyrinoids lacking one *meso* bridge, namely carbacorroles and N-confused corroles.

Attempts to synthesise 21-silaporphyrin resulted in the serendipitous discovery of a transformation of 21-silaphlorin into nonaromatic isocarbacorrole **S121-1**.<sup>272</sup> Similar trials to form 21-phosphaporphyrin led to the formation of the P-confused analogue.<sup>273</sup>

Insertion of silver or copper ions into isocarbacorrole **S121-1** (Scheme 121) gives two structurally related organometallic complexes of “true” carbacorrole (**S121-2** (Fig. 30) and **S121-3**) in which the metal(III) ions are bound by three pyrrolic nitrogen atoms and a tetrahedrally hybridised inner carbon atom of the cyclopentadiene ring with aryl substitution. The  $\text{Ag}-\text{C}(\text{sp}^3)$  (2.046(5) Å) bond length is similar to that in silver(III) carbaporphyrinoids in which a trigonal carbon atom coordinates to the metal ion.

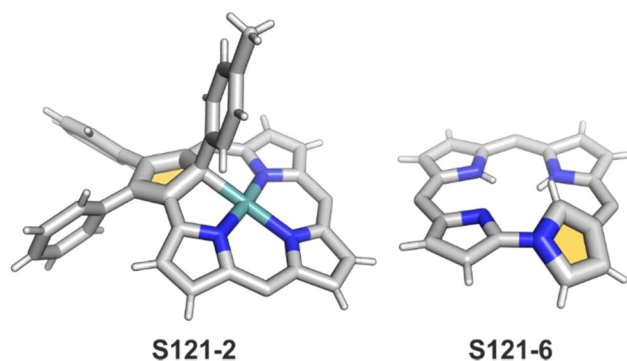
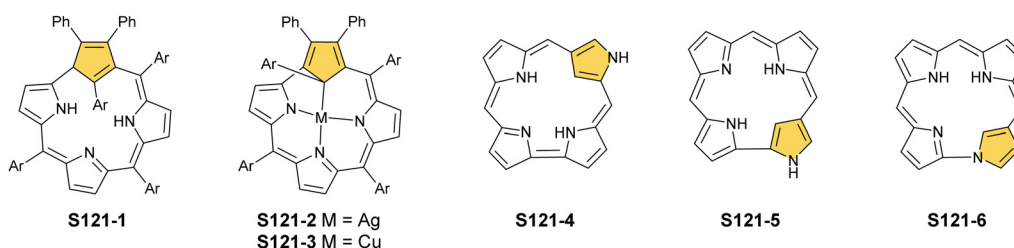
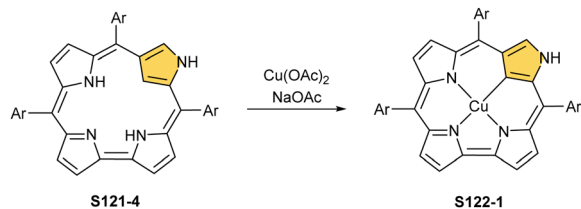


Fig. 30 Selected carbacorrole frameworks. *meso*-Substituents not shown.



Scheme 121 Carbacorroles.

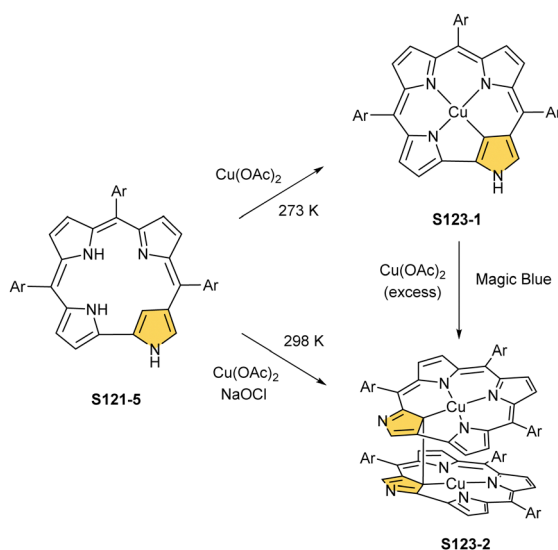


Scheme 122 Synthesis of copper(III) N-confused corrole **S122-1** from **S121-4**.

The appropriately designed substrates incorporating one 'N-confused pyrrolic ring' allowed for synthesising two types of modified carbabilanes (a noncyclic precursor of carbaporphyrin missing one *meso*-carbon link).<sup>274,275</sup> After oxidation of carbabilane, a C $\alpha$ -C $\alpha'$  pyrrole-pyrrole bond forms closing two macrocycles – N-confused corrole **S121-4** and **S121-5**. Alternatively, the N-C $\alpha$  pyrrole-pyrrole linkage yields the neo-confused version, *i.e.*, norrole **S121-6** (Fig. 30). Their <sup>1</sup>H NMR spectra indicate a significant degree of the diatropicity of these contracted carbaporphyrinoids with the inner CH signal located at  $-0.91$ ,  $1.84$ , and  $1.21$  ppm for **S121-4**, **S121-5**, and **S121-6**, respectively. It is despite a seemingly interrupted  $\pi$ -delocalization pathway in the typically shown resonance contributors. Also, the oxanorrole derivative has been recently synthesised.<sup>276</sup>

**S121-4** and **S121-5** accommodate copper(III), which seems to be a natural central cation for the trianionic cavity.<sup>275</sup> The insertion proceeds from copper(II) acetate and gives stable **S122-1** (Scheme 122) and **S123-1** (Scheme 123).

However, in contrast to **S122-1**, complex **S123-1** exhibits further reactivity. Under an excess of copper(II) salt or after adding the magic blue oxidant, it undergoes oxidative dimerization forming a C–C bond between inner coordinated carbon atoms yielding **S123-2** (Fig. 31). The C–C bond length equals  $1.552(7)$  Å, reflecting a single bond between two C(sp<sup>3</sup>) centres.



Scheme 123 Synthesis of copper(III) N-confused corrole **S123-1** and its dimer **S123-2** from **S121-5**.

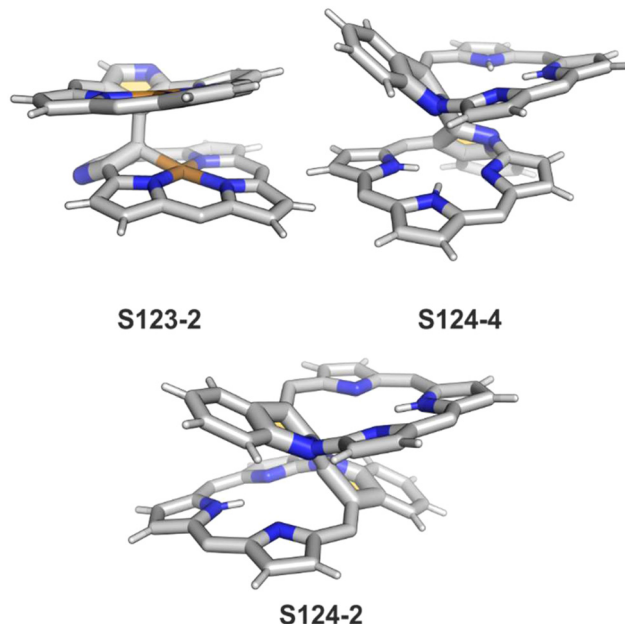
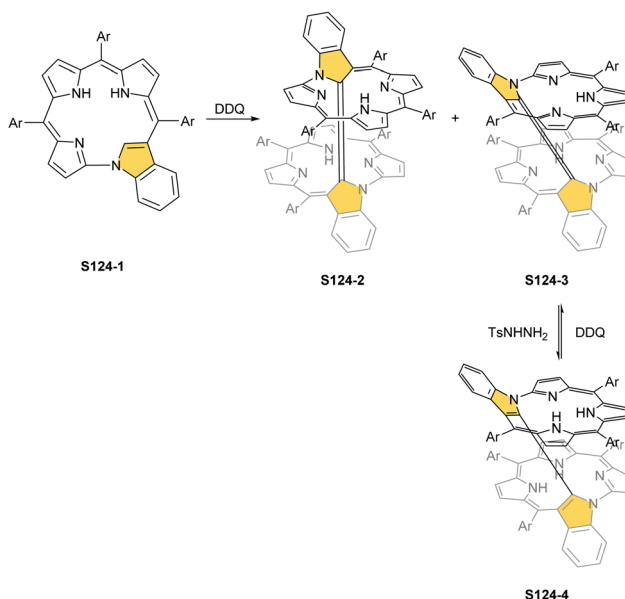
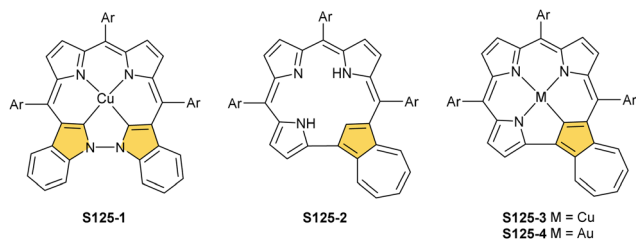


Fig. 31 Carbacorrole inner-C dimers. *meso*-Substituents not shown.

Similar to **S121-6**, benzonorrole **S124-1** (Scheme 124) can be obtained, first, as a copper(III) complex and then through demetallation.<sup>277</sup> Interestingly, **S124-1** in a free form can dimerise upon further oxidation, forming *trans* (**S124-2**; Fig. 31) and *cis* (**S124-3**) isomers with directly linked inner carbon atoms derived from each subunit. Solid-state structures indicated that the linkage is short enough ( $<1.36$  Å) to be described as a double bond. The confirmation comes from the test reduction of **S124-3** with the hydrazine derivative that gives **S124-4** (Fig. 31). Here, the C–C bond length increases to  $1.476(3)$  Å and the process can be reversed *via* reoxidation.



Scheme 124 Reactivity of benzonorrole **S124-1** with DDQ.



Scheme 125 Diazadicarborrole **S125-1** and carbacborrole, containing azulene.

Carbabilane with an indole moiety at each end of the acyclic molecule affords, after macrocyclisation, porphyrinoid **S125-1** (Scheme 125) linked through a direct N–N bond, among other products.<sup>278</sup> As shown in the scheme, the macrocycle is stabilised through the coordination of a copper(III) centre, which is inserted during macrocyclisation. Copper(III) removal with zinc and acid leads directly to starting carbabilane. An effective  $\pi$ -conjugation through the N–N linkage can be inferred, among others, from the  $^1\text{H}$  NMR spectra of **S125-1**.

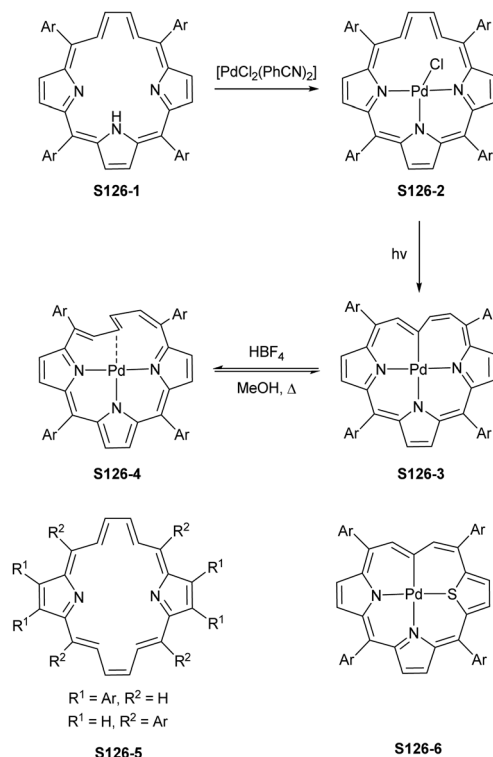
Finally, copper(III) was a central ion of choice to demonstrate the coordination abilities of carbacborrole, with one pyrrole replaced with an azulene fragment as seen in **S125-2**.<sup>279</sup> Interestingly, this carbaporphyrinoid is formed from simple substrates and the predesigned building blocks were not required. Azulene in **S125-2** forms a direct bond to one of pyrrole rings. The aromaticity level resembles that of regular azuliporphyrin **S64-2** (the inner H(21) chemical shift in **S125-2** equals 3.19 ppm). Three inner protons can be replaced easily with  $\text{M}^{\text{III}}$  cations; thus,  $\text{Cu}^{\text{III}}$  **S125-3** and  $\text{Au}^{\text{III}}$  **S125-4** complexes were isolated. The  $\text{Cu}^{\text{III}}$ –C(21) organometallic bond stabilised within the framework of **S125-3** is 1.886(10) Å long.

### Annulene-containing porphyrins

Vacataporphyrin **S126-1** (Scheme 126) represents a next macrocyclic frame to be mentioned, *i.e.*, a porphyrin deprived one inner nitrogen atom, which pushes it further on an axis from porphyrin to annulenes.

*meso*-Tetraarylvacataporphyrin **S126-1** was initially generated from 21-telluraporphyrin through acidolytic removal of the tellurium atom.<sup>280</sup> The macrocycle remains aromatic with the two inner CH protons from a remained diene fragment resonating at  $-2.50$  ppm. **S126-1** can be coordinated with palladium(II), among others.<sup>281</sup>

A reaction with  $[\text{PdCl}_2(\text{PhCN})_2]$  yields **S126-2** with no direct C–Pd bonding (Fig. 32), yet the forced proximity facilitates further transformations. After exposing the complex to light, the transformation occurs in which one of the carbon atoms gets coordinated, forming **S126-3**. The latter complex is still aromatic, as confirmed with the  $^1\text{H}$  NMR spectra, but the spectrum changes after either protonation or methylation with methyl iodide in the presence of a halide acceptor ( $\text{AgBF}_4$ ), indicating features of paratropicity. The  $\sigma$ -coordinated carbon atom accepts a proton (or methyl) forming **S126-4**, but because palladium(II) prefers a tetracoordinate environment, it strongly



Scheme 126 Vacata- (**S126-1**), divacata- (**S126-5**), and allyliporphyrin (**S126-6**) frameworks.

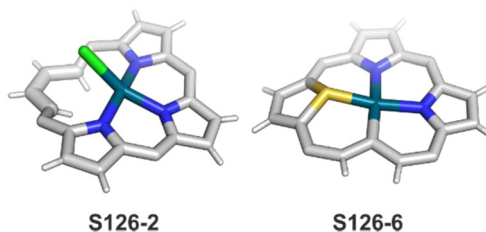


Fig. 32 Palladium(II) vacata- and allyliporphyrin complexes. *meso*-Substituents not shown.

interacts with the closest double bond ( $\eta^2$ -coordination), altering the conformation of a whole fragment and switching the topology of  $\pi$  orbitals from the Hückel aromatic to the Möbius antiaromatic  $18\pi$ -electron system.

A logical extension of a vacata-like annulene-porphyrin hybrid concept comes with divacataporphyrin **S126-5**. A half porphyrin-half annulene tetraphenyl- $\beta$ -substituted derivative was elegantly synthesized by Lash and co-workers in a McMurry coupling reaction.<sup>282</sup> Alternatively, an extrusion of two tellurium atoms from 21,23-ditelluraporphyrin yields *meso*-tetraaryl-21,23-divacataporphyrin.<sup>283</sup>

Allyliporphyrin constitutes another approach towards annulenes, in which one removes outer  $\beta$ -carbon atoms from a cyclopentadiene unit of theoretical carba(hetero)porphyrin.<sup>284</sup> The macrocycle forms in the course of a multistep reaction completed with condensation of an appropriate thiophene-allyl





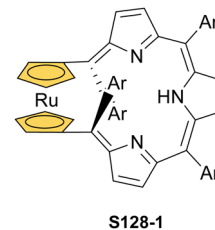
precursor with dipyrromethene. Similar to vacataporphyrins, this dynamic system also shows aromatic features and, due to the availability of two inner protons, forms the palladium(II) complex **S126-6** (Fig. 32) with direct Pd–C  $\sigma$ -bonding.

### Metalloceporphyrins

The final group of porphyrinoids to be discussed are classified as metalloceporphyrins, in which the annulene model of aromaticity is not natural at all. Ferrocene can be introduced into the porphyrinic framework through 1,3-positions from the same ring, replacing one of the pyrrolic rings. Then, the oxidation and work-up processes yield 21-carbaporphyrin (true carbaporphyrin) **S1-3**.<sup>213</sup>

An alternative incorporation mode of ferrocene was explored as well. Namely, the metallocene moiety can be also built-in through one carbon atom from each cyclopentadienyl ring (1,1'-binding mode) using appropriate precursors.<sup>29</sup> Consequently, a stable three-dimensional ferrocenothiaporphyrin **S127-1** (Scheme 127) is constructed (Fig. 33). Despite being highly nonplanar, the organometallic system seems to be fully conjugated. The <sup>1</sup>H NMR spectrum of **S127-1** shows antiaromatic features, with inner protons from the ferrocenyl unit located at 11.30 ppm. This peculiar metallamacrocycle can be reversibly reduced with two electrons providing **S127-3** – an aromatic congener. The later molecule exhibits the inner proton signal at 1.73 ppm as expected.

Similar molecular qualities are observed for ruthenoceno-thiaporphyrin **S127-2** and its reduced form **S127-4**.<sup>30</sup> The two Cp rings in **S127-2** adopt an anticlinal eclipsed



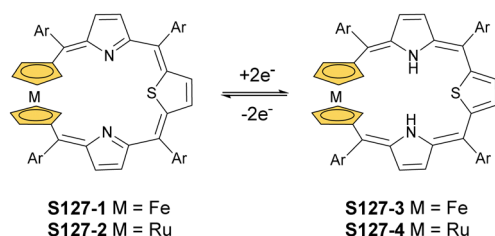
Scheme 128 Ruthenocenoporphyrin **S128-1**.

conformation. The most interesting electronic properties were detected for all-aza ruthenocenoporphyrin **S128-1** (Scheme 128) as it acquires a conformation completely different from **S127-1** or **S127-2**. The monoprotonated cation of **S128-1** adopts a peculiar conformation (Fig. 33), with the Cp rings almost eclipsed. It results in the macrocyclic diatropicity of **S128-1** and its protonated forms. It means that after changing the conformation from that of **S127-2** to that of **S128-1**, the antiaromaticity switches to aromaticity without changing the number of accessible  $\pi$ -electrons. Therefore, it has been confirmed that the macrocyclic  $\pi$  conjugation transmitted across a d-electron metallocene is conformationally controlled.

## Conclusions

The well-thought-out decision has been made to explore the “family ties” of carbaporphyrinoids starting from Vogel's original idea, namely, to approach carbaporphyrins from an annulene chemist's point of view.<sup>285–287</sup> According to our expectations, such an overview brings an appropriate perspective to the present achievements in the field. In longer distances, the promising perspectives can be founded presumably achievable *via* well-planned synthesis of intriguing structures still preserving the principal porphyrinic skeleton. Emanuel Vogel pioneered a very stimulating concept in his enlightening and stimulating overview, introducing the idea of novel porphyrin isomers. Namely, he approached a porphyrin frame from an “annulene-chemist perspective”. Thus, an all-carbon forefather of a porphyrin skeleton may be constructed by incorporating two CH<sub>2</sub> and two CH=CH bridges to the maternal [18]annulene **1**, resulting in peculiar aromatic tetracyclopentadienic hydrocarbon **4** (Scheme 129). To date, such hydrocarbon, later named quatyrin,<sup>238</sup> and its oxidised derivative didehydroquatyrin remain to be synthesised, albeit the importance of **4** to both annulene and porphyrin fields has been highlighted.<sup>288</sup> Significantly, the relevant molecular pattern has been identified in the tetraazuliporphyrin tetracation **S105-2**.<sup>241</sup>

Eventually, one can notice that Vogel's concept can be readily adapted to visualise many carbaporphyrins, which preserve the fundamental geometric features of regular porphyrin (Schemes 130–132). Accordingly, quatyrin **4** can be recognised as a fundamental molecular framework to be merely modified by “nitriding” [incorporating, *e.g.*, one (6 or 9), two (7 or 11), three (8 or 12) or four (5) nitrogen atoms in the location of



Scheme 127 Metalloceporphyrins.

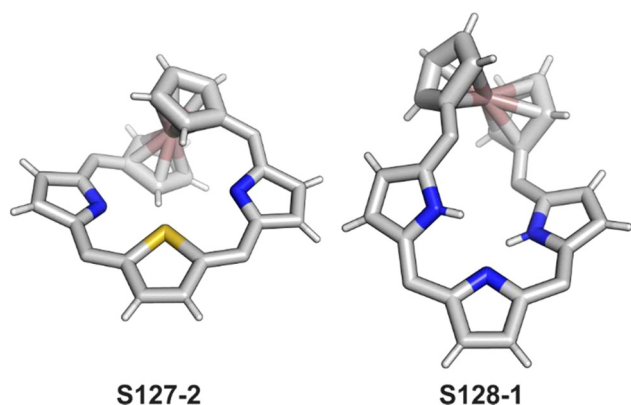
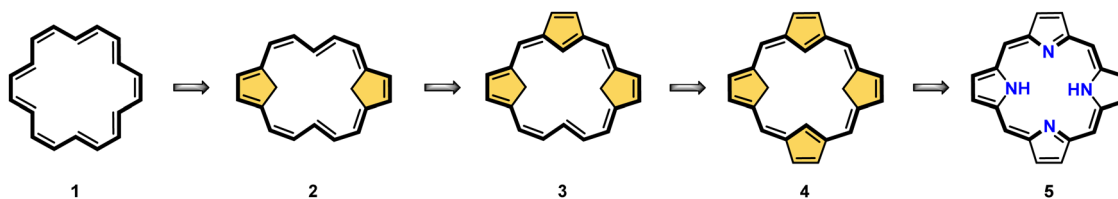
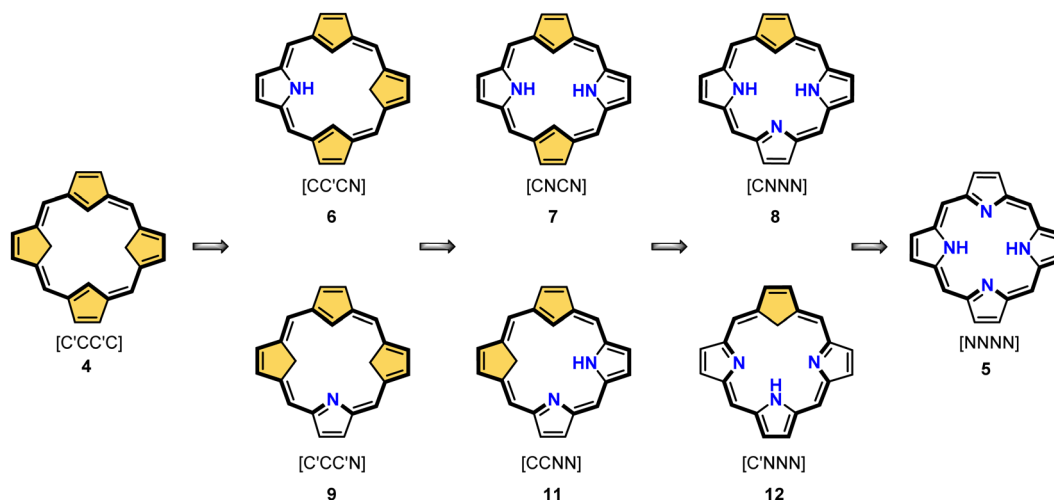


Fig. 33 Metalloceporphyrinoids. *meso*-Substituents not shown.





**Scheme 129** Visualisation of bridging patterns affording [18]annulene **1** transformation into quaterpyrin **4** and subsequently into porphyrin **5**.

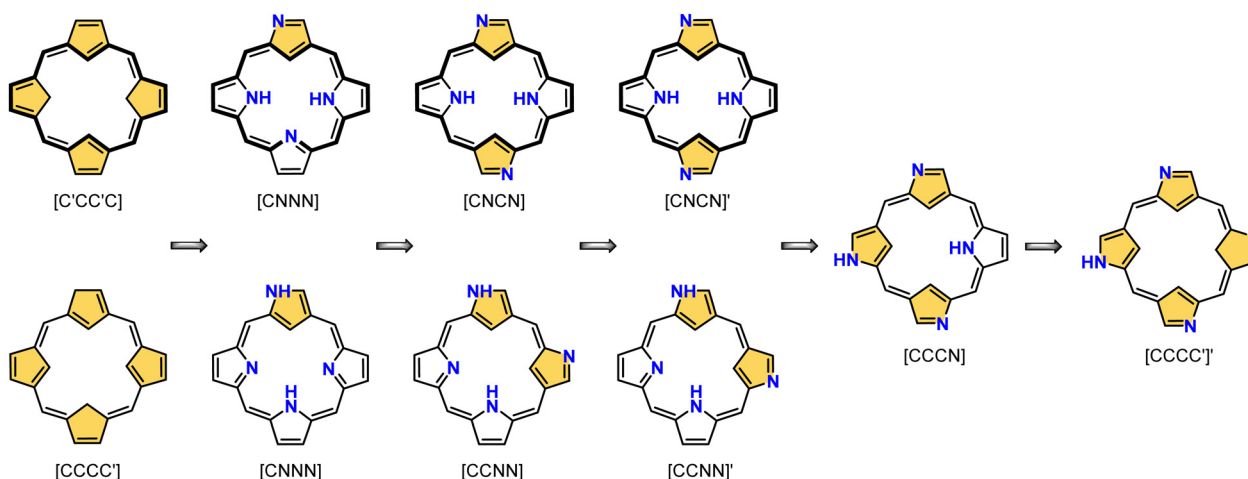


**Scheme 130** Inner core stepwise "nitriding" of quaterpyrin (an inner core described as: [set of donor atoms], hybridisations: C' tetrahedral, C trigonal, N trigonal).

choice instead of carbon atom(s)] (Scheme 130). In the limits of this review, one can present all feasible and equally intriguing structures resulting from the very conceptually rewarding visualisations. The most intriguing or the most promising have been arbitrarily selected, presenting the construction of regular carbaporphyrins (Scheme 130), N-confused porphyrins (Scheme 131, the whole set explored by using the

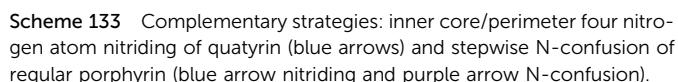
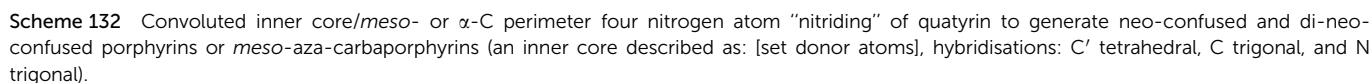
DFT approach<sup>289,290</sup>), neo-confused porphyrins (Scheme 132, the motif theoretically studied<sup>291</sup>), and *meso*-aza carbaporphyrins (Scheme 132).

Finally, regular porphyrin **5** and quaterpyrin **4** can be used as two opposite starting points to create prototypes of carbaporphyrinoids *via* N-confusion or nitriding concepts, respectively (Scheme 133).



**Scheme 131** Inner core/perimeter four nitrogen atom "nitriding" of quaterpyrin to generate N-confused and di-, tri-, and tetra-N-confused porphyrins (an inner core described as: [set donor atoms], hybridisations: C' tetrahedral, C trigonal, and N trigonal).





This all shows a plentiful set of ideas for forming porphyrins containing a carbon atom within the cavity exposed to interactions with a metal ion. As we presented, experimental explorations started in the 1990s are far from being completed. They should bring many new and original results and deepen our knowledge of organometallic chemistry under macrocyclic confinement and the further application of these fascinating systems in the years to come.

There are no conflicts to declare.

This work was supported by JSPS KAKENHI Grant Number JP20H00406 and NCN Grant Numbers 2020/39/D/ST4/00021 and 2019/35/D/ST4/00361. Publication of this article was supported by the Excellence Initiative – Research University program for the University of Wrocław.

- 1 T. D. Lash, *Chem. Rev.*, 2017, **117**, 2313–2446.
- 2 M. Toganoh and H. Furuta, *Chem. Commun.*, 2012, **48**, 937–954.
- 3 T. Tanaka and A. Osuka, *Chem. Rev.*, 2017, **117**, 2584–2640.
- 4 T. Chatterjee, V. S. Shetti, R. Sharma and M. Ravikanth, *Chem. Rev.*, 2017, **117**, 3254–3328.
- 5 L. Cuesta and J. L. Sessler, *Chem. Soc. Rev.*, 2009, **38**, 2716–2729.
- 6 G. Anguera and D. Sánchez-García, *Chem. Rev.*, 2017, **117**, 2481–2516.
- 7 S. Shimizu, *Chem. Rev.*, 2017, **117**, 2730–2784.
- 8 Y. Matano, *Chem. Rev.*, 2017, **117**, 3138–3191.
- 9 R. Orłowski, D. Gryko and D. T. Gryko, *Chem. Rev.*, 2017, **117**, 3102–3137.
- 10 C. Brückner, J. Akhigbe and L. P. Samankumara, *Handbook of Porphyrin Science*, World Scientific Publishing Company, 2012, vol. 31, pp. 1–275.
- 11 E. Vogel, M. Köcher, H. Schmickler and J. Lex, *Angew. Chem., Int. Ed. Engl.*, 1986, **25**, 257–259.
- 12 P. J. Chmielewski, L. Latos-Grażyński, K. Rachlewicz and T. Głowiak, *Angew. Chem., Int. Ed. Engl.*, 1994, **33**, 779–781.
- 13 H. Furuta, T. Asano and T. Ogawa, *J. Am. Chem. Soc.*, 1994, **116**, 767–768.
- 14 D. Dolphin, R. H. Felton, D. C. Borg and J. Fajer, *J. Am. Chem. Soc.*, 1970, **92**, 743–745.
- 15 M. O. Senge, *Angew. Chem., Int. Ed.*, 2011, **50**, 4272–4277.
- 16 M. J. Broadhurst, R. Grigg and A. W. Johnson, *J. Chem. Soc. C*, 1971, 3681–3690.

- 17 A. Ulman and J. Manassen, *J. Am. Chem. Soc.*, 1975, **97**, 6540–6544.
- 18 L. Latos-Grażyński, J. Lisowski, M. M. Olmstead and A. L. Balch, *J. Am. Chem. Soc.*, 1987, **109**, 4428–4429.
- 19 W. Haas, B. Knipp, M. Sicken, J. Lex and E. Vogel, *Angew. Chem., Int. Ed. Engl.*, 1988, **27**, 409–411.
- 20 E. Vogel, P. Röhrig, M. Sicken, B. Knipp, A. Herrmann, M. Pohl, H. Schmickler and J. Lex, *Angew. Chem., Int. Ed. Engl.*, 1989, **28**, 1651–1655.
- 21 M. Stępień, L. Latos-Grażyński, N. Sprutta, P. Chwalisz and L. Szterenber, *Angew. Chem., Int. Ed.*, 2007, **46**, 7869–7873.
- 22 A. Osuka and S. Saito, *Chem. Commun.*, 2011, **47**, 4330–4339.
- 23 M. Stępień, N. Sprutta and L. Latos-Grażyński, *Angew. Chem., Int. Ed.*, 2011, **50**, 4288–4340.
- 24 M. Pawlicki and L. Latos-Grażyński, *Chem. – Asian J.*, 2015, **10**, 1438–1451.
- 25 H. Maeda, Y. Ishikawa, T. Matsuda, A. Osuka and H. Furuta, *J. Am. Chem. Soc.*, 2003, **125**, 11822–11823.
- 26 N. Grzegorzec, M. Pawlicki, L. Szterenber and L. Latos-Grażyński, *J. Am. Chem. Soc.*, 2009, **131**, 7224–7225.
- 27 B. Szyszko, L. Latos-Grażyński and L. Szterenber, *Angew. Chem., Int. Ed.*, 2011, **50**, 6587–6591.
- 28 K. Hurej, M. Pawlicki, L. Szterenber and L. Latos-Grażyński, *Angew. Chem., Int. Ed.*, 2016, **55**, 1427–1431.
- 29 I. Simkova, L. Latos-Grażyński and M. Stępień, *Angew. Chem., Int. Ed.*, 2010, **49**, 7665–7669.
- 30 I. Grocka, L. Latos-Grażyński and M. Stępień, *Angew. Chem., Int. Ed.*, 2013, **52**, 1044–1048.
- 31 J. B. dela Cruz, M. Ruamps, S. Arco and C.-H. Hung, *Dalton Trans.*, 2019, **48**, 7527–7531.
- 32 J. B. dela Cruz and C.-H. Hung, *Catal. Sci. Technol.*, 2021, **11**, 2144–2154.
- 33 T. Miyazaki, T. Yamamoto, S. Mashita, Y. Deguchi, K. Fukuyama, M. Ishida, S. Mori and H. Furuta, *Eur. J. Inorg. Chem.*, 2018, 203–207.
- 34 K. Rachlewicz, L. Latos-Grażyński and E. Vogel, *Inorg. Chem.*, 2000, **39**, 3247–3251.
- 35 M. J. Bialek and L. Latos-Grażyński, *Chem. Commun.*, 2014, **50**, 9270–9272.
- 36 P. Rothmund, *J. Am. Chem. Soc.*, 1936, **58**, 625–627.
- 37 A. D. Adler, F. R. Longo, J. D. Finarelli, J. Goldmacher, J. Assour and L. Korsakoff, *J. Org. Chem.*, 1967, **32**, 476.
- 38 J. S. Lindsey, I. C. Schreiman, H. C. Hsu, P. C. Kearney and A. M. Marguerettaz, *J. Org. Chem.*, 1987, **52**, 827–836.
- 39 M. Pawlicki and L. Latos-Grażyński, *Handbook of Porphyrin Science*, World Scientific Publishing, Singapore, 2010, vol. 2, pp. 103–192.
- 40 A. Berlicka and L. Latos-Grażyński, *J. Porphyrins Phthalocyanines*, 2020, **24**, 1–20.
- 41 P. Pushpanandan and M. Ravikanth, *Top. Curr. Chem.*, 2021, **379**, 26.
- 42 M. Toganoh and H. Furuta, *Chem. Rev.*, 2022, **122**, 8313–8437.
- 43 T. D. Lash, *Acc. Chem. Res.*, 2016, **49**, 471–482.
- 44 K. Hurej and L. Latos-Grażyński, in *Metal-Ligand Co-operativity: Catalysis and the Pincer-Metal Platform*, ed. G. van Koten, K. Kirchner and M.-E. Moret, Springer International Publishing, Cham, 2021, pp. 181–225.
- 45 J. Zhang, G. Leitus, Y. Ben-David and D. Milstein, *Angew. Chem., Int. Ed.*, 2006, **45**, 1113–1115.
- 46 B. Guo, E. Otten and J. G. de Vries, in *Metal-Ligand Co-operativity: Catalysis and the Pincer-Metal Platform*, ed. G. van Koten, K. Kirchner and M.-E. Moret, Springer International Publishing, Cham, 2021, pp. 321–377.
- 47 H.-T. Zhang and M.-T. Zhang, in *Metal-Ligand Co-operativity: Catalysis and the Pincer-Metal Platform*, ed. G. van Koten, K. Kirchner and M.-E. Moret, Springer International Publishing, Cham, 2021, pp. 379–449.
- 48 S. Aronoff and M. Calvin, *J. Org. Chem.*, 1943, **08**, 205–223.
- 49 B. Y. Liu, C. Brückner and D. Dolphin, *Chem. Commun.*, 1996, 2141–2142.
- 50 G. R. Geier, D. M. Haynes and J. S. Lindsey, *Org. Lett.*, 1999, **1**, 1455–1458.
- 51 T. Morimoto, S. Taniguchi, A. Osuka and H. Furuta, *Eur. J. Org. Chem.*, 2005, 3887–3890.
- 52 H. Furuta, T. Ishizuka, A. Osuka, H. Dejima, H. Nakagawa and Y. Ishikawa, *J. Am. Chem. Soc.*, 2001, **123**, 6207–6208.
- 53 T. Ishizuka, R. Sakashita, O. Iwanaga, T. Morimoto, S. Mori, M. Ishida, M. Toganoh, K. Takegoshi, A. Osuka and H. Furuta, *J. Phys. Chem. A*, 2020, **124**, 5756–5769.
- 54 R. Sakashita, Y. Oka, H. Akimaru, P. E. Kesavan, M. Ishida, M. Toganoh, T. Ishizuka, S. Mori and H. Furuta, *J. Org. Chem.*, 2017, **82**, 8686–8696.
- 55 P. J. Chmielewski and L. Latos-Grażyński, *J. Chem. Soc., Perkin Trans. 2*, 1995, 503–509.
- 56 W. Qu, T. Ding, A. Cetin, J. D. Harvey, M. J. Taschner and C. J. Ziegler, *J. Org. Chem.*, 2006, **71**, 811–814.
- 57 M. Toganoh, T. Yamamoto, T. Hihara, H. Akimaru and H. Furuta, *Org. Biomol. Chem.*, 2012, **10**, 4367–4374.
- 58 P. J. Chmielewski, *Org. Lett.*, 2005, **7**, 1789–1792.
- 59 D. Ren, S. Koniarz, X. Li and P. J. Chmielewski, *Chem. Commun.*, 2020, **56**, 4836–4839.
- 60 X. Li, B. Liu, P. Yi, R. Yi, X. Yu and P. J. Chmielewski, *J. Org. Chem.*, 2011, **76**, 2345–2349.
- 61 I. Schmidt and P. J. Chmielewski, *Tetrahedron Lett.*, 2001, **42**, 6389–6392.
- 62 B. Liu, X. Li, X. Xu, M. Stępień and P. J. Chmielewski, *J. Org. Chem.*, 2013, **78**, 1354–1364.
- 63 P. J. Chmielewski, *Angew. Chem., Int. Ed.*, 2004, **43**, 5655–5658.
- 64 N. Grzegorzec, L. Latos-Grażyński and L. Szterenber, *Org. Biomol. Chem.*, 2012, **10**, 8064–8075.
- 65 Y. Ishikawa, I. Yoshida, K. Akaiwa, E. Koguchi, T. Sasaki and H. Furuta, *Chem. Lett.*, 1997, 453–454.
- 66 N. Kashiwagi, T. Akeda, T. Morimoto, T. Ishizuka and H. Furuta, *Org. Lett.*, 2007, **9**, 1733–1736.
- 67 B. Liu, X. Li, J. Maciolek, M. Stępień and P. J. Chmielewski, *J. Org. Chem.*, 2014, **79**, 3129–3139.
- 68 L. Szterenber and L. Latos-Grażyński, *J. Porphyrins Phthalocyanines*, 2001, **05**, 474–480.
- 69 M. Toganoh and H. Furuta, *J. Phys. Chem. A*, 2009, **113**, 13953–13963.





- 70 H. Furuta, T. Ishizuka, A. Osuka and T. Ogawa, *J. Am. Chem. Soc.*, 1999, **121**, 2945–2946.
- 71 M. Toganoh and H. Furuta, *Chem. Lett.*, 2019, **48**, 615–622.
- 72 S. Ikeda, M. Toganoh and H. Furuta, *Inorg. Chem.*, 2011, **50**, 6029–6043.
- 73 S. Touden, Y. Ikawa, R. Sakashita, M. Toganoh, S. Mori and H. Furuta, *Tetrahedron Lett.*, 2012, **53**, 6071–6074.
- 74 M. Toganoh, T. Kimura and H. Furuta, *Chem. – Eur. J.*, 2008, **14**, 10585–10594.
- 75 M. Toganoh, T. Kimura and H. Furuta, *Chem. Commun.*, 2008, 102–104.
- 76 T. Ishizuka, A. Osuka and H. Furuta, *Angew. Chem., Int. Ed.*, 2004, **43**, 5077–5081.
- 77 H. Furuta, T. Ishizuka and A. Osuka, *J. Am. Chem. Soc.*, 2002, **124**, 5622–5623.
- 78 H. Furuta, T. Morimoto and A. Osuka, *Inorg. Chem.*, 2004, **43**, 1618–1624.
- 79 Y.-C. Chen, J.-Y. Tung, T.-K. Liu, W.-J. Tsai, H.-Y. Lin, Y.-C. Chang and J.-H. Chen, *Dalton Trans.*, 2018, **47**, 14774–14784.
- 80 M. Siczek and P. J. Chmielewski, *Angew. Chem., Int. Ed.*, 2007, **46**, 7432–7436.
- 81 M. Toganoh, H. Ogawa, T. Morimoto and H. Furuta, *Supramol. Chem.*, 2009, **21**, 324–330.
- 82 T. Morimoto, H. Uno and H. Furuta, *Angew. Chem., Int. Ed.*, 2007, **46**, 3672–3675.
- 83 P. J. Chmielewski and L. Latos-Grażyński, *Inorg. Chem.*, 1997, **36**, 840–845.
- 84 Z. Xiao, B. O. Patrick and D. Dolphin, *Inorg. Chem.*, 2003, **42**, 8125–8127.
- 85 H. He, Z. Ye, D. Shimizu, I. Sumra, Y. Zhang, Z. Liang, Y. Zeng, L. Xu, A. Osuka, Z. Ke and H. W. Jiang, *Chem. – Eur. J.*, 2022, **28**, e202103272.
- 86 H.-W. Jiang, Q.-Y. Chen, J.-C. Xiao and Y.-C. Gu, *Chem. Commun.*, 2009, 3732–3734.
- 87 P. J. Chmielewski, L. Latos-Grażyński and T. Głowiak, *J. Am. Chem. Soc.*, 1996, **118**, 5690–5701.
- 88 T. D. Lash, D. T. Richter and C. M. Shiner, *J. Org. Chem.*, 1999, **64**, 7973–7982.
- 89 T. D. Lash and A. L. Von Ruden, *J. Org. Chem.*, 2008, **73**, 9417–9425.
- 90 H.-W. Jiang, Q.-Y. Chen, J.-C. Xiao and Y.-C. Gu, *Chem. Commun.*, 2008, 5435–5437.
- 91 I. Schmidt and P. J. Chmielewski, *Chem. Commun.*, 2002, 92–93.
- 92 A. Nakai, J. Kim, T. Tanaka, D. Kim and A. Osuka, *Angew. Chem., Int. Ed.*, 2021, **60**, 26540–26544.
- 93 H. Furuta, N. Kubo, H. Maeda, T. Ishizuka, A. Osuka, H. Nanami and T. Ogawa, *Inorg. Chem.*, 2000, **39**, 5424–5425.
- 94 D.-H. Won, M. Toganoh, H. Uno and H. Furuta, *Dalton Trans.*, 2009, 6151–6158.
- 95 T. Yoneda, S. Saito, H. Yorimitsu and A. Osuka, *Angew. Chem., Int. Ed.*, 2011, **50**, 3475–3478.
- 96 H. Furuta, K. Youfu, H. Maeda and A. Osuka, *Angew. Chem., Int. Ed.*, 2003, **42**, 2186–2188.
- 97 P. J. Chmielewski, B. Durlej, M. Siczek and L. Szterenber, *Angew. Chem., Int. Ed.*, 2009, **48**, 8736–8739.
- 98 H. Furuta, T. Ogawa, Y. Uwatoko and K. Araki, *Inorg. Chem.*, 1999, **38**, 2676–2682.
- 99 I. Sumra, M. Irfan, H. He, Y. Zhang, F. Hao, J. Lin, A. Osuka, Z. Zeng and H.-W. Jiang, *Eur. J. Org. Chem.*, 2021, 4440–4443.
- 100 M. Toganoh, T. Niino and H. Furuta, *Chem. Commun.*, 2008, 4070–4072.
- 101 N. Grzegorzec, M. Pawlicki and L. Latos-Grażyński, *J. Org. Chem.*, 2009, **74**, 8547–8553.
- 102 H.-W. Jiang, F. Hao, Q.-Y. Chen, J.-C. Xiao, S.-B. Liu and Y.-C. Gu, *J. Org. Chem.*, 2010, **75**, 3511–3514.
- 103 F. Hao, T. Zhang, D. Yu, X. Yang, H.-W. Jiang, J.-C. Xiao and Q.-Y. Chen, *Org. Lett.*, 2022, **24**, 1716–1721.
- 104 P. J. Chmielewski, *Angew. Chem., Int. Ed.*, 2005, **44**, 6417–6420.
- 105 P. J. Chmielewski, L. Latos-Grażyński and I. Schmidt, *Inorg. Chem.*, 2000, **39**, 5475–5482.
- 106 H. Maeda, A. Osuka, Y. Ishikawa, I. Aritome, Y. Hisaeda and H. Furuta, *Org. Lett.*, 2003, **5**, 1293–1296.
- 107 H. Furuta, H. Maeda and A. Osuka, *Org. Lett.*, 2002, **4**, 181–184.
- 108 J. Wojaczyński, M. Popiel, L. Szterenber and L. Latos-Grażyński, *J. Org. Chem.*, 2011, **76**, 9956–9961.
- 109 J. Wojaczyński and L. Latos-Grażyński, *Chem. – Eur. J.*, 2010, **16**, 2679–2682.
- 110 W.-C. Lin, D.-Z. Hsaio, W.-P. Chang, J.-H. Chen, S.-S. Wang and J.-Y. Tung, *Polyhedron*, 2012, **42**, 243–248.
- 111 N. Grzegorzec, E. Nojman, L. Szterenber and L. Latos-Grażyński, *Inorg. Chem.*, 2013, **52**, 2599–2606.
- 112 C.-H. Hung, C.-H. Peng, Y.-L. Shen, S.-L. Wang, C.-H. Chuang and H. M. Lee, *Eur. J. Inorg. Chem.*, 2008, 1196–1199.
- 113 I. Zilbermann, E. Maimon, R. Ydgar, A. I. Shames, E. Korin, L. Soifer and A. Bettelheim, *Inorg. Chem. Commun.*, 2004, **7**, 1238–1241.
- 114 K. B. Fields, J. T. Engle, S. Sripothongnak, C. Kim, X. P. Zhang and C. J. Ziegler, *Chem. Commun.*, 2011, **47**, 749–751.
- 115 J. D. Harvey and C. J. Ziegler, *Chem. Commun.*, 2004, 1666–1667.
- 116 C.-H. Chuang, W.-F. Liaw and C.-H. Hung, *Angew. Chem., Int. Ed.*, 2016, **55**, 5190–5194.
- 117 Y.-C. Chen, J.-Y. Tung, T.-K. Liu, W.-J. Tsai, C.-Y. Lin, H.-Y. Lin, S.-S. Li, J.-H. Chen and Y.-C. Chang, *Polyhedron*, 2019, **159**, 233–238.
- 118 Y.-C. Wang, J.-H. Chen, S.-S. Wang and J.-Y. Tung, *Inorg. Chem.*, 2013, **52**, 10711–10713.
- 119 Y.-Y. Lai, Y.-C. Chang, J.-H. Chen, S.-S. Wang and J.-Y. Tung, *Dalton Trans.*, 2016, **45**, 4854–4862.
- 120 A. Srinivasan, H. Furuta and A. Osuka, *Chem. Commun.*, 2001, 1666–1667.
- 121 A. Srinivasan, M. Toganoh, T. Niino, A. Osuka and H. Furuta, *Inorg. Chem.*, 2008, **47**, 11305–11313.
- 122 M. Toganoh, J. Konagawa and H. Furuta, *Inorg. Chem.*, 2006, **45**, 3852–3854.



- 123 T. Niino, M. Toganoh, B. Andrioletti and H. Furuta, *Chem. Commun.*, 2006, 4335–4337.
- 124 M. Toganoh, T. Niino, H. Maeda, B. Andrioletti and H. Furuta, *Inorg. Chem.*, 2006, **45**, 10428–10430.
- 125 K. Rachlewicz, S.-L. Wang, C.-H. Peng, C.-H. Hung and L. Latos-Grażyński, *Inorg. Chem.*, 2003, **42**, 7348–7350.
- 126 K. Rachlewicz, S.-L. Wang, J.-L. Ko, C.-H. Hung and L. Latos-Grażyński, *J. Am. Chem. Soc.*, 2004, **126**, 4420–4431.
- 127 K. Rachlewicz, D. Gorzelańczyk and L. Latos-Grażyński, *Inorg. Chem.*, 2006, **45**, 9742–9747.
- 128 W.-C. Chen and C.-H. Hung, *Inorg. Chem.*, 2001, **40**, 5070–5071.
- 129 C.-H. Hung, S.-L. Wang, J.-L. Ko, C.-H. Peng, C.-H. Hu and M.-T. Lee, *Org. Lett.*, 2004, **6**, 1393–1396.
- 130 C.-H. Hung, W.-M. Ching, G.-F. Chang, C.-H. Chuang, H.-W. Chu and W.-Z. Lee, *Inorg. Chem.*, 2007, **46**, 10941–10943.
- 131 W.-M. Ching and C.-H. Hung, *Chem. Commun.*, 2012, **48**, 4989–4991.
- 132 C.-H. Hung, W.-C. Chen, G.-H. Lee and S.-M. Peng, *Chem. Commun.*, 2002, 1516–1517.
- 133 C.-H. Hung, C.-H. Chang, W.-M. Ching and C.-H. Chuang, *Chem. Commun.*, 2006, 1866–1868.
- 134 T. Miyazaki, K. Fukuyama, S. Mashita, Y. Deguchi, T. Yamamoto, M. Ishida, S. Mori and H. Furuta, *ChemPlusChem*, 2019, **84**, 603–607.
- 135 O. Iwanaga, K. Fukuyama, S. Mori, J. T. Song, T. Ishihara, T. Miyazaki, M. Ishida and H. Furuta, *RSC Adv.*, 2021, **11**, 24575–24579.
- 136 T. Yamamoto, K. Mitsuno, S. Mori, S. Itoyama, Y. Shiota, K. Yoshizawa, M. Ishida and H. Furuta, *Chem. – Eur. J.*, 2018, **24**, 6742–6746.
- 137 D. S. Bohle, W.-C. Chen and C.-H. Hung, *Inorg. Chem.*, 2002, **41**, 3334–3336.
- 138 J. D. Harvey and C. J. Ziegler, *Chem. Commun.*, 2002, 1942–1943.
- 139 S.-H. Peng, M. H. R. Mahmood, H.-B. Zou, S.-B. Yang and H.-Y. Liu, *J. Mol. Catal. A: Chem.*, 2014, **395**, 180–185.
- 140 M. Toganoh, T. Ishizuka and H. Furuta, *Chem. Commun.*, 2004, 2464–2465.
- 141 M. Toganoh, S. Ikeda and H. Furuta, *Inorg. Chem.*, 2007, **46**, 10003–10015.
- 142 M. Toganoh and H. Furuta, *Chem. Lett.*, 2005, **34**, 1034–1035.
- 143 T. Yamamoto, M. Toganoh, S. Mori, H. Uno and H. Furuta, *Chem. Sci.*, 2012, **3**, 3241–3248.
- 144 T. Yamamoto, M. Toganoh and H. Furuta, *Dalton Trans.*, 2012, **41**, 9154–9157.
- 145 M. Toganoh, T. Hihara and H. Furuta, *Inorg. Chem.*, 2010, **49**, 8182–8184.
- 146 X. Zhu, W.-K. Wong, W.-K. Lo and W.-Y. Wong, *Chem. Commun.*, 2005, 1022–1024.
- 147 X.-J. Zhu, F.-L. Jiang, C.-T. Poon, W.-K. Wong and W.-Y. Wong, *Eur. J. Inorg. Chem.*, 2008, 3151–3162.
- 148 A. Młodzianowska, L. Latos-Grażyński, L. Szterenberga and M. Stępień, *Inorg. Chem.*, 2007, **46**, 6950–6957.
- 149 A. Młodzianowska, L. Latos-Grażyński and L. Szterenberga, *Inorg. Chem.*, 2008, **47**, 6364–6374.
- 150 J. Skonieczny, L. Latos-Grażyński and L. Szterenberga, *Inorg. Chem.*, 2009, **48**, 7394–7407.
- 151 J. D. Harvey, J. L. Shaw, R. S. Herrick and C. J. Ziegler, *Chem. Commun.*, 2005, 4663–4665.
- 152 B. Babu, J. Mack and T. Nyokong, *Dalton Trans.*, 2020, **49**, 15180–15183.
- 153 Y. Xie, T. Morimoto and H. Furuta, *Angew. Chem., Int. Ed.*, 2006, **45**, 6907–6910.
- 154 J.-C. Liu, T. Ishizuka, A. Osuka and H. Furuta, *Chem. Commun.*, 2003, 1908–1909.
- 155 T. Ogawa, H. Furuta, M. Takahashi, A. Morino and H. Uno, *J. Organomet. Chem.*, 2000, **611**, 551–557.
- 156 S. Sripathongnak and C. J. Ziegler, *Inorg. Chem.*, 2010, **49**, 5789–5791.
- 157 B. Szyszko, M. J. Bialek, E. Pacholska-Dudziak and L. Latos-Grażyński, *Chem. Rev.*, 2017, **117**, 2839–2909.
- 158 N. Sprutta and L. Latos-Grażyński, *Tetrahedron Lett.*, 1999, **40**, 8457–8460.
- 159 M. Pawlicki and L. Latos-Grażyński, *Chem. – Eur. J.*, 2003, **9**, 4650–4660.
- 160 M. Pawlicki and L. Latos-Grażyński, *J. Org. Chem.*, 2005, **70**, 9123–9130.
- 161 T. D. Lash, in *Advances in Heterocyclic Chemistry*, ed. E. F. V. Scriven and C. A. Ramsden, Academic Press, 2022, vol. 138, pp. 243–334.
- 162 I. Schmidt and P. J. Chmielewski, *Tetrahedron Lett.*, 2001, **42**, 1151–1154.
- 163 M. Pawlicki, L. Latos-Grażyński and L. Szterenberga, *Inorg. Chem.*, 2005, **44**, 9779–9786.
- 164 T. D. Lash, A. M. Young, A. L. Von Ruden and G. M. Ferrence, *Chem. Commun.*, 2008, 6309–6311.
- 165 M. Ishida, H. Fujimoto, T. Morimoto, S. Mori, M. Toganoh, S. Shimizu and H. Furuta, *Supramol. Chem.*, 2017, **29**, 8–16.
- 166 A. M. Young, A. L. Von Ruden and T. D. Lash, *Org. Biomol. Chem.*, 2011, **9**, 6293–6305.
- 167 T. D. Lash, A. D. Lammer and G. M. Ferrence, *Angew. Chem., Int. Ed.*, 2011, **50**, 9718–9721.
- 168 A. S. Almejbel and T. D. Lash, *Org. Biomol. Chem.*, 2020, **18**, 7336–7344.
- 169 R. Li, G. M. Ferrence and T. D. Lash, *Chem. Commun.*, 2013, **49**, 7537–7539.
- 170 M. J. Chmielewski, M. Pawlicki, N. Sprutta, L. Szterenberga and L. Latos-Grażyński, *Inorg. Chem.*, 2006, **45**, 8664–8671.
- 171 M. Pawlicki, I. Kańska and L. Latos-Grażyński, *Inorg. Chem.*, 2007, **46**, 6575–6584.
- 172 R. Li, A. D. Lammer, G. M. Ferrence and T. D. Lash, *J. Org. Chem.*, 2014, **79**, 4078–4093.
- 173 K. Berlin, C. Steinbeck and E. Breitmaier, *Synthesis*, 1996, 336–340.
- 174 T. D. Lash, *Chem. Commun.*, 1998, 1683–1684.
- 175 L. M. Stateman and T. D. Lash, *Org. Lett.*, 2015, **17**, 4522–4525.
- 176 T. Okujima, T. Kikkawa, H. Nakano, H. Kubota, N. Fukugami, N. Ono, H. Yamada and H. Uno, *Chem. – Eur. J.*, 2012, **18**, 12854–12863.



- 177 J. S. D. Moriones, A. N. Latham and T. D. Lash, *J. Porphyrins Phthalocyanines*, 2020, **24**, 817–829.
- 178 S. Venkatraman, V. G. Anand, V. PrabhuRaja, H. Rath, J. Sankar, T. K. Chandrashekar, W. J. Teng and K. R. Senge, *Chem. Commun.*, 2002, 1660–1661.
- 179 M. J. Bialek and L. Latos-Grażyński, *Inorg. Chem.*, 2016, **55**, 1758–1769.
- 180 T. D. Lash, D. I. AbuSalim and G. M. Ferrence, *Inorg. Chem.*, 2021, **60**, 9833–9847.
- 181 T. J. Smolczyk and T. D. Lash, *Chem. Commun.*, 2018, **54**, 9003–9006.
- 182 D. A. Colby and T. D. Lash, *Chem. – Eur. J.*, 2002, **8**, 5397–5402.
- 183 T. D. Lash, D. A. Colby and G. M. Ferrence, *Eur. J. Org. Chem.*, 2003, 4533–4548.
- 184 T. D. Lash and S. T. Chaney, *Angew. Chem., Int. Ed. Engl.*, 1997, **36**, 839–840.
- 185 A. Ghosh, S. Larsen, J. Conradie and C. Foroutan-Nejad, *Org. Biomol. Chem.*, 2018, **16**, 7964–7970.
- 186 V. A. K. Adiraju, G. M. Ferrence and T. D. Lash, *Org. Biomol. Chem.*, 2016, **14**, 10523–10533.
- 187 T. D. Lash, J. A. El-Beck and G. M. Ferrence, *Org. Biomol. Chem.*, 2014, **12**, 316–329.
- 188 T. D. Lash, D. A. Colby, S. R. Graham and S. T. Chaney, *J. Org. Chem.*, 2004, **69**, 8851–8864.
- 189 T. D. Lash, G. C. Gilot and D. I. AbuSalim, *J. Org. Chem.*, 2014, **79**, 9704–9716.
- 190 M. J. Hayes, J. D. Spence and T. D. Lash, *Chem. Commun.*, 1998, 2409–2410.
- 191 A. N. Latham, G. M. Ferrence and T. D. Lash, *Organometallics*, 2019, **38**, 575–585.
- 192 T. D. Lash, D. A. Colby and L. F. Szczepura, *Inorg. Chem.*, 2004, **43**, 5258–5267.
- 193 M. A. Muckey, L. F. Szczepura, G. M. Ferrence and T. D. Lash, *Inorg. Chem.*, 2002, **41**, 4840–4842.
- 194 E. Y. Grabowski, D. I. AbuSalim and T. D. Lash, *J. Org. Chem.*, 2018, **83**, 11825–11838.
- 195 D. A. Colby, G. M. Ferrence and T. D. Lash, *Angew. Chem., Int. Ed.*, 2004, **43**, 1346–1349.
- 196 M. J. Bialek, P. J. Chmielewski and L. Latos-Grażyński, *Chem. – Eur. J.*, 2019, **25**, 14536–14545.
- 197 T. D. Lash, D. A. Colby, J. A. El-Beck, D. I. AbuSalim and G. M. Ferrence, *Inorg. Chem.*, 2015, **54**, 9174–9187.
- 198 T. D. Lash, D. A. Colby, S. R. Graham, G. M. Ferrence and L. F. Szczepura, *Inorg. Chem.*, 2003, **42**, 7326–7338.
- 199 T. D. Lash and G. M. Ferrence, *Inorg. Chem.*, 2017, **56**, 11426–11434.
- 200 L. Latos-Grażyński, E. Pacholska, P. J. Chmielewski, M. M. Olmstead and A. L. Balch, *Angew. Chem., Int. Ed. Engl.*, 1995, **34**, 2252–2254.
- 201 T. D. Lash, *Org. Lett.*, 2011, **13**, 4632–4635.
- 202 M. J. Bialek, A. Białońska and L. Latos-Grażyński, *Inorg. Chem.*, 2015, **54**, 6184–6194.
- 203 V. A. K. Adiraju, G. M. Ferrence and T. D. Lash, *Dalton Trans.*, 2016, **45**, 13691–13694.
- 204 T. D. Lash, W. T. Darrow, A. N. Latham, N. Sahota and G. M. Ferrence, *Inorg. Chem.*, 2019, **58**, 7511–7526.
- 205 L. M. Stateman, G. M. Ferrence and T. D. Lash, *Organometallics*, 2015, **34**, 3842–3848.
- 206 K. Berlin, *Angew. Chem., Int. Ed. Engl.*, 1996, **35**, 1820–1822.
- 207 T. D. Lash and M. J. Hayes, *Angew. Chem., Int. Ed. Engl.*, 1997, **36**, 840–842.
- 208 M. J. Hayes and T. D. Lash, *Chem. – Eur. J.*, 1998, **4**, 508–511.
- 209 D. Li and T. D. Lash, *J. Org. Chem.*, 2014, **79**, 7112–7121.
- 210 D. Li and T. D. Lash, *Eur. J. Org. Chem.*, 2017, 6775–6780.
- 211 A. Berlicka, P. Dutka, L. Szterenberga and L. Latos-Grażyński, *Angew. Chem., Int. Ed.*, 2014, **53**, 4885–4889.
- 212 A. Berlicka, M. J. Bialek and L. Latos-Grażyński, *Angew. Chem., Int. Ed.*, 2016, **55**, 11231–11236.
- 213 M. Garbicz and L. Latos-Grażyński, *Angew. Chem., Int. Ed.*, 2019, **58**, 6089–6093.
- 214 N. Sahota, G. M. Ferrence and T. D. Lash, *J. Org. Chem.*, 2017, **82**, 9715–9730.
- 215 K. Hurej, M. Pawlicki and L. Latos-Grażyński, *Chem. – Eur. J.*, 2017, **23**, 2059–2066.
- 216 K. Hurej, M. Pawlicki and L. Latos-Grażyński, *Chem. – Eur. J.*, 2018, **24**, 115–126.
- 217 B. Szyszko, K. Kupietz, L. Szterenberga and L. Latos-Grażyński, *Chem. – Eur. J.*, 2014, **20**, 1376–1382.
- 218 B. Szyszko and L. Latos-Grażyński, *Organometallics*, 2011, **30**, 4354–4363.
- 219 A. Idec, L. Szterenberga and L. Latos-Grażyński, *Chem. – Eur. J.*, 2015, **21**, 12481–12487.
- 220 H. Furuta, H. Maeda and A. Osuka, *J. Am. Chem. Soc.*, 2000, **122**, 803–807.
- 221 H. Uno, K. Muramatsu, S. Hiraoka, H. Tahara, M. Hirose, E. Tamura, T. Shiraishi, J. Mack, N. Kobayashi, S. Mori, T. Okujima and M. Takase, *Chem. – Eur. J.*, 2020, **26**, 5701–5708.
- 222 H. Maeda, A. Osuka and H. Furuta, *J. Am. Chem. Soc.*, 2003, **125**, 15690–15691.
- 223 J. Yan, M. Takakusaki, Y. Yang, S. Mori, B. Zhang, Y. Feng, M. Ishida and H. Furuta, *Chem. Commun.*, 2014, **50**, 14593–14596.
- 224 N. Halder, M. Sangeetha, D. Usharani and H. Rath, *J. Org. Chem.*, 2020, **85**, 2059–2067.
- 225 N. Halder, R. Naryanasamy, D. Usharani and H. Rath, *Org. Chem. Front.*, 2022, **9**, 2333–2342.
- 226 Z. J. Zhang, G. M. Ferrence and T. D. Lash, *Org. Lett.*, 2009, **11**, 101–104.
- 227 D. I. AbuSalim, G. M. Ferrence and T. D. Lash, *J. Am. Chem. Soc.*, 2014, **136**, 6763–6772.
- 228 T. D. Lash, D. A. Colby, A. S. Idate and R. N. Davis, *J. Am. Chem. Soc.*, 2007, **129**, 13800–13801.
- 229 T. D. Lash, A. D. Lammer, A. S. Idate, D. A. Colby and K. White, *J. Org. Chem.*, 2012, **77**, 2368–2381.
- 230 T. D. Lash, D. I. AbuSalim and G. M. Ferrence, *Chem. Commun.*, 2015, **51**, 15952–15955.
- 231 T. D. Lash, J. L. Romanic, M. J. Hayes and J. D. Spence, *Chem. Commun.*, 1999, 819–820.
- 232 T. D. Lash, S. C. Fosu, T. J. Smolczyk and D. I. AbuSalim, *J. Org. Chem.*, 2018, **83**, 12619–12631.



- 233 S. R. Graham, D. A. Colby and T. D. Lash, *Angew. Chem., Int. Ed.*, 2002, **41**, 1371–1374.
- 234 N. Sprutta, M. Świdarska and L. Latos-Grażyński, *J. Am. Chem. Soc.*, 2005, **127**, 13108–13109.
- 235 N. Sprutta, M. Siczek, L. Latos-Grażyński, M. Pawlicki, L. Szterenber and T. Lis, *J. Org. Chem.*, 2007, **72**, 9501–9509.
- 236 S. Ahmad, A. Singhal, K. Nisa and S. M. S. Chauhan, *Inorg. Chem.*, 2018, **57**, 11333–11340.
- 237 T. Maulbetsch and D. Kunz, *Angew. Chem., Int. Ed.*, 2021, **60**, 2007–2012.
- 238 T. D. Lash, *Synlett*, 2000, 279–295.
- 239 N. Sprutta, M. Welnic, M. J. Bialek, T. Lis, L. Szterenber and L. Latos-Grażyński, *Chem. – Eur. J.*, 2016, **22**, 6974–6980.
- 240 D. A. Colby and T. D. Lash, *J. Org. Chem.*, 2002, **67**, 1031–1033.
- 241 N. Sprutta, S. Mackowiak, M. Kocik, L. Szterenber, T. Lis and L. Latos-Grażyński, *Angew. Chem., Int. Ed.*, 2009, **48**, 3337–3341.
- 242 G. G. Qiao, M. W. Wong and C. Wentrup, *J. Org. Chem.*, 1996, **61**, 8125–8131.
- 243 Y. Chun, N. J. Singh, I.-C. Hwang, J. W. Lee, S. U. Yu and K. S. Kim, *Nat. Commun.*, 2013, **4**, 1797.
- 244 M. R. Anneser, S. Haslinger, A. Pöthig, M. Cokoja, J.-M. Basset and F. E. Kühn, *Inorg. Chem.*, 2015, **54**, 3797–3804.
- 245 E. B. Bauer, M. A. Bernd, M. Schütz, J. Oberkofler, A. Pöthig, R. M. Reich and F. E. Kühn, *Dalton Trans.*, 2019, **48**, 16615–16625.
- 246 H. M. Bass, S. A. Cramer, A. S. McCullough, K. J. Bernstein, C. R. Murdock and D. M. Jenkins, *Organometallics*, 2013, **32**, 2160–2167.
- 247 M. R. Anneser, G. R. Elpitiya, X. B. Powers and D. M. Jenkins, *Organometallics*, 2019, **38**, 981–987.
- 248 A. Weiss, H. Pritzkow and W. Siebert, *Angew. Chem., Int. Ed.*, 2000, **39**, 547–549.
- 249 X. B. Carroll, D. Errulat, M. Murugesu and D. M. Jenkins, *Inorg. Chem.*, 2022, **61**, 1611–1619.
- 250 J. F. DeJesus, R. W. F. Kerr, D. A. Penchoff, X. B. Carroll, C. C. Peterson, P. L. Arnold and D. M. Jenkins, *Chem. Sci.*, 2021, **12**, 7882–7887.
- 251 M. R. Anneser, X. B. Powers, K. M. Peck, I. M. Jensen and D. M. Jenkins, *Organometallics*, 2019, **38**, 3369–3376.
- 252 H. Furuta, H. Maeda, A. Osuka, M. Yasutake, T. Shinmyozu and Y. Ishikawa, *Chem. Commun.*, 2000, 1143–1144.
- 253 J. Yan, Y. Yang, M. Ishida, S. Mori, B. Zhang, Y. Feng and H. Furuta, *Chem. – Eur. J.*, 2017, **23**, 11375–11384.
- 254 M. J. Bialek, N. Sprutta and L. Latos-Grażyński, *Inorg. Chem.*, 2016, **55**, 12061–12073.
- 255 P. J. Altmann, D. T. Weiss, C. Jandl and F. E. Kühn, *Chem. – Asian J.*, 2016, **11**, 1597–1605.
- 256 T. P. Schlachta, M. R. Anneser, J. F. Schlagintweit, C. H. G. Jako, C. Hintermeier, A. D. Böth, S. Haslinger, R. M. Reich and F. E. Kühn, *Chem. Commun.*, 2021, **57**, 6644–6647.
- 257 J. F. Schlagintweit, C. Hintermeier, M. R. Anneser, E.-M. H. J. Esslinger, S. Haslinger and F. E. Kühn, *Chem. – Asian J.*, 2020, **15**, 1896–1902.
- 258 M. R. Anneser, S. Haslinger, A. Pöthig, M. Cokoja, V. D'Elia, M. P. Högerl, J.-M. Basset and F. E. Kühn, *Dalton Trans.*, 2016, **45**, 6449–6455.
- 259 J. W. Kück, M. R. Anneser, B. Hofmann, A. Pöthig, M. Cokoja and F. E. Kühn, *ChemSusChem*, 2015, **8**, 4056–4063.
- 260 S. Meyer, I. Klawitter, S. Demeshko, E. Bill and F. Meyer, *Angew. Chem., Int. Ed.*, 2013, **52**, 901–905.
- 261 C. Cordes, M. Morganti, I. Klawitter, C. Schremmer, S. Dechert and F. Meyer, *Angew. Chem., Int. Ed.*, 2019, **58**, 10855–10858.
- 262 J. F. Schlagintweit, P. J. Altmann, A. D. Böth, B. J. Hofmann, C. Jandl, C. Kaußler, L. Nguyen, R. M. Reich, A. Pöthig and F. E. Kühn, *Chem. – Eur. J.*, 2021, **27**, 1311–1315.
- 263 Z. S. Ghavami, M. R. Anneser, F. Kaiser, P. J. Altmann, B. J. Hofmann, J. F. Schlagintweit, G. Grivani and F. E. Kühn, *Chem. Sci.*, 2018, **9**, 8307–8314.
- 264 F. E. Hahn, V. Langenhahn, T. Lügger, T. Pape and D. Le Van, *Angew. Chem., Int. Ed.*, 2005, **44**, 3759–3763.
- 265 H. Furuta, T. Ishizuka, A. Osuka, Y. Uwatoko and Y. Ishikawa, *Angew. Chem., Int. Ed.*, 2001, **40**, 2323–2325.
- 266 H. Furuta, T. Ishizuka and A. Osuka, *Inorg. Chem. Commun.*, 2003, **6**, 398–401.
- 267 P. Pushpanandan, Y. K. Maurya, T. Omagari, R. Hirose, M. Ishida, S. Mori, Y. Yasutake, S. Fukatsu, J. Mack, T. Nyokong and H. Furuta, *Inorg. Chem.*, 2017, **56**, 12572–12580.
- 268 N. Halder, M. H. Mahadavaiah, D. Usharani and H. Rath, *J. Porphyrins Phthalocyanines*, 2021, **25**, 966–974.
- 269 R. Nishiyabu, M. A. Palacios, W. Dehaen and P. Anzenbacher, *J. Am. Chem. Soc.*, 2006, **128**, 11496–11504.
- 270 P. Anzenbacher, R. Nishiyabu and M. A. Palacios, *Coord. Chem. Rev.*, 2006, **250**, 2929–2938.
- 271 Q. Chen, T. Wang, Y. Zhang, Q. Wang and J. Ma, *Synth. Commun.*, 2002, **32**, 1051–1058.
- 272 J. Skonieczny, L. Latos-Grażyński and L. Szterenber, *Chem. – Eur. J.*, 2008, **14**, 4861–4874.
- 273 Z. Duan, M. Clochard, B. Donnadieu, F. Mathey and F. S. Tham, *Organometallics*, 2007, **26**, 3617–3620.
- 274 K. Fujino, Y. Hirata, Y. Kawabe, T. Morimoto, A. Srinivasan, M. Toganoh, Y. Miseki, A. Kudo and H. Furuta, *Angew. Chem., Int. Ed.*, 2011, **50**, 6855–6859.
- 275 Y. K. Maurya, K. Noda, K. Yamasumi, S. Mori, T. Uchiyama, K. Kamitani, T. Hirai, K. Ninomiya, M. Nishibori, Y. Hori, Y. Shiota, K. Yoshizawa, M. Ishida and H. Furuta, *J. Am. Chem. Soc.*, 2018, **140**, 6883–6892.
- 276 P. Pushpanandan, V. Grover and M. Ravikanth, *Org. Lett.*, 2022, **24**, 3184–3188.
- 277 M. Toganoh, Y. Kawabe, H. Uno and H. Furuta, *Angew. Chem., Int. Ed.*, 2012, **51**, 8753–8756.
- 278 B. Basumatary, I. Hashiguchi, S. Mori, S. Shimizu, M. Ishida and H. Furuta, *Angew. Chem., Int. Ed.*, 2020, **59**, 15897–15901.
- 279 S. Larsen, L. J. McCormick-McPherson, S. J. Teat and A. Ghosh, *ACS Omega*, 2019, **4**, 6737–6745.





- 280 E. Pacholska, L. Latos-Grażyński and Z. Ciunik, *Chem. – Eur. J.*, 2002, **8**, 5403–5405.
- 281 E. Pacholska-Dudziak, J. Skonieczny, M. Pawlicki, L. Szterenber, Z. Ciunik and L. Latos-Grażyński, *J. Am. Chem. Soc.*, 2008, **130**, 6182–6195.
- 282 T. D. Lash, S. A. Jones and G. M. Ferrence, *J. Am. Chem. Soc.*, 2010, **132**, 12786–12787.
- 283 E. Pacholska-Dudziak, L. Szterenber and L. Latos-Grażyński, *Chem. – Eur. J.*, 2011, **17**, 3500–3511.
- 284 J.-H. Hong, A. S. Aslam, M.-S. Ko, J. Choi, Y. Lee and D.-G. Cho, *Chem. – Eur. J.*, 2018, **24**, 10054–10058.
- 285 E. Vogel, *Pure Appl. Chem.*, 1990, **62**, 557–564.
- 286 E. Vogel, *Pure Appl. Chem.*, 1993, **65**, 143–152.
- 287 E. Vogel, *Pure Appl. Chem.*, 1996, **68**, 1355–1360.
- 288 T. D. Lash, *J. Porphyrins Phthalocyanines*, 2012, **16**, 423–433.
- 289 H. Furuta, H. Maeda and A. Osuka, *J. Org. Chem.*, 2001, **66**, 8563–8572.
- 290 D. I. AbuSalim and T. D. Lash, *J. Org. Chem.*, 2013, **78**, 11535–11548.
- 291 D. I. AbuSalim and T. D. Lash, *J. Phys. Chem. A*, 2015, **119**, 11440–11453.

